Department of Meteorology
The University of Wisconsin
Madison, Wisconsin

Studies of Large Scale Atmospheric Energetics

Contributions by

A. Carasso
G. Gutman
D. R. Johnson
P. J. Smith
W. L. Smith
W. Schwerdtfeger

L. H. Horn, Principal Investigator

ANNUAL REPORT

The research reported in this document has been supported by the Meteorological Satellite Laboratory of the United States Weather Bureau Under Grant WBG 25

400-85

JUNE 1965

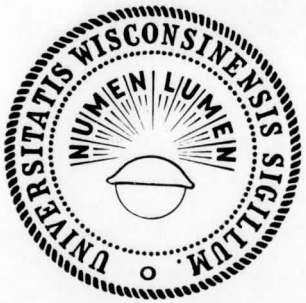

Department of Meteorology
The University of Wisconsin
Madison, Wisconsin

STUDIES OF LARGE SCALE ATMOSPHERIC ENERGETICS

Contributions by:

A. Carasso
G. Gutman
D. R. Johnson
P. J. Smith
W. L. Smith
W. Schwerdtfeger

L. H. Horn, Principal Investigator

ANNUAL REPORT

The research reported in this document has been supported by The Meteorological Satellite Laboratory of the United States Weather Bureau Under Grant WBG 25

JUNE 1965

ACKNOWLEDGMENTS

The authors would like to acknowledge the valuable suggestions, criticisms and assistance of Drs. Reid A. Bryson, P. M. Kuhn, H. H. Lettau, and F. Prohaska and Mr. Benjamin Bullock during the various phases of preparation of this report. The assistance of Mr. Charles Hutchins in computer programming is also acknowledged.

TABLE OF CONTENTS

GENERAL INTRODUCTION

The research presented here, in the form of an annual report, consists of five studies involving the large scale energetics of the atmosphere. They represent a continuation of work begun under U. S. Weather Bureau Contract CWB 10240 and U. S. Weather Bureau Grant WBG 10, Project 4.

The goal of this research is to obtain a better understanding of the mechanisms through which differential heating of the atmosphere produces and maintains the kinetic energy of various scales of atmospheric circulation. The increasing availability of meteorological satellite data is providing on a global scale the observational data necessary to understand the energetics of the atmosphere. Because the satellite radiation measurements have been in the infrared, the studies reported here center on the role of terrestrial radiation in the energy processes.

The five studies (1) establish on a firmer basis the relationship between satellite infrared measurements and the divergence of radiation within the atmosphere, (2) describe the areal scale of the time averaged and perturbation part of the infrared radiation field between 50° N and 50°S, (3) investigate the role of infrared cooling in the generation of available potential energy, (4) analyze time series of various energy parameters using variance spectra techniques, and (5) investigate the energy budget of the high level anticyclone found over the Altiplano of South America.

Lyle H. Horn
Principal Investigator

Madison, Wisconsin
June 1965

On the Relation Between TIROS Radiation Measurements and Atmospheric Infrared Cooling

William L. Smith
Lyle H. Horn
Donald R. Johnson

Department of Meteorology
University of Wisconsin

Abstract: TIROS II channel 2 and channel 4 measurements of infrared radiation are statistically correlated with corresponding radiometersonde measurements of radiation divergence within various layers of the atmosphere. Estimates of the correlation coefficient greater than 0.60 are obtained for all layers extending from the surface of the earth to levels beyond 600 mb.

The results of this study indicate that the satellite measured flux is most significantly related to the infrared cooling profile within the surface-600 mb layer. It is shown that good estimates of the infrared cooling profile might be obtained from satellite measurements if the general sky condition is also known.

1. Introduction

The importance of heat sources and sinks in maintaining the general circulation is well known. Many investigators have recognized the importance of the contribution of infrared cooling to the total heat budget of the atmosphere. Satellite measurements of the long-wave radiation leaving the earth-atmosphere system now offer a possibility of estimating the atmosphere's infrared cooling over large areas in a relatively small time interval (Sabatini and Suomi, 1962). From results based solely on radiometersonde data, Sabatini and Suomi (1962) have indicated that a high linear correlation should exist between the outgoing terrestrial

stream measured by a satellite and the mean infrared cooling of the entire atmospheric column. The objective of this research is to estimate the correlation between the infrared cooling of various layers within the atmospheric column determined from radiometersonde data and the TIROS II channel 2 and channel 4 measurements of infrared flux leaving the atmosphere.

2. Radiation Measurements and Infrared Cooling

The infrared cooling within the atmosphere, as well as the infrared flux leaving the atmosphere, is directly related to the air temperature, the emissivity and height of clouds, and the content and distribution of emitting and absorbing gases. Thus, variations in the upward flux at the top of the atmosphere due to variations of these atmospheric properties are related to variations of the heat loss by infrared radiation processes within the atmosphere.

An expression for the rate of heat loss within any atmospheric layer by infrared radiation processes may be obtained from the values of the net radiation at the top and bottom of the layer. Radiation in the atmosphere is emitted in all directions. When the atmosphere is assumed to be horizontally stratified, only the upward and downward flux need to be considered. The net radiation at any level is given by the difference between the upward and downward flux at that level. Thus, in a horizontally stratified medium, the mean rate of heat addition (loss), $\bar{Q}$, through infrared radiation processes experienced by a unit column between two isobaric surfaces, p_1 and p_2, is given by the vertical convergence (divergence) of the net radiation flux, F_n. Mathematically it may be expressed as

$$\bar{Q} = \frac{1}{p_2 - p_1} \int_{p_1}^{p_2} g \frac{\partial F_n}{\partial p} dp = g \frac{F_{n_2} - F_{n_1}}{p_2 - p_1} = g \frac{\Delta F_n}{\Delta p}$$

where g is the acceleration of gravity, and $\partial F_n / \partial p$ the divergence of the net infrared radiation, is hereafter noted simply as flux divergence. Measurements made by the Suomi-Kuhn radiometersonde (Suomi-Kuhn, 1958) can be used to estimate the flux divergence for any level in the atmosphere, thus providing a detailed profile of the infrared cooling throughout the atmosphere.

The channel 2 and channel 4 radiometers on board TIROS II, which measure radiation in the 7 - 13 micron region (i.e., the atmospheric window) and the 7 - 32 micron region, respectively, are capable of supplying reliable relative estimates of the infrared flux leaving the earth-atmosphere system. In general, channel 4 measurements which are sensitive to the radiation emitted by cloud and ground surfaces, as well as by most of the water vapor and carbon dioxide in the atmosphere, essentially represent the total upward flux at the top of the atmosphere. Channel 2 measurements, which are highly sensitive to radiation received through the atmospheric window where absorption by water vapor and carbon dioxide is at a minimum, represent energy being emitted from layers very near cloud or ground surfaces. In this study, an attempt is made to estimate the correlation between the flux divergence within the atmosphere observed by the Suomi-Kuhn radiometersonde and the radiation observed by the channel 2 and channel 4 radiometers of TIROS II.

3. Procedures

The basic flux divergence data for this study were provided by sixty-four nocturnal radiometersonde ascents which were made under the orbital paths of TIROS II during the period 19 December 1960 - 18 January 1961. The locations of the radiometersonde stations are illustrated in Figure 1. A summary of the net radiation flux data for these ascents is given in the Appendix. Using these data, the flux divergence was calculated for the fifty-five layers shown in Figure 2.

Because of the relatively large degradation of the channel 4 instrument beyond 6 January 1961 (TIROS II Radiation Data Users Manual, 1961), the entire collection of data was partitioned into two samples. The first sample includes both channel 4 and channel 2 data coinciding with the radiometersonde ascents between 19 December 1960 and 7 January 1961, whereas the second sample includes only channel 2 data coinciding with the radiometersonde ascents for the entire period (19 December 1960 - 18 January 1961). All the channel 4 and channel 2 measurements from the first sample were observed over a station within four hours of a radiometersonde ascent. However, the time interval between the two sets of observations reached as much as seven hours for a few of the cases beyond 6 January 1961. Since the synoptic conditions may change considerably between the times of these independent measurements, an attempt was made to screen from the initial sample those cases in which such changes occurred. Five cases in which large synoptic changes were indicated by the radiation measurements and surface observations were not included in this sample.

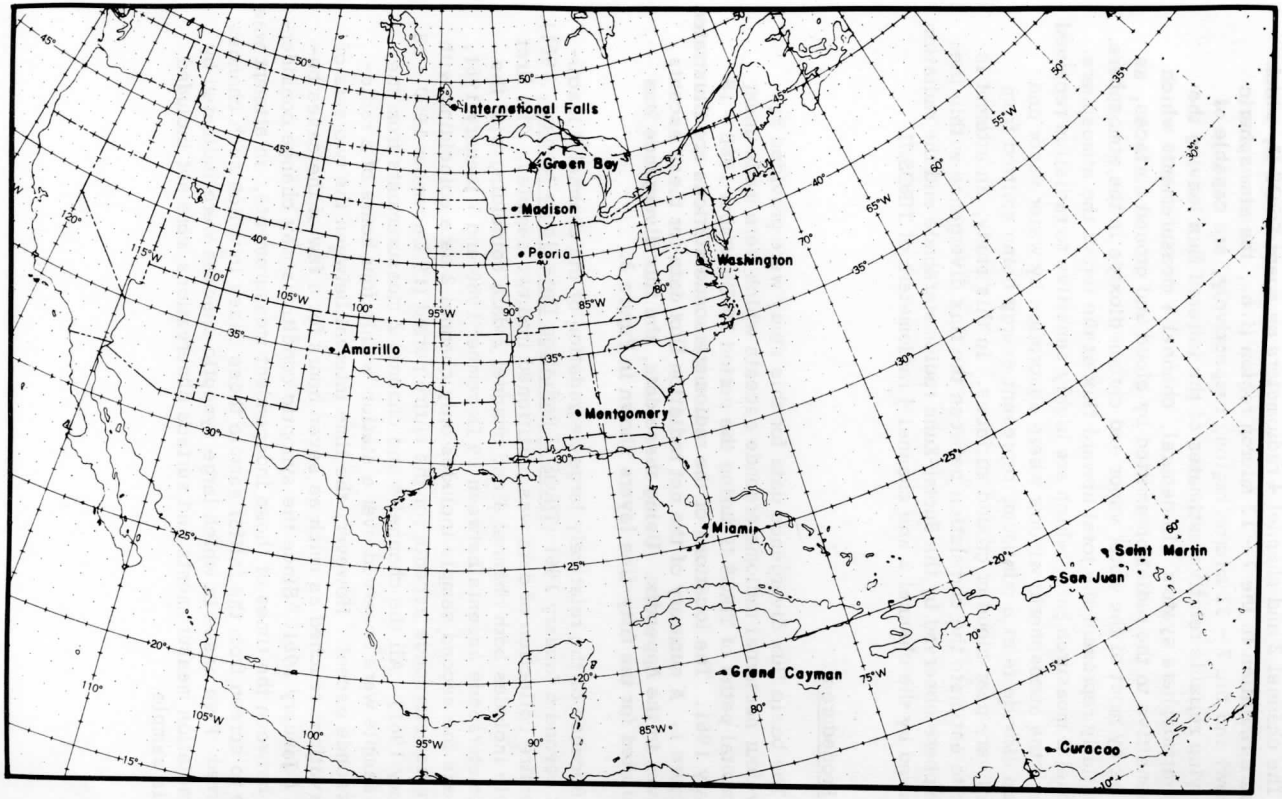

FIGURE 1. Station Locations

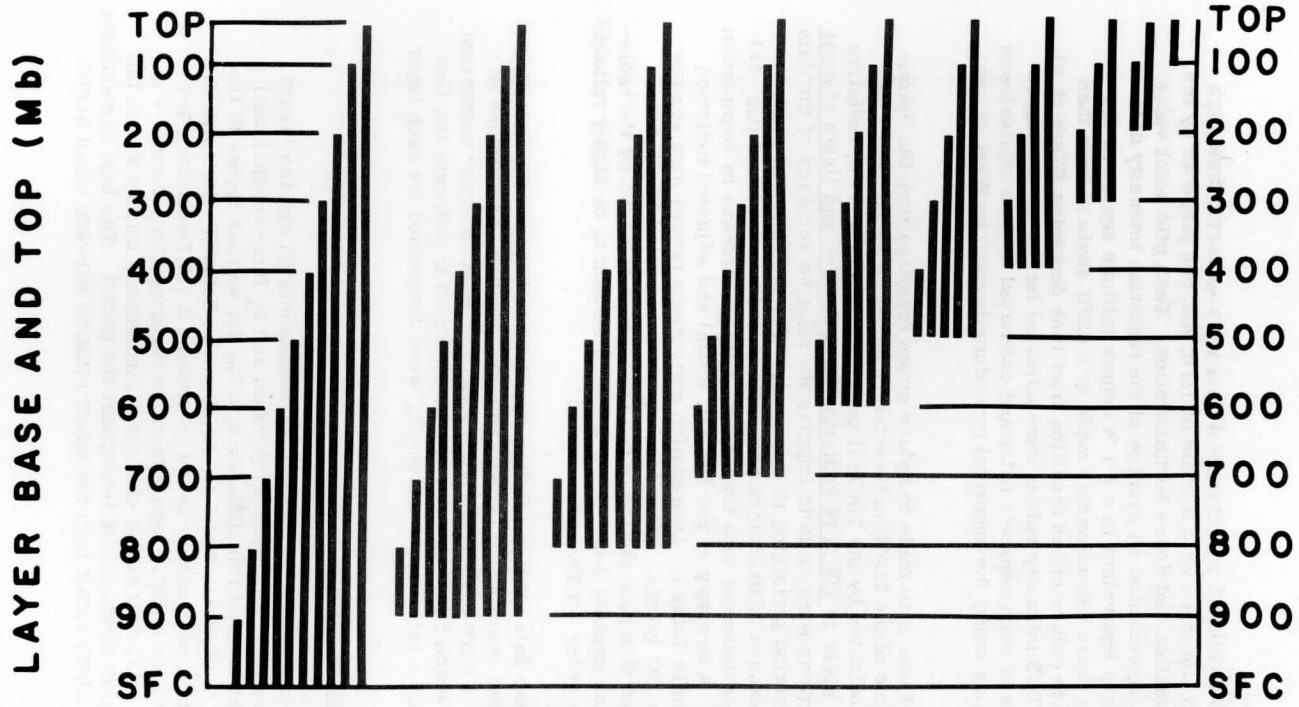

Figure 2 Atmospheric layers for which radiation divergence was computed from radiometersonde data.

The TIROS channel 2 and channel 4 data were extracted from high resolution mercator maps with a scale of 1:10,000,000 prepared by the National Aeronautics and Space Administration. Each grid point value on these maps represented an average of the radiation intensity data over a small area equivalent to a 1 1/4 degree latitude square at the equator. Only those measurements made at a nadir angle of less than 58° were used to reduce errors resulting from limb darkening (Wark et. al. 1962). The TIROS intensity values were adjusted for the transmittance characteristics of each sensor's filter and converted to their equivalence of blackbody flux using the empirical procedure devised by Wark et. al., (1962).

An attempt was also made to reduce errors resulting from the deterioration with time of the TIROS radiometers. Based on estimates of degradation as indicated by the TIROS II quasi-global (55°N-55°S) radiative energy budget given in TIROS IV Radiation Data Catalog and Users Manual (1963), corrections were made to improve the relative accuracy of the data over the time period pertaining to this study. For the period of study cumulative averages of irradiance presented in the users manual (fig. 46) showed a linear decrease with time; thus, a linear increase in degradation was assumed. A summary of the TIROS II initial and adjusted radiation values is given in Table I. Degradation corrections ranged from approximately .01 to .03 ly/min. After comparing the corrected TIROS data with the upward flux near the top of the atmosphere observed by the radiometersonde, the channel 2 and channel 4 data seemed to be highly reliable in the relative sense for the entire period.

Using these data, the correlation coefficients between the flux divergence of various atmospheric layers and corresponding observations in channel 2 and 4 were estimated. Furthermore, "least squares" regression coefficients, which could be used in a linear model to estimate the flux divergence from a satellite measurement, were determined for each layer.

4. Discussion of Results

Table II lists the linear correlation coefficients (r) and the "least square" regression coefficients b_o (ly/min) and b_1 (non-dimensional) relating the net infrared flux difference, ΔF_n, for various layers to the flux observed in channels 2 and 4. As shown in Table II, the estimates of the correlation coefficients based on channel 2 (19 December 1960 - 7 January 1961) are slightly higher than the corresponding channel 4 estimates. The relatively higher channel 2 correlations may be due to the greater reliability of channel 2 throughout the period. The high correlations for channel 2 likely result from the direct relation between cloud height

TABLE I: TIROS RADIATION DATA

Radiometersonde Ascents		Tiros II Radiation Values				
			Map Values (watts/m²)		Corrected Flux (ly/min)	
Station	Date (GMT)[1]	Orbits	Ch(2)	Ch(4)	Ch(2)	Ch(4)
Amarillo:	Dec 21 1960	405-407	28	37	.31	.29
	Dec 22 1960	419-421	28	34	.31	.27
	Dec 23 1960	433-436	29	37	.32	.29
	Dec 24 1960	447-450	26	35	.30	.28
	Jan 16 1961	794-798	32	-	.35	-
Curacao:	*Dec 23 1960	447-450	35	46	.35	.34
	Dec 27 1960	505	43	47	.39	.34
	*Jan 15 1961	779-782	35	-	.37	-
Grand Cayman:	Dec 24 1960	462-465	23	31	.28	.26
	Jan 06 1961	650-653	34	42	.35	.33
	Jan 09 1961	693-696	43	-	.39	-
	Jan 10 1961	707-711	33	-	.34	-
	Jan 12 1961	736-738	38	-	.38	-
	Jan 15 1961	779-782	36	-	.37	-
	Jan 16 1961	794-798	40	-	.39	-
Green Bay:	Jan 12 1961	736-738	27	-	.32	-
	Jan 15 1961	779-782	22	-	.29	-
	Jan 16 1961	794-798	28	-	.33	-
	Jan 17 1961	811-812	23	-	.30	-
	Jan 18 1961	823-827	29	-	.33	-
International Falls:	Dec 19 1960	390-392	20	29	.26	.24
	Dec 20 1960	405-407	24	35	.28	.28
	Dec 21 1960	419-421	21	28	.27	.24
	Dec 22 1960	433-436	20	28	.27	.24
	Dec 23 1960	447-450	21	33	.27	.25
	Dec 24 1960	462-465	24	33	.29	.25
	Jan 07 1961	667	22	39	.28	.31
	Jan 09 1961	693-696	23	-	.29	-
	Jan 10 1961	707-711	24	-	.30	-
	Jan 11 1961	723-724	21	-	.29	-
	Jan 15 1961	779-782	14	-	.25	-
	Jan 17 1961	811-812	23	-	.30	-
Madison:	Dec 22 1960	433-436	23	32	.28	.26
	Jan 10 1961	707-711	24	-	.30	-
	Jan 11 1961	723-724	24	-	.31	-
Miami:	Jan 06 1961	650-653	34	44	.35	.34
	Jan 10 1961	707-711	38	-	.37	-
	Jan 15 1961	779-782	34	-	.36	-
Montgomery:	Dec 22 1960	433-436	33	42	.34	.32
	Jan 06 1961	650-653	26	37	.30	.30
	Jan 09 1961	693-696	33	-	.34	-
	Jan 15 1961	779-782	33	-	.35	-
	Jan 16 1961	794-798	34	-	.36	-
	Jan 18 1961	823-827	26	-	.31	-
Peoria:	Dec 22 1960	433-436	23	32	.28	.26
	Dec 23 1960	447-450	23	35	.28	.28
	Jan 09 1961	693-696	27	-	.31	-
	Jan 10 1961	707-711	26	-	.30	-
	Jan 11 1961	723-724	29	-	.33	-
	Jan 12 1961	736-738	26	-	.31	-
Saint Martin:	*Dec 25 1960	476-479	31	37	.33	.30
	Dec 28 1960	519-521	40	53	.38	.38
San Juan:	Dec 23 1960	447-450	40	50	.37	.36
	Dec 25 1960	476-479	26	32	.30	.27
	Jan 15 1961	779-782	40	50	.39	-
Washington:	Dec 19 1960	390-392	31	39	.32	.30
	*Dec 25 1960	462-465	32	40	.34	.31
	Jan 06 1961	650-653	35	41	.35	.32
	Jan 09 1961	693-696	31	-	.33	-
	Jan 10 1961	707-711	31	-	.33	-
	*Jan 11 1961	723-724	34	-	.36	-
	Jan 12 1961	736-738	27	-	.32	-
	Jan 16 1961	794-798	27	-	.32	-
	Jan 17 1961	811-812	28	-	.33	-

[1] All radiometersondes were released between 2300 and 0030 GMT.

*This TIROS data was positioned 1 grid point from the station.

TABLE II

SUMMARY OF LINEAR CORRELATION COEFFICIENTS (r) AND REGRESSION COEFFICIENTS (b_0 and b_1).

Sample	1:	Dec 19 1960 — Jan 7 1961						2:	Dec 19 1960 — Jan 18 1961		
Layer		Channel 2			Channel 4				Channel 2		
	N	r	b_0	b_1	r	b_0	b_1	N	r	b_0	b_1
SFC-900	24	.13	-.0011	.0868	.06	.0136	.0418	59	.14	-.0050	.0945
-800	27	.26	-.0288	.2193	.26	-.0230	.2142	63	.32	-.0308	.2361
-700	27	.32	-.0433	.3601	.27	-.0183	.2989	63	.36	-.0395	.3504
-600	27	.74	-.1745	.8621	.73	-.1501	.8366	63	.61	-.1151	.6543
-500	27	.68	-.2036	1.0095	.69	-.1801	.9967	63	.65	-.1491	.8162
-400	27	.75	-.1609	.9494	.70	-.1205	.8655	62	.71	-.1275	.8077
-300	27	.80	-.1741	1.0252	.76	-.1330	.9537	60	.75	-.1216	.8325
-200	27	.83	-.1798	1.0298	.79	-.1395	.9613	59	.79	-.1354	.8751
-100	26	.87	-.2549	1.2508	.83	-.2070	1.1715	57	.78	-.1816	1.0068
SFC-TOP	23	.88	-.2925	1.4269	.78	-.2445	1.3598	53	.79	-.1833	1.0739
900-800	25	.22	-.0213	.1228	.28	-.0283	.1545	60	.24	-.0178	.1214
-700	25	.28	-.0344	.2634	.24	-.0183	.2253	60	.29	-.0253	.2336
-600	25	.64	-.1653	.7662	.64	-.1513	.7666	60	.52	-.1015	.5398
-500	25	.60	-.1985	.9207	.62	-.1890	.9462	60	.57	-.1407	.7165
-400	25	.64	-.1552	.8503	.62	-.1282	.8118	59	.62	-.1205	.7140
-300	25	.69	-.1700	.9360	.68	-.1460	.9132	57	.64	-.1161	.7416
-200	25	.73	-.1709	.9332	.72	-.1475	.9119	56	.67	-.1206	.7615
-100	24	.77	-.2155	1.0707	.74	-.1812	1.0213	54	.69	-.1503	.8506
900-TOP	21	.78	-.2457	1.1972	.69	-.2127	1.1604	50	.67	-.1527	.9081
800-700	28	.16	-.0151	.1415	.10	.0040	.0855	64	.18	-.0093	.1157
-600	28	.52	-.1467	.6439	.51	-.1281	.6236	64	.44	-.0849	.4195
-500	28	.51	-.1760	.7916	.52	-.1583	.7840	64	.48	-.1191	.5820
-400	28	.52	-.1336	.7229	.48	-.0990	.6532	63	.51	-.0974	.5736
-300	28	.56	-.1477	.8087	.53	-.1124	.7426	61	.52	-.0949	.6090
-200	28	.62	-.1515	.8111	.58	-.1170	.7476	60	.57	-.1021	.6342
-100	27	.67	-.2209	1.0145	.63	-.1794	.9413	58	.58	-.1465	.7062
800-TOP	24	.71	-.2212	1.0568	.56	-.1569	.9082	54	.61	-.1401	.7988
700-600	28	.53	-.1315	.5023	.58	-.1321	.5381	64	.42	-.0755	.3038
-500	28	.52	-.1609	.6500	.57	-.1623	.6985	64	.46	-.1096	.4660
-400	28	.51	-.1184	.5813	.51	-.1030	.5677	63	.47	-.0880	.4578
-300	28	.52	-.1325	.6672	.52	-.1165	.6571	61	.47	-.0907	.5106
-200	28	.52	-.1363	.6695	.52	-.1210	.6621	60	.48	-.0990	.5390
-100	27	.56	-.2067	.8759	.56	-.1857	.8631	58	.49	-.1447	.6687
700-TOP	24	.68	-.1646	.7989	.49	-.0985	.6262	54	.53	-.1157	.6459
600-500	28	.18	-.0966	.3285	.28	-.1385	.4936	64	.22	-.0769	.2803
-400	28	.16	-.0130	.0790	.06	.0290	.0295	63	.27	-.0131	.1549
-300	28	.25	-.0010	.1648	.18	.0156	.1189	61	.31	-.0193	.2196
-200	28	.23	-.0048	.1671	.17	.0111	.1240	60	.32	-.0290	.2517
-100	27	.36	-.0702	.3590	.31	-.0480	.3076	58	.35	-.0730	.3768
600-TOP	24	.56	-.1096	.5574	.38	-.0542	.4052	54	.43	-.0791	.4702
500-400	28	.11	-.0424	-.0686	-.22	.0592	-.1307	63	-.01	.0212	-.0078
-300	28	.02	.0283	.0171	-.05	.0458	-.0413	61	.05	.0214	.0352
-200	28	.02	.0245	.0194	-.03	.0412	-.0363	60	.09	.0097	.0727
-100	27	.15	-.0359	.1968	.10	-.0130	.1320	58	.17	-.0308	.1879
500-TOP	24	.35	-.0833	.4252	.18	-.0208	.2392	54	.26	-.0363	.2796
400-300	28	.25	-.0140	.0858	.26	-.0134	.0893	61	.09	.0028	.0340
-200	28	.14	-.0178	.0881	.15	-.0179	.0944	60	.12	-.0084	.0706
-100	27	.29	-.0790	.2671	.30	-.0744	.2695	58	.21	-.0471	.1803
400-TOP	24	.50	-.1290	.4975	.39	-.0966	.4205	54	.28	-.0542	.2731
300-200	28	.00	-.0037	.0023	.00	-.0045	.0050	60	.06	-.0098	.0326
-100	27	.22	-.0640	.1788	.22	-.0601	.1774	58	.18	-.0472	.1390
300-TOP	24	.47	-.1322	.4639	.38	-.1046	.4010	54	.27	-.0620	.2518
200-100	27	.24	-.0528	.1546	.24	-.0487	.1508	58	.23	-.0442	.1333
200-TOP	24	.54	-.1091	.3889	.39	-.0757	.3007	54	.26	-.0476	.2021
100-TOP	23	.30	-.0650	.2547	.16	-.0291	.1496	53	.15	-.0207	.1255

(and amount) and atmospheric flux divergence. The influence of clouds is to reduce the flux divergence within the column beneath the clouds, the magnitude of the reduction being proportional to the cloud height and amount. Since channel 2 measurements are more distinctly related to the energy emitted by cloud surfaces (and, hence, cloud heights and amounts) than are channel 4 measurements, the somewhat higher channel 2 correlation seems to be physically significant.

As also shown in Table II, the estimates of the correlation coefficients pertaining to each channel increase as the thickness of the layers approaches the thickness of the entire atmospheric column. This trend results because the downward flux becomes extremely small compared to the upward flux as the top of the atmosphere is approached; consequently, variations in the outgoing flux as measured by TIROS essentially represent variations in the net flux near the top of the atmosphere. Since the net radiation near the surface of the earth is a relatively small value whose variation is significantly less than the upward flux at the top of the atmosphere, a high correlation will always exist between the outgoing flux and the mean flux divergence for the thicker atmospheric layers. However, an accurate estimate of the mean infrared cooling of the entire atmospheric column is not necessarily representative of the cooling profile throughout the column. For example, this tendency is evident in Table II where the channel 4 correlation is + 0.58 for the 700-600 mb layer, but -0.22 for the 500-400 mb layer. Thus, one particular satellite measurement may be related to the relative cooling of one layer, but also to the relative warming of another layer. Such a result would be physically significant for a cloudy atmosphere where there is relative heating beneath the cloud layer, but strong flux divergence (cooling) above the cloud layer.

Figure 3 graphically illustrates the relation between the channel 2 and channel 4 flux and the net infrared flux divergence for the various atmospheric layers extending from the earth's surface. As shown, both the channel 2 and channel 4 estimates of the correlation coefficients increase substantially to high values as the top of the atmospheric layer approaches the 600 mb level. The slight decrease and subsequent slight increase as the top surface is extended above the 600 mb level indicate that variations in the TIROS measured flux are most distinctly related to the variations of the infrared cooling of the lower troposphere. This result may be indicative of an overwhelming effect by middle clouds on the infrared cooling distribution of the atmosphere.

In order to distinguish more clearly between the contribution of cloud and water vapor variations to the correlation estimates shown in Figure 3, the entire sample of data was partitioned into two sub-samples. One sample includes only observations made in clear and scattered sky

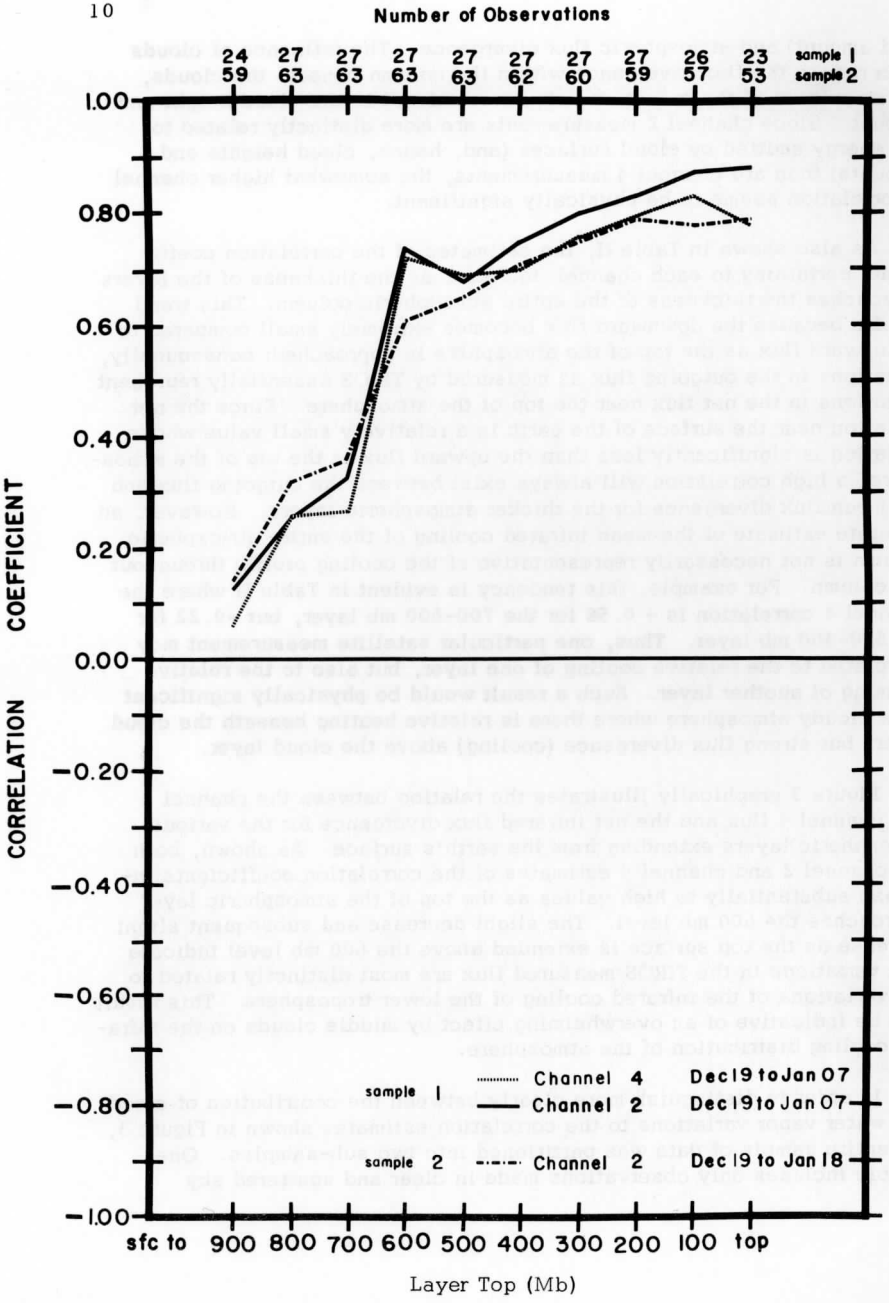

FIGURE 3. All Cases.

conditions, while the other sample includes only observations made in broken and overcast sky conditions. Figures 4 and 5 illustrate the distribution of the correlation coefficient estimates pertaining to these samples for various atmospheric layers based at the earth's surface. As shown for the clear and scattered cases (Figure 4), the channel 4 correlation estimates are higher than the channel 2 estimates when only the lower atmospheric layers are considered. This seems to be significant since the variation of the flux divergence of the lower atmospheric layers in a relatively clear atmosphere is distinctly related to variation of the water vapor content. The reason the channel 4 correlation estimates do not increase above 800 mb is likely due to the very small water vapor content and variability above this level.

An examination of Table III A (clear and scattered cases), which presents the channel 2 and channel 4 estimates for individual layers, reveals that the satellite measured flux is positively correlated with the flux divergence of each layer below the 600 mb level, but only slightly correlated with the flux divergence of any layer above this level. Thus, it seems that within a relatively clear atmosphere satellite measurements may provide physically significant estimates of the infrared cooling profile from the surface to 600 mb. However, the low correlations above 600 mb indicate that although a satellite measurement provides a good estimate of the mean cooling of the entire column, it generally is not representative of the infrared cooling profile within the entire column.

As shown in Figure 5 for the cloudy sky cases, the TIROS measured flux is negatively correlated with the mean flux divergence of the layers extending from the earth's surface to 700 mb, but positively correlated with the mean divergence of the layers extending from the earth's surface to and beyond the 600 mb level. Thus, even though a satellite measurement might provide reasonable estimates of the mean infrared cooling of the surface - 600 mb layer, such estimates for a cloudy atmosphere may indeed be ambiguous since they fail to describe the infrared cooling profile within this layer. A more meaningful estimate of the infrared cooling profile within the cloudy atmosphere may be given by individual relations between satellite measurements and the mean flux divergence of each 100 mb layer. Table II B (broken and overcast cases) illustrates these relations as estimated from the first data sample. The correlations, as well as the sample means of net infrared flux difference shown in this table, clearly depict the effect of the clouds between the 900 and 700 mb levels. In general, the lower the cloud height the greater the relative warming will be near the earth's surface. In the situation where only a low overcast exists, the relatively high values of satellite flux (compared with the flux associated with a higher overcast) are related to the relative

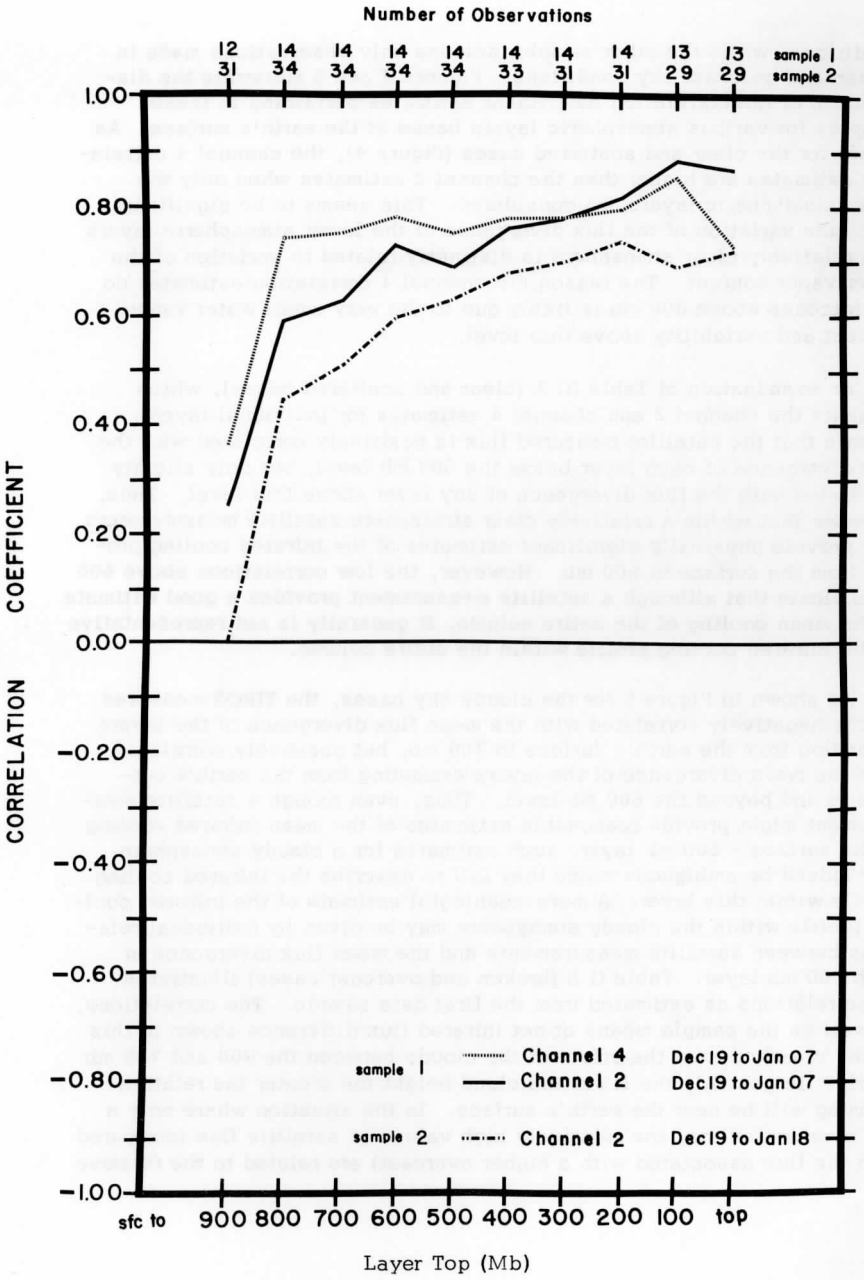

FIGURE 4. Clear and Scattered Cases.

warming below the cloud layer as well as to the strong cooling above. This result is indicated by the significant negative and positive correlations obtained for the surface - 900 mb and 700 - 600 mb layers, respectively. The positive correlation for the 400 - 300 mb layer indicates the presence of cirriform clouds. It is possible that the vertical variation of correlation coefficients noted here indicate the tendency for the existence of a separate cirriform cloud layer above the middle clouds with little cloudiness in between.

Both Figure 5 and Table III suggest that variations in the satellite measured flux from a cloudy atmosphere are most distinctly related to variations of the flux divergence profile within the atmosphere below the 600 mb level. Hence, it seems that for the cloudy as well as the clear atmosphere, satellite measurements might be used with considerable accuracy to estimate the differential infrared cooling distribution of the lower atmosphere. From the results derived from this study, however, such estimates will be more meaningful if the sky condition is also known, since a relatively high satellite flux measurement indicates both relatively strong infrared cooling in the lower layers of a clear atmosphere and significant relative warming in the lower layers of a cloudy atmosphere. Furthermore, although satellite measurements provide reasonable estimates of the mean infrared cooling of large layers, these infrared cooling estimates are not always representative, especially in a cloudy sky, of the infrared cooling at any point within the layer. More meaningful estimates might be obtained, however, by constructing infrared cooling profiles from satellite measurements. The profiles might be constructed by using a regression model relating the satellite observations to the mean infrared cooling of the various 100 mb layers of the atmosphere. Admittedly, the regression equations derived from the limited sample of data used in this study are insufficient to develop an accurate model, yet the physical significance of the correlation obtained in this study seems to warrant its consideration. The ultimate regression equations which might be used as a model of the infrared cooling profile of the atmosphere would indeed have to be developed from large samples of data and include other dependent variables for latitude, general sky conditions (i.e., clear or cloudy), surface (i.e., land or ocean), and season.

Although major attention has been focused on the vertical variation of the correlation coefficients, and not their magnitude, it is noteworthy that some estimates exceeding 0.80 are achieved. It is possible that latitudinal variations between the stations contributed to such high correlation estimates (i.e., the outgoing flux and infrared cooling tend to be higher in low latitudes). However, this effect does not appear to have been as significant as the cloud distribution. An analysis of the correlation estimates achieved when the data were partitioned into low and high

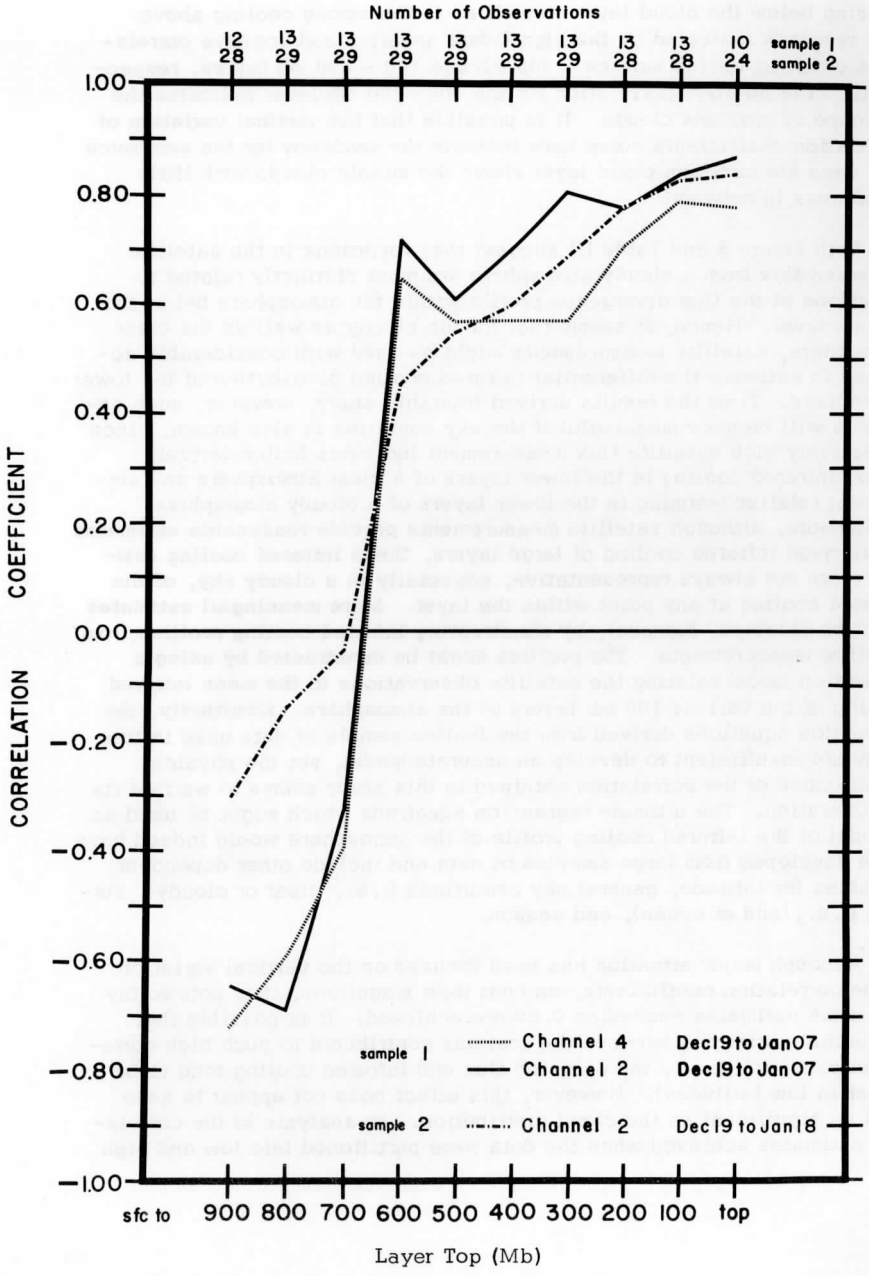

FIGURE 5. Broken and Overcast Cases.

TABLE III

Correlation and regression coefficients (r, b_o, b_1) and means of net infrared radiation differences as obtained from data sample 1 for individual 100 mb layers.

A. Clear and Scattered Cases:

		Channel 2			Channel 4			
Layer	N	r	b_0	b_1	r	b_0	b_1	Fn
Sfc-900	12	.26	.0002	.1253	.37	-.0212	.2021	.0417
900-800	13	.29	-.0340	.1751	.30	-.0397	.2041	.0235
800-700	15	.49	-.0681	.2862	.54	-.0787	.3409	.0256
700-600	15	.78	-.0578	.2435	.54	-.0344	.1837	.0218
600-500	15	.00	.0219	.0000	.06	-.0145	.0240	.0219
500-400	15	.10	.0076	.0302	-.06	.0235	-.0196	.0175
400-300	15	.31	-.0205	.0993	.21	-.0110	.0753	.0119
300-200	15	-.05	.0116	-.0332	-.09	.0018	-.0591	.0008
200-100	14	.30	-.0716	.2027	.23	-.0569	.1695	-.0043

B. Broken and Overcast Cases:

Layer	N	r	b_0	b_1	r	b_0	b_1	Fn
Sfc-900	12	-.65	.1435	-.4517	-.72	.1267	-.4194	.0103
900-800	12	-.19	.0420	-.1083	.04	.0043	.0208	.0191
800-700	13	.11	-.0114	.1506	-.02	.0392	-.0220	.0044
700-600	13	.82	-.3519	1.2918	.83	-.2742	1.0941	.0296
600-500	13	.12	-.1216	.3701	.27	-.1979	.6684	-.0123
500-400	13	-.12	.0591	-.1158	-.23	.0761	-.1843	.0249
400-300	13	.32	-.0290	.1443	.40	-.0272	.1472	.0136
300-200	13	-.14	.0203	-.0942	-.05	.0011	-.0311	-.0075
200-100	13	.27	-.0690	.2195	.30	-.0606	.2031	-.0042

latitudes revealed that although slightly lower estimates were achieved for the higher latitudes, the correlation estimates were in general not much different than those achieved for the entire sample.

5. Conclusions

The basic conclusion of this investigation is that a significant linear relationship exists between TIROS II channel 2 and channel 4 flux measurements and the infrared cooling distribution of the surface - 600 mb layer. Although satellite measurements provide a reasonable estimate of the mean cooling of the entire atmospheric column, regardless of sky conditions, it does not necessarily describe the infrared cooling profile within the column.

It should be noted that since only a limited sample of data was considered, and since the results are statistical, different relations may apply to different seasons, synoptic conditions, areas, and to different satellite instruments. Additional statistical investigations which employ large samples of data covering a wider range of latitudes, synoptic conditions, and seasons must be made before such statistical relations might be used with a high degree of accuracy. The results of this study seem to warrant such future investigations.

6. References

Sabatini, R.R. and V.E. Suomi, 1962: On the Possibility of Atmospheric Infrared Cooling Estimates from Satellite Observations, Journal of the Atmospheric Sciences, Vol. 19, No. 4.

Suomi, V.E., and P. M. Kuhn, 1958: An Economical Net Radiometer, Tellus, Vol. 10, No. 1.

TIROS II Radiation Data User's Manual, 1961: NASA, Goddard Space Flight Center, Greenbelt, Maryland, May 15.

TIROS IV Radiation Data Catalog and User's Manual, 1963: NASA, Goddard Space Flight Center, Greenbelt, Maryland, December 15.

Wark, D.Q., G. Yamamoto and J.H. Lienesch, 1962: Infrared Flux and Surface Temperature Determinations from TIROS Radiometer Measurements, Meteorological Satellite Laboratory Report No. 10, August.

Wark, D.Q., G. Yamamoto and J.H. Lienesch, 1963: Meteorological Satellite Laboratory Supplement to Report No. 10, April.

APPENDIX

SUMMARY OF NET INFRARED RADIATION FLUX (F_N) IN LANGLEYS PER MINUTE AND PRESSURE (P) IN MILLIBARS

Amarillo:

Dec 21 1960		Dec 22 1960		Dec 23 1960		Dec 24 1960		Jan 16 1961	
P	F_N	P	F_N	P	F_N	P	F_N	P	F_N
900	.0287	890	.0704	890	.0609	890	.0803	880	.0768
800	.1034	800	.0927	800	.1059	800	.1085	800	.1420
700	.1207	700	.1067	700	.1171	700	.1256	700	.1687
600	.1397	600	.1282	600	.1347	600	.1401	600	.1922
500	.1520	500	.1565	500	.1604	500	.1767	500	.1972
400	.1679	400	.1799	400	.1785	400	.1917	400	.1955
300	.1645	300	.2102	300	.1946	300	.2006	300	.2150
200	.1948	200	.2140	200	.1778	200	.1733	200	**.2057**
100	.1822	100	.1688	100	.1693	100	.1440	100	.1713
20	.2224	40	.2430	20	.2052	40	.1901	20	.2584

Curacao:

Dec 23 1960	
P	F_N
1010	.0399
1000	.0519
900	.0964
800	.1221
700	.1846
600	.2042
500	.2323
400	**.2326**
300	.2385
200	.2159
120	.1867

Grand Cayman:

Dec 27 1960		Jan 15 1961	
P	F_N	P	F_N
1010	.0622	975	.0891
1000	.0617	900	.1255
900	.1115	800	.1495
800	.1309	700	.1913
700	.1709	600	.2180
600	.2171	500	.2372
500	.2278		
400	.2423		
300	.2594		
200	.2919		
100	.2855		
30	.3249		

Dec 24 1960		Jan 06 1961		Jan 09 1961		Jan 10 1961	
P	F_N	P	F_N	P	F_N	P	F_N
990	.0265	990	.0527	970	.0811	1010	.0101
900	.0554	900	.1051	900	.0839	1000	.0191
800	.0655	800	.1216	800	.1244	900	.0707
700	.0654	700	.1489	700	.1780	800	.1104
600	.0606	600	.1824	600	.1905	700	.1553
500	.0100	500	.2384	500	.2243	600	.1748
400	.0833	400	.2549	400	**.2456**	500	.1992
300	.1101	300	**.2849**	300	.2570	400	.1568
200	.0903	200	.2341	200	.2788	300	.1833
100	.1380	100	.2734	100	.2714	200	.1795
80	.1154	30	.2264	40	.2710	110	.1907

Green Bay:

Jan 12 1961		Jan 15 1961		Jan 16 1961	
P	F_N	P	F_N	P	F_N
990	.0714	990	.0524	990	.0664
900	.1161	900	.0313	900	.1132
800	.1468	800	.0971	800	.1406
700	.1641	700	.1497	700	.1634
600	.1987	600	.1729	600	.1659
500	.2409	500	.2114	500	.1865
400	.2632	400	.2301	400	.2308
300	.2685	300	.2601	300	.2577
200	.2883	200	.2696	200	.2495
100	.2729	100	.2624	100	.2562
30	.3009	30	.2715	20	.2879

Jan 12 1961		Jan 15 1961		Jan 16 1961	
P	F_N	P	F_N	P	F_N
950	.0401	980	.0376	970	.0721
900	.0472	900	.0925	900	.0733
800	.0651	800	.1067	800	.1056
700	.0745	700	.1232	700	.1172
600	.0783	600	.1272	600	.1292
500	.0863	500	.1265	500	.1466
400	.1226	400	.1478	400	.1668
300	.1481	300	.1703	300	.1886
200	.1486	290	.1740	200	.2021
100	.1787			100	.2111
30	.2117			20	.2302

International Falls:

Jan 17 1961		Jan 18 1961	
P	F_N	P	F_N
960	.0959	980	.0216
900	.1155	900	.0354
800	.1357	800	.1000
700	.1659	700	.1306
600	.1819	600	.1447
500	.1904	500	.1484
400	.1898	400	.1695
300	.2179	300	.1748
200	.2198	200	.1677
100	.2283	100	.1517
30	.2633	30	.1924

Dec 19 1960		Dec 20 1960		Dec 21 1960		Dec 22 1960	
P	F_N	P	F_N	P	F_N	P	F_N
960	.0347	980	.0349	960	.0406	970	.0405
900	.0944	900	.0231	900	.0765	900	.0664
800	.0748	800	.0858	800	.0646	800	.0774
700	.0946	700	.1071	700	.0990	700	.0803
600	.1029	600	.1187	600	.1182	600	.1093
500	.1211	500	.1337	500	.1359	500	.1254
400	.1446	400	.1480	400	.1439	400	.1365
300	.1544	300	.1465	300	.1370	300	.1541
200	.1651	200	.1558	200	.1430	200	.1596
110	.1685	100	.1359	100	.1249	100	.1045
		40	.1296	100	.1249	70	.1207

Dec 23 1960		Dec 24 1960		Jan 07 1961		Jan 09 1961		Jan 10 1961		Jan 11 1961		Jan 15 1961	
P	F_N	P	F_N	P	F_N	P	F_N	P	F_N	P	F_N	P	F_N
950	.0489	940	-.0109	980	.0464	950	.0507	970	.0577	990	.0617	960	.0604
900	.0748	900	.0057	900	.0962	900	.0461	900	.0746	900	.1009	900	.0586
800	.0845	800	.0000	800	.1164	800	.0779	800	.0990	800	.1209	800	.1002
700	.0975	700	.0360	700	.1344	700	.0902	700	.1234	700	.1567	700	.1283
600	.1022	600	.0426	600	.1445	600	.0759	600	.1301	600	.1839	600	.1319
500	.1163	500	.0243	500	.1752	500	.0669	500	.1429	500	.1979	500	.1499
400	.1327	400	.1328	400	.1754	400	.1240	400	.1535	400	.2122	400	.1518
300	.1607	300	.1493	300	.1834	300	.1534	300	.1815	300	.2243	300	.1459
200	.1264	200	.1512	200	.1840	200	.1710	200	.1691	200	.2048	200	.1623
100	.1340	100	.1358	100	.1598	100	.1456	100	.1587	100	.1805	100	.1612
40	.1181	50	.1294	70	.1340	30	.1379	30	.1419	30	.1871	30	.1573

Madison:

Jan 17 1961		Dec 22 1960		Jan 10 1961		Jan 11 1961	
P	F_N	P	F_N	P	F_N	P	F_N
950	.0622	1000	.0625	950	.0497	970	.0595
900	.0443	900	.0961	900	.0741	900	.0890
800	.0867	800	.1081	800	.0820	800	.1031
700	.1161	700	.1150	700	.1008	700	.1465
600	.1458	600	.1246	600	.1216	600	.1695
500	.1596	500	.1306	500	.1394	500	.1779
400	.1679	400	.1424	400	.1628	400	.2268
300	.1797	300	.1461	300	.1900	300	.2122
200	.1785	200	.1544	240	.2016	200	.2186
100	.1431	100	.1717			100	.2288
30	.2239	70	.1568			30	.2489

Miami:

Jan 06 1961	
P	F_N
990	.0796
900	.1146
800	.1361
700	.1489
600	.1635
500	.1877
400	.2203
300	.2492
200	.2638
100	.2664
30	.2941

Montgomery:

Jan 10 1961		Jan 15 1961		Dec 22 1960		Jan 06 1961		Jan 09 1961		Jan 15 1961	
P	F_N	P	F_N	P	F_N	P	F_N	P	F_N	P	F_N
1020	.0019	975	.0827	1020	.0095	1010	.0427	1020	.0953	980	.0154
1000	.0139	900	.1114	1000	.0270	1000	.0506	1000	.1211	900	.0115
900	.0203	800	.1352	900	.0295	900	.0525	900	.1153	800	.0170
800	.0681	700	.1493	800	.0319	800	.0786	800	.1315	700	.0360
700	.1231	600	.1823	700	.1058	700	.0973	700	.1608	600	.0387
600	.1852	500	.2068	600	.1541	600	.1031	600	.1954	500	.1068
500	.1849	400	.2370	500	.1690	500	.0865	500	.2127	400	.1308
450	.1920	300	.2703	400	.1733	400	.1070	400	.2255	300	.1409
		200	.2795	300	.1834	300	.1416	300	.2285	200	.1652
		100	.2873	200	.1967	200	.1567	200	.2279	100	.1874
		20	.2762	100	.2009	100	.1584	100	.2225	20	.2389
				40	.2382	20	.1909	30	.2374		

Peoria:

Jan 16 1961		Jan 18 1961		Dec 22 1960		Dec 23 1960		Jan 09 1961		Jan 10 1961	
P	F_N	P	F_N	P	F_N	P	F_N	P	F_N	P	F_N
990	.0711	990	.0742	960	.1040	980	.0143	1000	.0857	990	.0448
900	.1021	900	.1165	900	.1056	900	.0026	900	.0977	900	.0558
800	.1138	800	.1368	800	.1006	800	.0061	800	.1135	800	.0748
700	.1466	700	.1669	700	.1131	700	.0592	700	.1430	700	.0935
600	.1762	600	.1810	600	.1288	600	.1045	600	.1605	600	.0944
500	.1963	500	.2033	500	.1432	500	.1396	500	.1882	500	.1010
400	.2145	400	.2224	400	.1548	400	.1587	400	.1809	400	.0769
300	.2198	300	.2339	300	.1520	300	.1677	300	.2032	300	.1145
200	.2031	200	.2326	200	.1561	200	.1664	200	.2046	200	.1318
100	.1617	100	.2120	100	.1600	100	.1777	100	.2042	100	.1472
30	.2257	30	.2513	20	.1677	20	.1939	20	.2307	30	.1697

Jan 11 1961

P	F_N
1000	.0660
900	.1054
800	.1283
700	.1499
600	.1670
500	.1872
400	.2121
300	.2146
200	.2267
100	.2412
20	.2547

Jan 12 1961

P	F_N
990	.0611
900	.1150
800	.1342
700	.1567
600	.1780
500	.1900
400	.1939
300	.2102
200	.2096
100	.2108
20	.2321

Saint Martin:

Dec 25 1960

P	F_N
1010	.0601
1000	.0777
900	.1020
800	.1330
700	.1855
600	.2056
500	.2278
400	.2404
300	.2378
200	.2236
100	.2095
30	.2520

Dec 28 1960

P	F_N
1010	.0364
1000	.0236
900	-.0025
800	-.0026
700	-.0034
600	.1865
500	.2234
400	.2399
300	.2744
200	.2503
160	.2650

San Juan:

Dec 23 1960

P	F_N
1010	.0425
1000	.0512
900	.1049
800	.1210
700	.1881
600	.2201
500	.2329
400	.2574
300	.2702
200	.2729
100	.2767
30	.2882

Dec 25 1960

P	F_N
950	.0598
900	.0493
800	.0507
700	.2045
600	.2099
500	.2430
400	.2485
300	.2440
200	.1935
100	.1721
100	.1721

Jan 15 1961

P	F_N
1000	.0387
900	.0940
800	.1258
700	.1686
600	.2144
500	.2326
400	.2481
300	.2647
200	.2629
100	.2380
40	.2874

Washington:

Dec 19 1960

P	F_N
1010	.0797
1000	.0853
900	.1031
800	.1450
700	.1398
600	.1491
500	.1615
400	.1918
300	.2036
200	.2141
100	.2217
20	.2352

Dec 25 1960

P	F_N
1010	.0363
1000	.0376
900	.0781
800	.0815
700	.1167
600	.1507
500	.1709
400	.1881
300	.2084
200	.2102
100	.2379
30	.2440

Jan 06 1961

P	F_N
1000	.0496
900	.0995
800	.1364
700	.1524
600	.1906
500	.2095
400	.2203
300	.2234
200	.2268
100	.2311
10	.2734

Jan 09 1961

P	F_N
1020	.0869
1000	.1033
900	.1220
800	.1198
700	.1344
600	.1553
500	.1793
400	.2024
300	.2193
200	.2194
100	.2242
30	.2488

Jan 10 1961

P	F_N
1020	.0310
1000	.0868
900	.0896
800	.1017
700	.1239
600	.1447
500	.1580
400	.1819
300	.1992
200	.2037
100	.2190
20	.2379

Jan 11 1961

P	F_N
1010	.0427
1000	.0560
900	.1106
800	.1230
700	.1562
600	.1792
500	.1949
400	.2154
300	.2245
200	.2110
100	.2331
20	.2516

Jan 12 1961

P	F_N
1010	.0343
1000	.0543
900	.0751
800	.0907
700	.1205
600	.1167
500	.1414
470	.1530

Jan 16 1961

P	F_N
1000	.0276
900	.0198
800	.0212
700	.0236
600	.0932
500	.1624
400	.1668
300	.1775
200	.1852
100	.1980
10	.2582

Jan 17 1961

P	F_N
980	.0622
900	.0986
800	.1198
700	.1409
600	.1603
500	.1861
400	.2042
300	.2278
200	.2143
100	.2296
10	.2632

A Harmonic Analysis of TIROS IV Infrared Radiation Measurements

Phillip J. Smith
Lyle H. Horn
Donald R. Johnson

Abstract: The method of harmonic analysis is used to describe the infrared radiation field as measured by the channel 2 radiometer aboard TIROS IV during April, 1962.

The analysis, which is done along satellite orbits, includes a partitioning of the resulting spectra into time-averaged and perturbation components. The time-averaged portion of the spectrum clearly describes the mean latitudinal profile of the infrared radiation, while the perturbation portion describes the effect of longitudinal deviations from the mean profile and of transient weather systems. The study reveals that the longitudinally varying and transient features of the infrared radiation field are more significant than is usually thought.

1. Introduction

Although on a global scale the earth-atmosphere system emits to space an amount of infrared radiation equal to the amount of solar radiation it receives, there are considerable areal variations of these quantities within the system. Because of the earth's spherical shape, the variations of incoming solar radiation received at the earth's surface are almost entirely latitudinal. However, because of the complexity of the energy processes which occur within the atmosphere before this energy is returned to space, the major areal variations of outgoing infrared radiation are less easily described. Theoretical studies of the earth's heat budget have indicated that while the principal variation of

the mean infrared radiation is also latitudinal, this variation is considerably smaller than the latitudinal variation of solar radiation.

The advent of the artificial earth satellite has made possible the first direct measurements on a quasi-global scale of the infrared radiation emitted to space. Winston and Rao (1962) and Astling and Horn (1964) have prepared mean latitudinal profiles of infrared radiation from data obtained by TIROS II. Although the profiles, extending from 50° S to 50 °N, show a definite decrease of infrared radiation with increasing latitude, they also reveal two distinct maxima over the relatively clear and dry subtropics thus giving a somewhat M-shaped profile. Weinstein and Suomi (1961), using EXPLORER VII data, found significant variations of infrared radiation on a synoptic scale. The work of Corcoran and Horn (1964), using TIROS II data, revealed that the areal variations of infrared radiation are quite dependent on the scale of the synoptic features. Thus, areal variations of infrared radiation are influenced both by climatological and synoptic phenomena in the atmosphere.

In this paper the areal variations of infrared radiation are further investigated by using the technique of harmonic analysis to describe the scale of the infrared radiation patterns along the orbits of TIROS IV. In addition, the individual harmonic terms are partitioned into time-averaged and perturbation parts which are useful in determining the relative significance of the climatological and synoptic features of the infrared radiation field.

2. Data Preparation

The data used in this study consisted of 30 days (April, 1962) of TIROS IV, channel 2 observations. Channel 2 records infrared radiation in the 8-12 micron atmospheric window. Thus, the channel is relatively sensitive to changes in the height and amount of any existing clouds. For a more detailed discussion of the TIROS IV radiometer see the TIROS IV Radiation Data Catalogue and Users' Manual (1963).

Because of the inclination angle of the satellite orbit the area of available data is restricted to a latitudinal belt extending from about 50°N to 50°S. During each rotation of the satellite about its axis at least one sensor scans a portion of the earth (swath) and records a series of data values at various nadir angles. Data in this study were restricted to that obtained from every fifth rotational swath and that measured at nadir angles less than 26°. The second restriction was imposed to minimize the limb darkening errors. At nadir angles less than 26° the limb darkening error should be less than two percent (Wark, et al., 1962).

Each orbit was divided into 36, ten degree arcs, numbered consecutively beginning at the ascending node, i.e., the longitude at which the satellite crosses the equator in its northward journey. A mean radiation value was computed for each arc that contained one or more observations. To insure 36 equally spaced data points, mean radiation values for arcs lacking observations were computed by linear interpolation. If any orbit contained more than three consecutive arcs with no data points, the orbit was not used. Using these procedures 36 equally spaced radiation values were obtained for 139 usable orbits.

3. Harmonic Analysis Procedures

During each orbit of the satellite the infrared radiation varies as a function of the orbital arc (herein referred to as λ). Since each orbit represents one complete period, the method of harmonic analysis can be used to describe these variations.

Normally a harmonic analysis of a meteorological parameter is applied to data points spaced along a parallel of latitude; however, because of the incomplete data coverage provided by the satellite, it was necessary to use observations made along the satellite path. Since 36 equally spaced pieces of data are available along each orbit, the radiation field given by these 36 mean values can be completely described by a total of 18 harmonics. The basic harmonic equation, which describes the radiation as a function of arc, is

$$R(\lambda) = \frac{a_0}{2} + \sum_{n=1}^{18} (a_n \cos n\lambda + b_n \sin n\lambda) \qquad (1)$$

where

$$a_0 = \frac{1}{18} \sum_{i=0}^{35} R(\lambda_i),$$

$$a_n = \frac{1}{18} \sum_{i=0}^{35} R(\lambda_i) \cos(2\pi ni/36),$$

$$b_n = \frac{1}{18} \sum_{i=0}^{35} R(\lambda_i) \sin(2\pi ni/36),$$

where i is the orbital arc number and n is the harmonic ($n = 1 - 18$).

Using appropriate trigonometric identities (1) can be written as a sum of n cosine functions each with a phase ϕ_n and amplitude C_n,

$$R(\lambda) = C_0 + \sum_{n=1}^{18} C_n \cos(n\lambda - \phi_n) \qquad (2)$$

where

$C_0 = \frac{a_0}{2}$ is the mean radiation for the orbit,

$C_n = (a_n^2 + b_n^2)^{1/2}$ (for n = 1-17) and

$C_{18} = \sqrt{(a_{18}/2)^2}$

$\phi_n = \arctan \frac{b_n}{a_n}$

See Panofsky and Brier (1958) for details of the methods of harmonic analysis.

The results of the harmonic analysis of 139 orbits were used to obtain the total mean spectrum ($\overline{C_n^2}$, n = 1-18) of the variations of infrared radiation. The total mean spectrum was then partitioned into two components—a time-averaged part and a perturbation part. The partitioning was accomplished by computing mean values of a_n and b_n over all orbits and then expressing a_n and b_n for individual orbits as the sum of the mean value and a deviation from the mean. Thus C_n can be expressed as

$$C_n = [(\bar{a}_n + a'_n)^2 + (\bar{b}_n + b'_n)^2]^{1/2} \qquad (3)$$

where $\bar{a}_n$ and $\bar{b}_n$ are the mean values and a'_n and b'_n are the deviations. Squaring (3) and averaging over all orbits gives an expression for the total mean spectrum,

$$\overline{C_n^2} = \overline{(\bar{a}_n^2 + \bar{b}_n^2)} + \overline{[(a'_n)^2 + (b'_n)^2]} \qquad (4)$$

where $\overline{(\bar{a}_n^2 + \bar{b}_n^2)}$ represents the spectrum of the time-averaged field of radiation and $\overline{[(a'_n)^2 + (b'_n)^2]}$ the spectrum of the perturbation field of radiation.

In this study the relative importance of the time-averaged and perturbation portions of each harmonic was described by expressing them as percentages of the total mean variance for the 139 orbits. The total mean variance ($\overline{\sigma_T^2}$) for the 139 orbits is given by

$$\overline{\sigma_T^2} = \sum_{n=1}^{17} \frac{\overline{C_n^2}}{2} + \overline{C_{18}^2} \qquad (5)$$

The percentage of the total mean variance explained by the n^{th} harmonic is

$$\bar{V}_n = \overline{C_n^2} / 2\,\overline{\sigma_T^2} \quad \text{for } n = 1\text{-}17 \text{ and} \qquad (6)$$

$$\bar{V}_{18} = \overline{C_{18}^2} / \overline{\sigma_T^2} \quad \text{for } n = 18. \qquad (7)$$

The percentage of the total mean variance explained by the perturbation component is

$$(V_n)_p = \overline{([(a'_n)^2 + (b'_n)^2]} / \overline{C_n^2})\,(\bar{V}_n) \qquad (8)$$

and the time-averaged percentage is given by the difference between equation 6 (or 7) and 8.

4. Results

The results obtained using the procedures described above are presented in Figure 1, which portrays the percentage of the total mean variance of the infrared radiation field explained by each harmonic. The shaded portion represents the total variance explained by the perturbation component, and the unshaded portion the percentage explained by the time-averaged component.

Before discussing the results in more detail, it might be well to briefly consider the significance of the time-averaged and perturbation components of the spectrum. Since the satellite orbit precesses westward, the infrared radiation measurements for a given arc number i occur at varying longitudes. However, since the arcs are numbered beginning at the equator, the latitude associated with a given arc number does not vary. Because the latitudinal range of each arc remains constant, the mean radiation values obtained from 139 orbits essentially define a mean latitudinal profile. It is this profile which determines the characteristics of the time-averaged part of the total spectrum. On the other hand, the perturbation component of the spectrum is produced by deviations from the mean latitudinal profile. These deviations are due to longitudinal variations of the climatic features as well as to transient weather systems. If the ascending node of the satellite were fixed, the deviations would be produced entirely by transient weather systems; however, since the ascending node precesses, the deviations are in part

due to longitudinal variations in the climatic features (for example, longitudinal variations in the structure of the sub-tropical highs).

An examination of Figure 1 reveals basic differences in the characteristics of the time-averaged and perturbation spectra. The time-averaged spectrum is prominent only at the lower wave numbers. The prominence of the even harmonics (2, 4, 6) must be attributed to the nearly symmetrical distribution of the mean radiation field with respect to the earth's equator, while that of the odd harmonics (1, 5) results from certain asymmetric influences on this mean radiation field. In the case of the perturbation spectrum there are no pronounced harmonics, indicating the lack of systematic variations favoring any particular harmonic.

Certain of the individual harmonics can be interpreted as resulting from explainable features of the infrared radiation field. For example, the first harmonic, which explains 9.4 percent of the total variance, may be considered as resulting from larger infrared emissions under one-half of the orbit than the other. The time-averaged component of this harmonic (only 1.4 percent of the total variance) can be attributed to the asymmetry of the mean M-shaped north-south profile. This asymmetry is a result of greater infrared emissions in one-half of the orbit than the other. Possible physical causes include 1) greater emission from the summer hemisphere than the winter hemisphere (unlikely in this case since the data were for April), 2) a different emission from the water hemisphere (southern) than the land hemisphere (northern), or 3) a greater emission from the sunlit half of the orbit than the nighttime half.

The perturbation component, which accounts for most of the first harmonic variance (8.0 percent), is produced by variations from orbit to orbit of the locations of the high and low emission halves of each orbit. Of the features mentioned previously as contributing to the variance of the time-averaged component of the first harmonic, the effect of a water hemisphere versus a land hemisphere probably makes the most significant contribution to the perturbation component. This is because the location and amount of land over which the satellite passes varies more from orbit to orbit than do other features which might contribute to this harmonic. Also important is the influence of the sunlit verus the nighttime halves of the orbit. This is due to the sizeable change of the local time of the ascending node of the orbits over the 30 day period of this data. As noted above, the use of April data practically eliminates the effect of summer versus winter hemispheres; however, it should be kept in mind that this feature can produce high and low emission hemispheres and in other data samples may contribute significantly to this perturbation component.

FIGURE 1

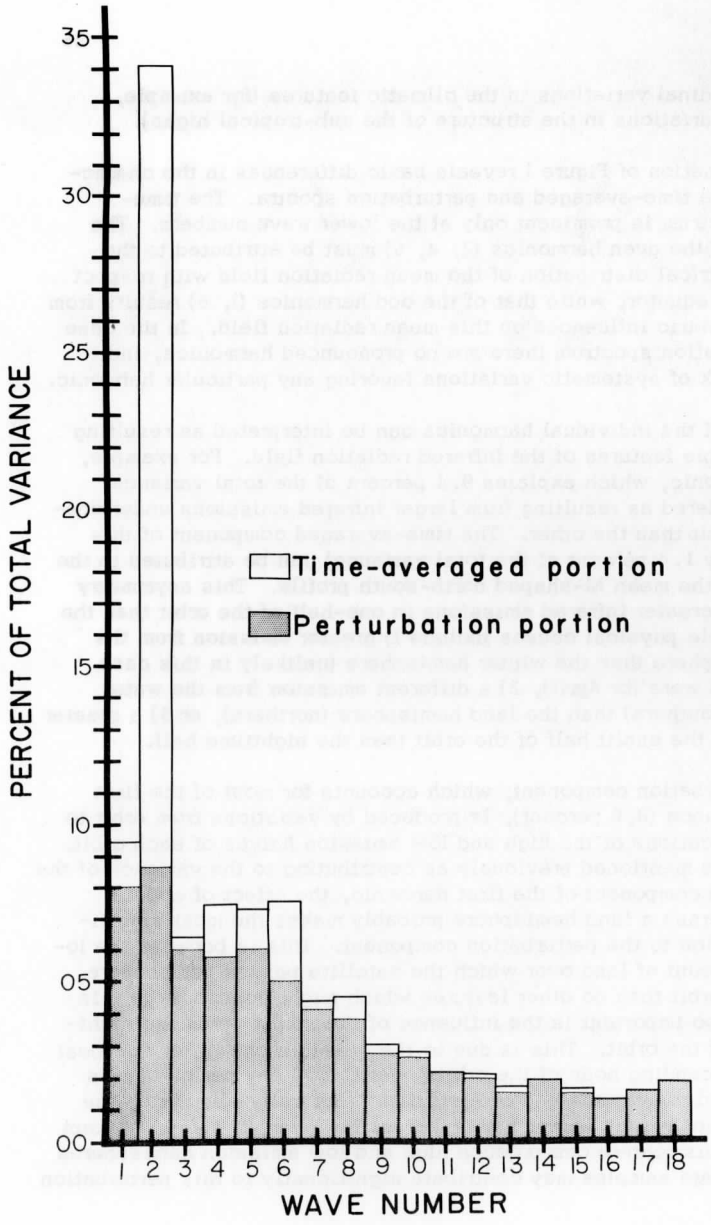

FIGURE 1. Normalized Time-Averaged and Perturbation Spectra of Tiros IV Infrared Measurements (April, 1962).

The second harmonic, which explains 34.1 percent of the total variance, is produced by differences in the infrared emission between low and high latitudes. As expected, the second harmonic indicates that these differences are the single most prominent feature of the earth's infrared radiation field. The time-averaged component (25.4 percent) is much larger than the perturbation component (8.7 percent), indicating that, with respect to this harmonic, the latitudinal variations are considerably larger and more constant with time than the longitudinal and temporal variations. Using an argument similar to that used in the first harmonic, the perturbation component is seen to result from factors such as the varying amounts of land versus ocean, cloudy versus clear areas, etc., seen by the satellite sensor as the ascending node precesses with time.

A further examination of Figure 1 reveals that of the remaining harmonics the fourth, fifth, and sixth are the largest. The fourth and sixth harmonics tend to emphasize the latitudinal symmetry of the infrared profile, and they are undoubtedly the result of the M-shape of the latitudinal profile. That is, as the satellite moves through its range of latitudes (50°N to 50°S and back), it senses maxima of radiation over the relatively clear subtropics and minima over the cloudier equatorial and higher latitude regions. The relatively prominent fifth harmonic is probably an asymmetric component needed to more completely describe the M-shaped feature of the mean meridional profile.

It is important to note that in this data sample the significant time-averaged spectra occur at the first, second, fourth, fifth, and sixth harmonics. Thus, it appears that the first six harmonics adequately describe the general characteristics of mean latitudinal profiles for this season.

Although the third, seventh, and eighth harmonics each explain about four to six percent of the total variance, they are produced almost entirely by perturbation effects. Likewise, the spectral components of all higher harmonics (i.e. greater than eight) are almost entirely produced by perturbation effects. As seen from an inspection of Figure 1 there are no particular scale sizes dominating the perturbation spectra. It seems likely that the perturbation part of the lower harmonics are probably produced by longitudinal variations in climatic features, while those of the higher harmonics are associated with transient weather systems.

It is important to note that of the total variance, 33.7 percent is explained by the time-averaged spectrum and 66.3 percent by the perturbation spectrum. The relative magnitude of these percentages indicates that the longitudinal and transient variations of the infrared emission are important in the consideration of atmospheric energetics.

5. Conclusions

The results of this study indicate that a number of significant characteristics of the earth's infrared radiation field can be described by harmonic analysis of data taken along satellite orbits. The following characteristics stand out:

1. The spectrum described through harmonic analysis can be successfully partitioned into time-averaged and perturbation parts. The time-averaged component is produced by the mean-latitudinal variations, and the perturbation component by longitudinally varying climatic features and transient weather systems.

2. The mean latitudinal profile of infrared radiation can be described by a relatively few number of harmonics. Because of the symmetry of the profile with respect to the equator, the even harmonics at low wave numbers, especially n = 2, tend to be dominant. Superimposed on the symmetrical profile are asymmetric properties which influence wave numbers one and five.

3. The relatively uniform decrease of the perturbation spectrum with increasing harmonics indicates that there are no preferred scale sizes in the variations described by the infrared perturbation field.

4. Since the variance due to the perturbation spectrum represents about 2/3 of the total variance, it appears that longitudinal and transient variations of infrared radiation are very important contributors to the energetics of the atmosphere.

The moderate success achieved by this rather primitive analysis of infrared radiation during one month suggests that this method may be useful to a study of seasonal changes in the infrared radiation patterns. It may also be valuable in making more detailed analyses of the infrared radiation data from individual orbits or groups of orbits.

6. References

Astling, E. G., and L. H. Horn, 1964: Some Geographical Variations of Terrestrial Radiation Measured by TIROS II. Journal of Atmospheric Sciences, 21, 30-34.

Corcoran, J., and L. H. Horn, 1964: The Role of Synoptic Scale Variations of Infrared Radiation in the Generation of Available Potential Energy. Annual Report, U. S. Weather Bureau Grant WBG-10, Project 4.

Panofsky, H. A., and G. W. Brier, 1958: Some Applications of Statistics to Meteorology, University Park, Pennsylvania, The Pennsylvania State University, 224 pp.

Staff Members, 1963: TIROS IV Radiation Data Catalogue and Users' Manual. Greenbelt, Md., Goddard Space Flight Center, 250 pp.

Wark, D. Q., G. Yamamoto, and J. H. Lienesch, 1962: Methods of Estimating Infrared Flux and Surface Temperature from Meteorological Satellites. Journal of Atmospheric Sciences, 19, 369-384.

Weinstein, M., and V. E. Suomi, 1961: Analysis of Satellite Infrared Radiation Measurements on a Synoptic Scale. Monthly Weather Review, 89, 419-428.

Winston, J. S., and P. K. Rao, 1962: Preliminary Study of Planetary-Scale Outgoing Long Wave Radiation as Derived from TIROS II Measurements. Monthly Weather Review, 90, 307-310.

The Role of Terrestrial Radiation in the Generation of Available Potential Energy

Donald R. Johnson

1. Introduction

Until very recently it has been customary to disregard the spatial distribution of heat sources and sinks within the atmosphere except for their latitudinal variation. Since the sun is the principle source of atmospheric energy, the emphasis on the latitudinal variation of heat sources and sinks within the atmosphere is largely a consequence of the solar-terrestrial geometry. Low latitudes receive the major portion of the solar radiation intercepted by the earth, while the terrestrial radiation losses occur relatively uniformly over the earth's surface. As a result, there is a meridional thermal contrast within the troposphere. This thermal contrast has been considered the sources of potential energy for the circulation of the atmosphere.

According to earlier theories of the general circulation, (Hadley 1735, Ferrel 1889, Rossby 1941) the potential energy was thought to be continually transformed into kinetic energy by the general rising of air at lower latitudes and the sinking of air at higher latitudes in the form of overturnings in the meridional planes. The action of the earth's rotation on the meridional cells produced the observed broad zonal currents, easterlies in the tropics and westerlies in the middle latitudes. The cyclones and anticyclones in the middle latitudes were regarded as turbulent elements in the frictional depletion of the kinetic energy of the zonal current. From energy considerations the meridional theory is consistent and complete. The source of potential energy is balanced by the sink of kinetic energy due to frictional dissipation. Implied but not stressed in this theory is the concept of differential heating due to the latitudinal variation of solar radiation.

The validity of the meridional circulation was seriously questioned when the additional measurements made by the expanded observational network established during World War II provided evidence which indicated that the middle latitude cyclones are not merely turbulent elements in the frictional dissipation of the westerlies, but rather are an essential mechanism in the redistribution of heat, momentum, and water vapor of the atmosphere. As more evidence was uncovered, it became evident that the anticyclones and cyclones are the sites of a substantial conversion of potential to kinetic energy, a concept which is diametrically opposed to their assigned role in the meridional theory. Because these secondary circulation features are an important site of the conversion process, increased attention has been given to the mechanisms which produce the necessary thermal variance within them. In this paper, the contribution of infrared cooling in the maintenance of the thermal contrast is examined. In particular, the vertical variation of this contribution to the secondary circulation is considered.

Apart from scientific inquiry "to know," there is an economic justification for the determination of the contribution of infrared cooling in atmospheric energetics. This need is primarily the result of recent scientific and engineering advances. One advance, the satellite, provides a means of determining the global coverage of heat sources and sinks within the atmosphere (Sabatini and Suomi, 1962; Smith, 1964) while the other, the giant digital computer, provides the means of utilizing the satellite observations in expanded numerical weather prediction models which incorporate atmospheric heat sources and sinks. Thus, the immediate justification of this study is to determine if the satellite observations of infrared cooling are an essential item of information in an energetically consistent numerical model where the heat sources and sinks of potential energy balance the frictional dissipation of kinetic energy. From energy considerations it seems that satellite observations of infrared cooling would be essential information if the magnitude or the range of the generation of potential energy is nearly equal to or greater than the magnitude or range of the frictional dissipation of kinetic energy.

Before designing a diagnostic model with sufficient resolution and reliability to estimate the vertical distribution of the generation of potential energy, let us review the development of the concepts which have lead to the recognition of the importance of the secondary circulation in the energetics of the general circulation. In 1933 Jeffreys showed that a transport of angular momentum by the cyclones and anticyclones is required to offset the earth-atmosphere's frictional coupling of the steady systematic surface circulation (i.e., the tropical easterlies and middle latitude westerlies). By the late 1940's Starr (1948) in an extension of Jeffrey's argument postulated that the asymmetry of the secondary

circulation features is the principle mechanism for transporting the necessary momentum. Rossby (1949) noting the observational inconsistencies of the meridional theory from his work with the jet stream stated, "The conversion of the potential energy supply of the atmosphere into motion may to a large extent occur in the local baroclinic circulation pattern. The kinetic energy thus gained must ultimately, through dispersion followed by mixing, accumulate in the jet stream zone." This statement was a marked revision of his earlier concepts of 1941 of the general circulation.

By the mid 1950's, Starr (1956, 1958), Phillips (1956), Kuo (1956a, 1956b), Lorenz (1955) and others had formulated and verified by observational evidence a new concept of the general circulation. In their concept, potential and latent energy are continually created in the low latitudes by solar energy. The poleward advection of heat, momentum, energy, and water vapor is performed by the broad scale horizontal secondary circulation features. Through the action of the horizontal eddies, an east-west thermal contrast is created. This east-west thermal contrast is a store of potential energy which is available for conversion to kinetic energy. The conversion process occurs in the east-west overturnings associated with baroclinic disturbances in the westerlies of middle latitudes.

In 1955 Lorenz produced a mathematical model for the general circulation energetics by expanding Margules' (1903) concept of the separation of total potential energy into a portion not available for conversion into kinetic energy and a portion available for conversion. Lorenz defines available potential energy as the difference between the total potential energy of an arbitrary atmosphere and that which would exist after adiabatic redistribution of the mass to a state of stable, horizontal density stratification. The available potential energy, which he partitions into zonal and eddy portions, is created by the differential heating or cooling of the atmosphere. The zonal portion is determined by the strength of the north-south thermal variance of the zonal mean temperatures and is principally produced by the latitudinal covariance of zonal means of diabatic heating and temperatures. The eddy portion is a measure of the east-west thermal variance and is principally produced either indirectly by the action of the eddies on the zonal available potential energy or directly by the east-west covariance of diabatic heating and temperature.

An implication of modern theory is that differential cooling may be equally as important as differential heating in the generation of available potential energy. Hence, the differential cooling of the atmosphere by long wave radiation, although always a sink of total potential energy, may be either a source or sink of available potential energy. On a

latitudinal scale the differential cooling by infrared radiation destroys zonal available potential energy. However, within the smaller scales of the secondary circulation the infrared cooling may generate eddy available potential energy. For example, the warm cloudy regions of some cyclones lose less heat than cool clear regions of anticyclones, generating eddy available potential energy at this scale. Therefore, it seems important to consider the role that organized heating and temperature fields of the secondary circulation play in the generation of eddy available potential energy for the atmosphere's circulation.

In this paper both the vertical and horizontal variations of cooling by infrared radiation are examined. Emphasis is placed on the role of the vertical variation of infrared cooling in the generation of eddy available potential energy and the design of a diagnostic model with sufficient resolution and reliability to estimate this quantity. Data from radiometersonde flights are used to obtain continuous profiles of temperature and net radiation. A polynomial technique is developed which permits the vertical integration of continuous profiles of infrared cooling and temperature. These integrals of the covariance of temperature and heating fields are used to estimate the height variation of the generation of eddy available potential energy within the atmosphere's secondary circulation. In the next section the physical model which is used in obtaining these estimates is developed.

2. Development and discussion of the physical model

The set of energy equations developed by Lorenz (1955) provides the framework upon which the physical model used in this study is based. In this chapter the essential equations are presented and their physical significance discussed with emphasis on the role of infrared cooling in the generation of eddy available potential energy.

According to Lorenz, the average available potential energy per unit area of the earth's surface is

$$A = \frac{1}{2} \int_0^{\bar{\bar{p}}_0} \frac{\bar{\bar{T}}}{(\Gamma_d - \bar{\bar{\Gamma}})} \left(\frac{\overline{\overline{T''}}}{\bar{\bar{T}}}\right)^2 dp \qquad (2.1)$$

where Γ_d is the dry adiabatic lapse rate, $\bar{\bar{\Gamma}}$ is the mean lapse rate of the earth's horizontally averaged temperature field, $\bar{\bar{T}}$, and T'' is the deviation of temperature from its horizontal average. The pressure, p, is the independent variable serving as the vertical coordinate with boundary values $p = 0$ at the top of the atmosphere and $p = p_0$ at the earth's

surface. In general in this paper the operator $(\overline{\overline{\overline{\ }}})$ represents an average taken with respect to the horizontal projection of the surface of the independent variable, while (") represents a deviation from the horizontal average. Thus, the available potential energy is a vertically weighted measure of the horizontal variance of the temperature field. In Lorenz' development, the energy equations are based on integration over the entire mass of the atmosphere.

According to Lorenz the time rate of change of available potential energy is

$$\frac{\partial A}{\partial t} = - C + G \tag{2.2}$$

where C, the conversion of available potential energy, is

$$C = - \frac{R}{g} \int_0^{\overline{\overline{p_0}}} \frac{1}{p} \overline{\overline{\overline{T''\omega}}}\, dp \tag{2.3}$$

and G, the generation of available potential energy, is

$$G = \frac{1}{g} \int_0^{\overline{\overline{p_0}}} \frac{\Gamma_d}{(\Gamma_d - \overline{\overline{\Gamma}})\overline{\overline{T}}} \overline{\overline{\overline{T''Q''}}}\, dp \tag{2.4}$$

where Q is the rate of addition of heat per unit mass, and $\omega = \frac{dp}{dt}$ is the individual pressure change which is regarded as a measure of the vertical velocity in the free atmosphere.

The average horizontal kinetic energy, K, per unit area of the earth's surface is

$$K = \frac{1}{2g} \int_0^{\overline{\overline{p_0}}} \overline{\overline{\overline{\vec{V}_h \cdot \vec{V}_h}}}\, dp \tag{2.5}$$

where g is the acceleration of gravity and $\vec{V}_h$ is the horizontal wind velocity.

The time rate of change of kinetic energy is

$$\frac{\partial K}{\partial t} = C - D \tag{2.6}$$

where D, the dissipation of kinetic energy by frictional dissipation, is

$$D = - \frac{1}{g} \int_0^{\overline{\overline{p_0}}} \vec{V} \cdot \vec{F}\, dp \tag{2.7}$$

and $\vec{F}$ is the horizontal force of friction per unit mass.

The first term of the right hand side of equations (2.2) and (2.6) represents the conversion between available potential energy and kinetic energy. A positive contribution to this integral is given by warm air rising and cold air sinking, a process which converts available potential energy to kinetic energy. The generation, G, of available potential energy is positive when, relative to horizontal averages, the warmer air is heated and the colder air is cooled, thus, increasing the horizontal variance of temperature. The frictional dissipation integral, D, of equation (2.7) is regarded by Lorenz as the unique sink for kinetic energy. Concerning this integral Lorenz states, "The only non-adiabatic process which directly alters kinetic energy is friction which ordinarily generates internal energy while it destroys kinetic energy." Physically, this statement is true; however, by adding equations (2.2) and (2.6)

$$\frac{\partial}{\partial t}(A + K) = G - D \tag{2.8}$$

it is evident that the sum of the time rate of change of the available potential energy and kinetic energy is equal to the sources and sinks of both forms of energy. Thus in an open system differential heating may serve as a source or sink of horizontal kinetic energy, while the available potential energy for the atmosphere is a constant. Physically, this condition exists when the rate of decrease of the horizontal thermal variance by diabatic processes is exactly balanced by the increase of the thermal variance by the action of the vertical velocity field on the temperature field (mathematically, the conversion integral is equal to both the generation integral and the time rate of change of kinetic energy.) Therefore, both the kinetic energy and available potential energy implicitly depend on the generation integral, although in Lorenz' equation (2.6) the kinetic energy appears to be independent of the generation integral. One notes, however, from equation (2.8) that positive (negative) generation causes an increase (decrease) in the sum of the two forms of energy.

Within the troposphere and lower stratosphere the generation of available potential energy can be attributed to five physical processes causing differential heating: (1) direct absorption by solar radiation; (2) emission of long wave radiation; (3) release of latent heat; (4) sensible heat transfer through the earth-atmosphere interface; and (5) frictional dissipation. Thus, the generation integral can be divided into five linear components corresponding to each physical process,

$$G = \sum_{i=1}^{5} G_i = \sum_{i=1}^{5} \frac{1}{g} \int_0^{\overline{\overline{p_0}}} \frac{\Gamma_d}{(\Gamma_d - \overline{\overline{\Gamma}})\,\overline{\overline{T}}} \overline{\overline{T''Q_i''}}\, dp \tag{2.9}$$

where the index, i, represents a physical process, and Q_i'' is the deviation of the rate of heat addition by the i-th component from its horizontal mean, Q_i. Furthermore, to separate the contribution of the systematic zonal heating field from the organized heating fields of other scales of atmospheric disturbances, the total generation integral is divided into a zonal component (after Lorenz)

$$G_Z = \sum_{i=1}^{5} G_{Z_i} = \sum_{i=1}^{5} \frac{1}{g} \int_0^{\overline{\overline{p_0}}} \frac{\Gamma_d}{(\Gamma_d - \overline{\overline{\Gamma}})\,\overline{\overline{T}}} [T]''[Q]_i'' \, dp \qquad (2.10)$$

and an eddy component

$$G_E = \sum_{i=1}^{5} G_{E_i} = \sum_{i=1}^{5} \frac{1}{g} \int_0^{\overline{\overline{p_0}}} \frac{\Gamma_d}{(\Gamma_d - \overline{\overline{\Gamma}})\,\overline{\overline{T}}} \overline{\overline{T^* Q_i^*}} \, dp \qquad (2.11)$$

The brackets represent a zonal mean on a pressure surface and the asterisk a departure from a zonal mean. As previously noted, the zonal generation is determined by the covariance of the temperature and heating deviations of the zonal means from the horizontal means, while the eddy generation is determined by the covariance of the temperature and heating deviations from the zonal means. The zonal and eddy generation can be further divided into a stationary and transient contribution by expressing the areal deviations as

$$T''_{(x,\,y,\,p,\,t)} = [\overline{T}]''_{(y,\,p)} + ([T]')''_{(y,\,p,\,t)} + \overline{T}^*_{(x,\,y,\,p)} + (T')^*_{(x,\,y,\,p,\,t)} \qquad (2.12)$$

and

$$Q''_{(x,\,y,\,p,\,t)} = [\overline{Q}]''_{(y,\,p)} + ([Q]')''_{(y,\,p,\,t)} + \overline{Q}^*_{(x,\,y,\,p)} + (Q')^*_{(x,\,y,\,p,\,t)} \qquad (2.13)$$

where the operator (—) represents a time average and a single prime (') the deviation from a time average. The first and third terms on the right hand side of (2.12) and (2.13) are the time averaged stationary deviations while the second and fourth are the transient deviations. The partitioning is similar to that used by Murakami (1960). It can be shown that substitution of equations (2.12) and (2.13) into (2.9) gives the following expression for the total time average generation

$$\overline{G} = \sum_{i=1}^{5} \overline{G}_i = \sum_{i=1}^{5} (G_{ZS_i} + G_{ZT_i} + G_{ES_i} + G_{ET_i}) \qquad (2.14)$$

where the order of integration for space and time are interchanged. Thus the total averaged generation, G, is divided into four scales and five

components of diabatic heating. The scales of atmospheric circulation are defined as follows:

$$G_{ZS} = \frac{1}{g}\int_0^{\overline{\overline{p_0}}} \frac{\Gamma_d}{(\Gamma_d - \overline{\overline{\Gamma}})\,\overline{\overline{T}}}\,\overline{\overline{[\overline{T}]''[\overline{Q}]''}}\,dp \qquad (2.15)$$

where G_{ZS} is the generation at the stationary zonal scale.

$$G_{ZT} = \frac{1}{g}\int_0^{\overline{\overline{p_0}}} \frac{\Gamma_d}{(\Gamma_d - \overline{\overline{\Gamma}})\,\overline{\overline{T}}}\,\overline{\overline{([T]')''([Q]')''}}\,dp \qquad (2.16)$$

where G_{ZT} is the generation at the transient zonal scale associated with an expansion or contraction of the westerlies.

$$G_{ES} = \frac{1}{g}\int_0^{\overline{\overline{p_0}}} \frac{\Gamma_d}{(\Gamma_d - \overline{\overline{\Gamma}})\,\overline{\overline{T}}}\,\overline{\overline{T^*\,\overline{Q}^*}}\,dp \qquad (2.17)$$

where G_{ES} is the generation at the stationary or standing eddy scale. It is associated with both the long planetary waves and continents or oceans, when the time interval of averaging is a few days. For longer time intervals, this term must be identified with stationary features due to the continents and oceans since even the long planetary waves are quasi-transient features of the atmospheric circulation.

$$G_{ET} = \frac{1}{g}\int_0^{\overline{\overline{p_0}}} \frac{\Gamma_d}{(\Gamma_d - \overline{\overline{\Gamma}})\,\overline{\overline{T}}}\,\overline{\overline{(T')^*(Q')^*}}\,dp \qquad (2.18)$$

where G_{ET} is the generation by the transient eddies primarily associated with surface cyclones, anti-cyclones or upper air traveling waves.

This division of the time averaged generation into four scales of atmospheric circulation defines one additional scale, the transient zonal circulation, which was not included by Murakami (1960). It may be an important scale in energy studies of the general circulation since the weather patterns and the distribution of kinetic and potential energy associated with an expanded or contracted zonal scale are quite different.

The total contributions to the generation by the five diabatic components at the various scales is still an unresolved problem. With regard to the overall generation at the eddy scale, Lorenz (1955) states

that "presumably it is negative, in view of the probable warming of cold air masses and cooling of warm air masses in middle latitudes, but the possible preference of warm longitudes for the release of latent heat may suppress this negative value." Although this postulate may be true, it is exceedingly difficult to verify or reject. In other diagnostic studies there are results which indicate that several of the diabatic contributions may be important in generating eddy available potential energy while at least one, the eddy conduction component, destroys available potential energy.

Wiin Nielsen and Brown (1962) estimated that the eddy generation by all physical processes is -3.5 watts/m^2, apparently confirming Lorenz' postulate. In their study, which was based on a quasi-geostrophic model, the principal diabatic component destroying available potential energy was the sensible heat transfer by eddy conduction by the warm ocean currents to the cold air flowing eastward from the Asian and North American continents (See Figure 2 of their paper). On the other hand, Clapp (1961) obtained an estimate of +0.26 watts/m^2 for the time averaged semi-permanent circulation in winter.

In studies of the individual components, the positive generation by latent heat seems to have been well established by Palmen (1960), Clapp and Winninghoff (1963), and Murakami (1960). Palmen estimated that an average of 53 watts/m^2 of kinetic energy was created for 1/35 of the polar cap north of latitude 30°N by the latent heat released in an intense extra-tropical cyclone (Hazel). From this estimate he stated that three extra-tropical disturbances of the same intensity as "Hazel" would suffice to produce the necessary kinetic energy to offset a frictional dissipation estimate of 5 watts/m^2 for the polar cap. Using data from one station (Washington, D.C.) Clapp (1963) estimated an eddy generation of 1.8 watts/m^2, the principle eddy generation component being the differential heating by the release of latent heat by thunderstorms. Since the summer thunderstorms at Washington, D.C., are usually identified with transient disturbances, Clapp's estimate does not contradict Murakami's (1960) estimate of 0.47 watts/m^2 for the eddy generation by the latent heat release in the stationary disturbances. One would expect transient disturbances to be more efficient than the stationary features in generating available potential energy, since the largest positive vertical velocities and greatest amounts of water vapor are found within the warm air of the transient scales. Thus, the large positive contribution due to the latent heat component provides support to Lorenz' qualifying statement that the release of latent heat might suppress the negative generation.

Another diabatic component that may generate eddy available potential energy is the direct absorption of solar energy. Korb and Moller (1961) found that the direct solar absorption in warm, moist air may be twice as great as in clear, dry air. The presence of clouds in the warm, moist air increases the direct solar absorption. Since the greater heating occurs in the warm air, a positive generation results.

Merely from physical considerations, the component of differential heating by frictional dissipation can be dismissed as a negligible contribution. The total heating by frictional dissipation within the planetary boundary layer may reach several degrees per day; however, there does not appear to be any systematic effect leading to greater frictional heating in the warm air than in the cold air or vice versa.

Generation estimates of the remaining diabatic component, the cooling by infrared radiation, have been established by the use of satellite measurements. Suomi and Shen (1963) obtained a mean generation of +0.583 watts/m^2 for 12 selected days of Explorer VII data. In a later analysis of 30 days of Explorer VII data, Shen's mean estimate (1963) was 0.260 watts/m^2. In a study of the generation associated with 500 mb waves using Tiros II data, Corcoran and Horn (1964) obtained a mean estimate of 0.055 watts/m^2. Although the latter two generation estimates are small, both studies indicated that at the smaller scale eddies, the generation is approximately 0.2 watts/m^2, while the largest scales destroy available potential energy, approximately -0.1 watts/m^2. Thus, two tentative conclusions are: (1) cooling by radiation is not a large sink of eddy available potential energy, and (2) generation of available potential energy by the infrared component is a function of scale size.

The positive generation within these smaller scale transient disturbances is undoubtedly the result of the distribution of clouds. Extensive cloudiness in the warm air, including the broad expanse of cirrus in the high troposphere ahead of the approaching wave, appreciably reduces the cooling by the infrared component. Within the cold, clear descending air of the disturbance the infrared radiation stream to space is a maximum. Thus, beneath the clouds, the warm air will cool less than will the cold air at corresponding heights. The result is an infrared contribution toward the positive generation of eddy available potential energy. Above the level of the clouds the horizontal differential heating fields are reversed (i.e., the warm air above the level of the clouds cools more than the cold air at equivalent heights). At these greater heights the eddy generation is then negative. Consequently, the vertical variation of the generation of available potential energy by the infrared component may be an important element within a transient disturbance. In the next two chapters, two polynomial techniques are developed and

applied to radiometersonde data so that the vertical variation of the covariance of temperature and infrared cooling may be investigated and the generation by the infrared component estimated.

3. Procedures for estimating temperature and cooling profiles from radiometersonde data

As the result of instrumental developments during the last decade, measurements of the vertical distribution of the flux of infrared radiation have become feasible. Concurrently with the radiation measurements by Brewer and Houghton (1956), Pohl (1956), and Gergen (1957), the Suomi-Kuhn (1958) balloon-borne net radiometersonde was developed at the University of Wisconsin to provide measurements of the upward, downward, and net flux of infrared radiation. Radiometersonde flights conducted during the last five years have provided data for research into the nature of the infrared cooling of the atmosphere.

From this five year period, the only data sample providing adequate coverage to study the generation of available potential energy consists of the 198 individual night time flights made during December, 1960 and January, 1961. These flights were conducted by thirteen radiometersonde stations over the eastern half of the United States and the Caribbean. The radiometersonde flights provided discrete observations of temperature, net radiation, and pressure at approximately 600-800 foot intervals of height. Only nocturnal flights were made in order to avoid direct solar heating of the radiometersonde's infrared sensors. In Table I, the stations, their locations and an identifying zonal ring are given, while Table II presents the date of each flight. Although there are missing observations in the time series for each station, this is not a serious defect since only time averaged estimates will be considered in this study.

To apply the radiometersonde data to the problem at hand, a number of difficulties had to be overcome.* The first was to obtain accurate profiles of temperature and cooling. The second was to develop a method of integration using a polynomial description for the temperature and cooling profiles. Previous generation studies employed satellite infrared radiation measurements. As a result, the generation integral was evaluated by assuming that a vertical mean value for the temperature and the cooling profiles was representative of their vertical distribution within

*To successfully pursue the investigation, it was necessary to apply a number of statistical techniques. Because some of the techniques require lengthy proofs, they were developed as five separate appendices in the original thesis (Johnson, 1965).

TABLE 1

RADIOMETERSONDE STATIONS

Index No.	Station	Location
	Zone I (38.5° - 51.5°N)	
72405	Washington, D.C.	38°- 51"N - 77°-02"W
72532	Peoria, Illinois	40°-40"N - 89°-41"W
72641	Madison, Wisconsin	43°-08"N - 89°-24"W
72645	Green Bay, Wisconsin	44°-29"N - 88°-08"W
72747	International Falls, Minnesota	48°-34"N - 93°-26"W
	Zone II (25.5° - 38.5°N)	
72202	Miami, Florida	25°-49"N - 80°-17"W
72226	Montgomery, Alabama	32°-18"N - 86°-24"W
72363	Amarillo, Texas	35°-14"N - 101°-42"W
	Zone III (12.5° - 25.5°N)	
78383	Grand Cayman, Cayman Islands	19°-15"N - 85°-25"W
78525	San Juan, Puerto Rico	18°-28"N - 66°-07"W
78866	Phillipsburg, St. Maarten	18°-02"N - 63°06"W
78967	Chagmaramus Bay, Trinidad	10°-11"N - 61°-37"W
78988	Willemstad, Curacao	12°-11"N - 68°-59"W

TABLE 2

OBSERVATIONAL DATES OF RADIOMETERSONDE FLIGHTS (0000Z)

	Station	December 1960									January 1961														Total
		20	21	22	23	24	25	26	27	28	7	8	9	10	11	12	13	14	15	16	17	18	19	20	21	
Zone I	405	X	X	X	X	X		X	X	X	X	X	X	X	X	X	X	X	X		X	X				19
	532	X		X	X	X	X				X	X	X	X	X	X	X	X	X		X	X				16
	641				X					X			X		X	X										6
	645																X	X	X	X	X	X	X	X	X	9
	747	X	X	X	X	X	X			X	X	X	X	X	X	X	X	X	X	X	X	X				19
Zone II	202									X	X	X	X		X	X	X	X		X						9
	226		X	X	X			X		X	X	X	X	X	X	X		X	X	X	X	X	X			17
	363			X	X	X	X	X			X	X	X	X	X			X	X	X	X	X	X			16
Zone III	383	X	X	X	X	X	X	X	X	X	X	X	X	X	X	X	X	X	X	X	X					20
	525		X	X	X	X	X	X	X		X	X	X	X	X			X	X	X	X	X	X	X		19
	866	X	X		X	X	X	X	X	X		X	X	X	X	X	X	X	X	X						17
	967			X	X	X		X	X	X					X	X			X	X	X					11
	988	X	X	X	X	X	X	X	X	X		X	X	X	X	X	X	X	X	X	X	X				20

an entire atmospheric unit column, thus ignoring the height dependency of both variables. Since a strong correlation exists between both the temperature and the heating fields with height (Clapp and Winninghoff, 1963), it is quite probable that the correlation between temperature and atmospheric cooling will also vary as a function of height. To avoid the use of mean values, a diagnostic model was designed in which the generation of available potential energy is evaluated by dividing the atmosphere into seven levels. Within these seven levels, the temperature and infrared cooling profiles are described by approximating polynomials and the correlation between the two fields is then integrated.

As previously noted, the data used are air temperature and net radiation observations, which are the dependent variables, and the pressure observation, which is the independent variable. Since these measurements involve several sources of error, one must regard each observation as being composed of a true function on which is superimposed an instrumental error component. Thus, let

$$y_i = \eta_i + \epsilon_i \tag{3.1}$$

where y_i is the i-th observation of the true function η_i, and ϵ_i is the instrumental error component. If the observations are biased, then the expected value of the instrumental error is

$$E(\epsilon_i) = \lambda_i \tag{3.2}$$

and

$$y_i = \eta_i + \lambda_i + \epsilon_{R_i} \tag{3.3}$$

where λ_i is the bias component and ϵ_{R_i} is the random error component with expectation zero. It is the random error component of the observations of net radiation which causes the computational problem, since the estimation of atmospheric cooling from the observation of net radiation is obtained from second differences. The air temperature and pressure observations are used directly and do not present any computational difficulties. Since pressure is used as an independent variable, it is regarded as an exact measurement, allowing cooling rates to be efficiently estimated. The effect of this assumption is discussed at the end of this chapter. Because the estimation of temperature profiles follows directly from the techniques and criteria developed in solving the infrared cooling problem, the method of estimating temperature profiles is discussed after the procedure for estimating vertical profiles of cooling is developed.

The observations of net radiation are a linear combination of two temperature measurements by a top and a bottom sensor of the radiometer

(Suomi, Staley, and Kuhn, 1958). In Appendix I of the original thesis (Johnson, 1965), the validity of regarding the net radiation observation as being a measurement of a smooth true function with a superimposed random error component is established. In this development the mean and the variance of the net radiation flux are equated to the moments of the random error distribution of the observed temperatures (i.e., the top and bottom sensors of the radiometer). Thus, the net radiative flux is

$$R_{n_i} = \gamma_{n_i} + \lambda_{n_i} + \epsilon_{n_{R_i}} \tag{3.4}$$

where γ_{n_i} is a linear combination of the two true temperature functions, λ_{n_i} is a linear combination of all bias error terms, and $\epsilon_{n_{R_i}}$ is a linear combination of the random error components.

The local cooling or warming of an atmospheric layer due to the divergence of infrared radiation is given by

$$Q = g \frac{\partial R_n}{\partial p} \tag{3.5}$$

where Q is the rate of addition of heat per unit mass. Substitution of (3.4) into (3.5) yields

$$Q = g \frac{\partial}{\partial p} (\gamma_n + \lambda_n + \epsilon_{n_R}) \tag{3.6}$$

Since one wishes to estimate the vertical derivative, $\frac{\partial}{\partial p} \gamma_n$, but is possibly forced to estimate $\frac{\partial}{\partial p} (\gamma_n + \lambda_n)$, a biased estimate, the optimum estimates of the derivative will be provided by filtering the random component before any form of differentiation is attempted (Hildebrand, 1956).

Since the data contain a random error component, "least squares" approximating polynomials rather than an exact polynomial description were selected for the filtering. With an approximating polynomial the estimating function is free to determine a new point at each level of the independent variable, thus avoiding the consequences of an exact polynomial fit (i.e., the determination of an estimating function which passes through each observation but oscillates about the true function). Furthermore, any attempt to differentiate an exact polynomial description of net radiation to determine cooling by equation (3.6) would only amplify the oscillations due to the random error component and would prevent any form of convergence to the true profile, $\partial \gamma_n / \partial p$.

The approximating polynomial for the observations of net radiation is

$$\hat{R}_{n_i} = B_0 + B_1 x_i + \cdots B_k x_i^k \tag{3.7}$$

where x_i, the scale independent variable of pressure for each atmospheric layer, is

$$x_i = \frac{p_i - \frac{1}{2}(p_{s+1} + p_s)}{\frac{1}{2}(p_{s+1} - p_s)} \qquad \begin{matrix} p_s \geq p \geq p_{s+1} \\ -1 \leq \chi \leq +1 \end{matrix} \tag{3.8}$$

$$x_i = \frac{p_i - C_{1s}}{C_{2s}} \tag{3.9}$$

where C_{1s} is the mean value and C_{2s} is one-half the range of the pressure interval, p_s to p_{s+1}. The independent variable was scaled to range between -1 and +1 for the atmospheric layer (Plackett, 1960). In matrix notation

$$\hat{\underset{\sim}{R}}_n = \underset{\sim}{X}\,\underset{\sim}{B} \tag{3.10}$$

where $\hat{\underset{\sim}{R}}_n$ is the $(n \times 1)$ vector of predicted values of net radiation for the n observations of net radiation within each atmospheric layer, $\underset{\sim}{X}$ is the $n \times (k+1)$ design matrix of the independent variable, and $\underset{\sim}{B}$ is the $(k+1) \times 1$ vector of polynomial coefficients. The solution to the polynomial coefficients is

$$\underset{\sim}{B} = [\underset{\sim}{X}^T \underset{\sim}{X}]^{-1} \underset{\sim}{X}^T \underset{\sim}{R}_n \tag{3.11}$$

where $\underset{\sim}{R}_n$ is the $(n \times 1)$ vector of observations for each atmospheric layer. The relation of the predicted values to the observed values is given by substituting equation (3.11) into (3.10) yielding

$$\hat{\underset{\sim}{R}}_n = \underset{\sim}{X}[\underset{\sim}{X}^T \underset{\sim}{X}]^{-1} \underset{\sim}{X}^T \underset{\sim}{R}_n \tag{3.12}$$

Thus, the predicted values for the net radiation are a linear transformation of the observations.

If the approximating polynomial is unbiased, so that

$$E(\hat{\underset{\sim}{R}}_n) = \underset{\sim}{X}[\underset{\sim}{X}^T \underset{\sim}{X}]^{-1} \underset{\sim}{X}^T E(\underset{\sim}{R}_n) \tag{3.13}$$

then, substitution of the expected value of R_n from equation (3.4) yields

$$E(\underset{\sim}{\hat{R}}_n) = \underset{\sim}{X}[\underset{\sim}{X}^T\underset{\sim}{X}]^{-1}\,\underset{\sim}{X}^T(\underset{\sim}{\gamma}_n + \underset{\sim}{\lambda}_n) \tag{3.14}$$

From this equation it is evident that even though the approximating polynomial is an unbiased estimate of the observation, R_{n_i}, the predicted values, $\hat{R}_{n_i}$, are really estimating the function $(\gamma_{n_i} + \lambda_{n_i})$. Thus, if the approximating polynomial is unbiased, and since it is a linear transformation of the observations, one may use Gauss' Theorem to state, "of all the possible linear transformations, the estimates of R_n are minimum variance estimates for net radiative flux, $(\gamma_{n_i} + \lambda_{n_i})$" (Box, 1962). It is logical to extend the argument, primarily because of this theorem, and state that a net radiative flux estimate by an unbiased approximating polynomial is the best linear estimate of the true continuous function, $(\gamma_n + \lambda_n)$.

Before proceeding further, let us distinguish between the two bias errors in order to establish their effect on the estimation of the cooling profiles. The first, the bias error of measurement, λ_{n_i}, of equation (3.4) is a combination of the bias errors in the temperature measurements and the neglect of high order terms in defining a set of equations for the radiometersonde (Suomi, Staley and Kuhn, 1958). The second, the bias error due to "lack of fit" of the approximating polynomials to the observations within the atmospheric layer, is from either the improper selection of an r-th degree polynomial for the unbiased k-th degree polynomial, or from the choice of an atmospheric layer so large that the functional form of R_n cannot be adequately represented by an approximating polynomial. Since the approximating polynomial attempts to fit $(\gamma_n + \lambda_n)$, the expected value of R_n with a bias term due to lack of fit is

$$E(\hat{R}_{n_i}) = (\gamma_{n_i} + \lambda_{n_i}) + \lambda_{B_i} \tag{3.15}$$

where λ_{B_i} is the systematic bias error from the lack of fit. Remembering that the relation between the true function of cooling, χ, and the vertical distribution of the true net radiative flux is

$$\chi = g\,\frac{\partial \gamma_n}{\partial p} \tag{3.16}$$

the substitution of the expected value of R_n from (3.16) for R_n of (3.5) yields

$$E(Q) = g\left(\frac{\partial \gamma_n}{\partial p} + \frac{\partial \lambda_n}{\partial p} + \frac{\partial \lambda_B}{\partial p}\right) \tag{3.17}$$

Thus, it is clear that both bias errors will cause errors in the estimation of cooling rates. In considering the effect of the first bias error, the experimental work of Bushnell (1962) indicates that instrumental bias

errors are negligible at pressures greater than 30 mb. It is important to note that any bias error in the telementry system of the radiometersonde will have a negligible influence on estimates of net radiation since the bias errors in the top and bottom temperature measurements cancel each other. (Appendix I, Johnson, 1965). For a constant bias error of either sensor, cooling estimates are unbiased since the derivative, $\partial\lambda_n/\partial p$, is zero. Furthermore, if a systematic bias error exists which is a function of pressure only, the generation estimates will not be influenced, for when subtracting to determine the field of heating deviations the bias errors of both the mean profile and arbitrary profiles cancel each other. Therefore, the possibility of any bias error in the measurements affecting the estimates of the generation of the available potential energy is dismissed.

The possibility of the second bias error, the lack of fit, is minimized by satisfying several criteria (Johnson, 1965). Briefly, these criteria are: (1) the selection of a "region of immediate interest" from the entire function, γ_n, so that within this region R_n may be described by a low order unbiased k-th degree polynomial, (2) the RMS error estimate from the residual sums of squares of the unbiased k-th degree polynomial is nearly equal to the RM S error estimate determined from a laboratory or a replicated experiment, and (3) the number of observations within the "region of immediate interest" is large compared to the degree, k.

The first criteria is partially satisfied by dividing the atmosphere into seven layers. This division is both meteorologically and statistically sound since the generation may be studied as a function of height and the entire span of pressure is reduced to several "regions of immediate interest." Within each "region of immediate interest" the appropriate unbiased k-th order polynomial is selected by comparing the estimates of error variance, σ^2_R, of the 0-th through the 4-th degree polynomials.

$$\hat{\sigma}^2_R = \frac{(\underset{\sim}{\hat{R}}_n - \underset{\sim}{\hat{R}}_n)'(\underset{\sim}{R}_n - \underset{\sim}{\hat{R}}_n)}{n - (r+1)} \qquad (3.18)$$

Here, n is the number of observations and r the appropriate degree. In the first test, each estimate of the error variance by the r-th degree polynomial was compared with the (r+1)-th degree for polynomial orders zero through four. If the estimate r was less than the estimate (r+1), the r-th degree was selected as the optimum k-th degree, provided it satisfied appropriate tests for criteria two and three. The specific criteria chosen were that the estimate of the error variance for the k-th degree polynomial would not exceed 4.00×10^{-4} ly^2/min^2 ($\hat{\sigma}_R$ = 0.020 ly/min) and that the number of observations within the layer

would exceed $4(r+1)$. The upper limit of $\hat{\sigma}^2$, allowing for sampling variations, is based on Bushnell's estimate of 0.36×10^{-4} ly^2/min^2 ($\sigma_R = 0.006$) for the random error variance. In these results the lowest order r-th degree polynomial satisfying these tests is selected as the optimum k-th degree polynomial. If no local minimum for $\hat{\sigma}^2_R$ occurs, the 4-th degree is selected provided criteria two and three are satisfied; otherwise, the layer is rejected. However, in 86 percent of the layers, an optimum degree was selected by the test for a local minimum. The local minimum for $\hat{\sigma}^2$ as a function of r in (3.18) occurs when the rate of the monotonically decreasing numerator is insufficient to offset the influence of the larger denominator for each higher (r+1)-th degree. In this study the unbiased estimate of the error variance, $\hat{\sigma}^2_r$, served as an excellent discriminator for the selection of the appropriate k-th degree unbiased approximating polynomial. It should also be noted that all layers contained more than ten points since the three observations outside of the layer but adjacent to the upper and lower boundaries were included. This was necessary to achieve continuity for the estimate of cooling across the boundaries. Furthermore, the highest layer used in each flight was required to have at least three observations above its upper boundary.

After the selection of the k-th degree polynomial as the best estimate of R_n over the "region of immediate interest," the polynomial is differentiated.[2]

$$\frac{\partial \hat{R}_n(x)}{\partial p} = \frac{\partial x}{\partial p}\left(B_1 + 2B_2 x + \ldots + k\,B_k x^{k-1}\right) \qquad (3.19)$$

In matrix notation the $n \times 1$ vector of derivatives of the net radiative flux is

$$\frac{\partial \hat{\underset{\sim}{R}}_n}{\partial p} = C_{2s}^{-1} \underset{\sim}{X}\,\underset{\sim}{C}\,\underset{\sim}{B} \qquad (3.20)$$

[2] One notes that $\frac{\partial \hat{R}_n}{\partial x}$ is defined by $\lim_{h \to 0} \frac{\hat{R}(x+h) - \hat{R}(x)}{h}$. If actual observations of the derivative of R_n, $(\partial \hat{R}_n/\partial x)$ were available, the individual coefficients of $\underset{\sim}{A}$, a $(k+1) \times 1$ vector in the "least squares" polynomial representation $(\partial \hat{R}_n/\partial x) = \underset{\sim}{X}, \underset{\sim}{A}$, are estimates of the individual coefficients of B according to the relation $A_i = i\,B_{i-1}$ for $i = 0, \ldots, (k-1)$ where $\hat{R}(x) = \underset{\sim}{X}, \underset{\sim}{B}$. Furthermore, the estimates of the derivatives by a differentiated unbiased approximating polynomial are also unbiased (Johnson, 1965).

where $\underset{\sim}{C}$ is a (k+1) diagonal matrix with diagonal elements given by $(i-1)/x$ for $i = 1, \ldots, (k+1)$. The $(n \times 1)$ vector of cooling estimates given by substitution of equation (3.7) into (3.1) is

$$\underset{\sim}{Q} = g\, C_{2s}^{-1} \underset{\sim}{X}\, \underset{\sim}{C}\, \underset{\sim}{B} \tag{3.21}$$

where Q is a $n \times 1$ vector of the estimate of infrared cooling (i.e., rate of addition of heat per unit mass). Substitution of equation (3.11) into (3.21) yields

$$\underset{\sim}{Q} = g\, C_{2s}^{-1} \underset{\sim}{X}\, \underset{\sim}{C} [\underset{\sim}{X}^T \underset{\sim}{X}]^{-1} \underset{\sim}{X}^T \underset{\sim}{R}_n \tag{3.22}$$

Since the infrared cooling estimates are linearly related to the observations of net radiation, one may again use Gauss' Theorem to state, "of all the possible linear transformations for the 'immediate region of interest,' the estimates of Q by the unbiased k-th degree polynomial are minimum variance estimates for infrared cooling." (Johnson, 1965).

The criteria for the estimation of infrared cooling was developed by analyzing atmospheric cross-sections from International Falls to Curacao, Venezuela, for January 7 and 9, 1961. In the analysis, using estimates by this method, the tests leading to the three criteria provided consistent profiles of atmospheric cooling. The critical factors necessary to provide consistent estimates were: (1) an estimate of error variance nearly equal to the estimate by Bushnell (1962), and (2) a greater number of observations within each atmospheric layer as the order, k, of the unbiased approximating polynomial increased.

Estimates of the random error variance of atmospheric cooling estimates by this technique can be determined by relating the variance of the local rate of atmospheric cooling to the variance of net radiation, or by comparing individual estimates from the net radiation observations from two radiometers mounted on the same radiosonde. The equations for the first method which are developed in Appendix IV of the basic thesis show that the variance of the infrared cooling estimates is a function of the scaled variable within each atmospheric layer, a maximum at the boundaries and a minimum at the midpoint of the layer.

The latter method is used since one can determine, not only an estimate for the variance, but more important whether the technique developed in this chapter and applied separately to data from each radiometer provides consistent estimates for the true profiles of atmospheric cooling. The data were available from a "doubleheader" radiometersonde flight in which the telemetry system alternately transmitted observations from the two radiometers mounted on the same radiosonde.

The k-th degree polynomial for each layer was determined from the data for each radiometer and was used to individually estimate the true continuous cooling profiles. The maximum estimate of cooling was -3.2°C/day at 310 mb and the minimum estimate 30.6°C/day at 470 mb for both radiometers. The averaged RMS estimate of the error obtained by the differences between the two cooling curves at 25 mb intervals at pressures greater than 100 mb and at 10 mb intervals at pressures less than 100 mb is $\pm$0.22°C/day. This RMS estimate of the error for cooling by this method can be compared with Kuhn's results (1961). Kuhn determined that the RMS estimate of the random error for the mean cooling for a 100 mb layer is 0.34°C/day. This estimate is based on a RMS error estimate of $\pm$0.004 ly/min for the net radiation observations, while if $\pm$0.006 ly/min (Bushnell, 1962) is used, the RMS error estimate of cooling is 0.51°C/day. Thus, the polynomial technique provides continuous estimates of the vertical profile of atmospheric cooling with greater reliability and avoids the overly smooth mean estimates by 100 mb finite differences. This improvement in estimation of atmospheric cooling rates is due to the utilization of all the information from the observations within the "region of immediate interest" and the ability of the "least squares" method to redistribute the random error component of each observation over a predicted function in a manner similar to its superposition on the measurements of the true function.

The estimates of the temperature profiles were also determined by approximating polynomials; however, the criteria determining the k-th degree unbiased polynomials were not as stringent. Only polynomial orders through the second degree were compared to determine if a local minimum for the estimate of the random error variance occurred before the second degree, since the description by a second order polynomial was sufficient to describe the vertical variation of temperature within each atmospheric layer. If a local minimum occurred, the 0-th or 1-st degree became the k-th degree polynomial, however, if not, the second degree was used as the k-th order unbiased estimate provided that the RMS error estimate was less than 4°C. The latter test was necessary to determine errors resulting from faulty data processing. The nearly perfect description of the temperature profile is indicated by the value of the RMS error estimate from the residual sums of squares. This estimate was usually between $\pm$0.3 to $\pm$0.4°C, a value close to the random instrumental error component of air temperature (AWS TR-105-133, 1955). Although in this study pressure is regarded as an exact measurement, in reality there exists a small error component in the observation. Consequently, this effect reduces the magnitude of the regression coefficients (Kendall and Stuart, 1961) of both the approximating polynomials for net radiation and temperature, causing the variation in the profiles to be slightly underestimated. However, since the RMS error is approximately

$\pm$0.3 mb while the range of atmospheric pressure for each layer is at least 25 mb, this effect can be disregarded as negligible. In the next chapter the method of integrating these approximating polynomial functions to estimate the generation of available potential energy will be presented.

4. Generation Estimates by Approximating Polynomial Integrals

In the previous chapter it was shown that approximating polynomials can be used to provide consistent estimates of temperature and cooling profiles. Since the polynomial coefficients may be averaged to provide the space and time means from which the deviations of temperature and infrared cooling are determined, optimum estimates of Lorenz' generation integral can be obtained for the generation at the various scales of atmospheric circulation. To realize this advantage a diagnostic model is designed which incorporates the polynomial coefficients into a method of integration. Integration over each of the seven layers describes the vertical distribution of the generation of available potential energy. The diagnostic model is based on the technique of integrating two polynomial functions. General development of this technique is presented in Appendix V of the original thesis (Johnson, 1965).

The predicted polynomial functions for temperature (T) and the rate of heat addition (Q) for an arbitrary atmospheric layer may be expressed as

$$\hat{T} = \underset{\sim}{x}_1 \underset{\sim}{A} \tag{4.1}$$

$$\hat{Q} = g \frac{\partial x}{\partial p} \underset{\sim}{x}_2 \underset{\sim}{C} \underset{\sim}{B} \tag{4.2}$$

where $\underset{\sim}{A}$ and $\underset{\sim}{B}$ are $(k+1) \times 1$ and $(q+1) \times 1$ vectors of unbiased polynomial coefficients, $\underset{\sim}{x}_1$ and $\underset{\sim}{x}_2$ are the corresponding $1 \times (k+1)$ and $1 \times (q+1)$ vectors of the powers of the independent variables, $[1, x, x^2 \cdots x^k]$, and g, $\frac{\partial x}{\partial p}$, and $\underset{\sim}{C}$ are previously defined in Chapter 3. The space averaged profiles of (4.1) and (4.2) are

$$\overline{\hat{T}} = \underset{\sim}{x}_1 \overline{\underset{\sim}{A}} \tag{4.3}$$

$$\overline{\hat{Q}} = \underset{\sim}{x}_3 \overline{\underset{\sim}{B}} \tag{4.4}$$

where the vector $\underset{\sim}{x}_3$ is equal to the vector $(g \frac{\partial x}{\partial p} \underset{\sim}{x}_2 \underset{\sim}{C})$ of equation (4.2), and the space deviations are

$$\hat{\underset{\sim}{T}}'' = \underset{\sim}{x}_1(\underset{\sim}{A} - \bar{\bar{\underset{\sim}{A}}}) = \underset{\sim}{x}_1 \underset{\sim}{A}'' \tag{4.5}$$

$$\hat{\underset{\sim}{Q}}'' = \underset{\sim}{x}_3(\underset{\sim}{B} - \bar{\bar{\underset{\sim}{B}}}) = \underset{\sim}{x}_3 \underset{\sim}{B}'' \tag{4.6}$$

Substitution of (4.5) and (4.6) into the generation integral, (2.4), yields

$$G = \frac{1}{g}\sum_{s=1}^{7} \int_{p_0+1}^{p_s} \frac{\Gamma_d}{(\Gamma_d - \bar{\bar{\Gamma}}_s)\bar{\bar{T}}_s} A_s''^T \underset{\sim}{x}_1^T \underset{\sim}{x}_3 \underset{\sim}{B}_s'' dp \tag{4.7}$$

where the atmosphere is divided into seven layers ($s = 1, \ldots, 7$). For an atmosphere in local hydrostatic equilibrium and possessing a linear lapse rate, the horizontally averaged temperature profile within an arbitrary layer, s, is

$$\bar{\bar{T}}_s = \bar{\bar{T}}_{0s}\left(\frac{p}{p_{0s}}\right)^{\frac{R\bar{\bar{\Gamma}}_s}{g}} \tag{4.8}$$

where $\bar{\bar{T}}_0$ and p_{0s} are the lower boundary values of temperatures and pressure, $\bar{\bar{\Gamma}}_s$ is the lapse rate and R is the specific gas constant for dry air. Substituting (4.8) into (4.7) gives

$$G = \frac{1}{g}\sum_{s=1}^{7} \frac{(p_{0s})^{\frac{R\bar{\bar{\Gamma}}_s}{g}}}{(1 - \bar{\bar{\Gamma}}_s/\Gamma_d)\bar{\bar{T}}_{0s}} \underset{\sim}{A}_s''^T \left\{ \int_{p_s+1}^{p_s} p^{-\frac{R\bar{\bar{\Gamma}}_s}{g}} \underset{\sim}{x}_1^T \underset{\sim}{x}_3 dp \right\} \underset{\sim}{B}_s'' \tag{4.9}$$

Since the polynomial coefficients are constants with respect to each layer, the diagnostic model may be expressed as

$$G = \sum_{s=1}^{7} C_s \underset{\sim}{A}_s''^T \underset{\sim}{X}_s \underset{\sim}{B}_s'' \tag{4.10}$$

where the constant C_s for at atmospheric layer is

$$C_s = \frac{p_{0s}^{R\bar{\bar{\Gamma}}_s/g}}{(1 - \bar{\bar{\Gamma}}_s/\Gamma_d)\bar{\bar{T}}_{0s} C_{2s}} \tag{4.11}$$

and the elements x_{ij} of the $(k+1) \times (q+1)$ matrix, $\underset{\sim}{X}_s$, are

$$x_{ij} = \int_{p_{s+1}}^{p_s} (j-1)p^{-\frac{R\bar{\bar{\Gamma}}_s}{g}} \left(\frac{P - C_{1s}}{C_{2s}}\right)^{(i+j)-3} dp \qquad (4.12)$$

A binomial expansion of (4.12) and term-wise integration leads to the solution for the element ij of $\underset{\sim}{X}_s$

$$x_{ij} = \sum_{k=0}^{(i+j-3)} \frac{(i+j-3)!\,(j-1)(C_{2s})^{3-(i+j)}(-C_{1s})^{\ell}}{\ell!\,(i+j-3-\ell)!\,[(i+j)-(2+\ell+(R\bar{\bar{\Gamma}}_s/g))]} \left[p^{(i+j)-(2+\ell+R\bar{\bar{\Gamma}}_s)} \right]_{p_{s+1}}^{p_s} \qquad (4.13)$$

The integral solution of (4.10) may be time averaged to yield the generation due to the infrared component of heating. The resulting expression may be partitioned among the four scales of atmospheric circulation by substituting the time averaged form of (4.10) into equation (2.14).

$$\bar{G} = \sum_{s=1}^{7} \left\{ \overline{\overline{[\bar{A}]''_s \underset{\sim}{X}_s [\bar{B}]''_s}} + \overline{\overline{([\underset{\sim}{A}]')''_s \underset{\sim}{X}_s ([\underset{\sim}{B}]')''_s}} + \overline{\overline{\bar{\underset{\sim}{A}}^*_s \underset{\sim}{X}_s \bar{\underset{\sim}{B}}^*_s}} + \right. \qquad (4.14)$$

$$\left. + \overline{\overline{(\underset{\sim}{A}')^*_s \underset{\sim}{X}_s (\underset{\sim}{B}')^*_s}} \right\}$$

The advantages of expressing the generation in this form are: (1) the vertical description of both temperature and heating allow the generation to be estimated as a function of pressure, (2) a variable static stability can be used in the integration model, and (3) the diagnostic model provides unbiased estimates of the generation (Appendix V, Johnson, 1965).

The most serious limitation of this study is the small data sample. The thirteen radiometersonde stations represent a limited area, the eastern half of the United States and the Carribbean. Thus, the estimates based on these thirteen stations represent only a linear contribution to the global generation integral. On the other hand, studies involving only data from limited areas have advantages. For example, if one wishes to study the linear contribution of the smaller scales which might be contained within the data region, many of the physical processes expressed by the covariant terms in Lorenz' equations will attain their maximum values. When only two or three of these features are averaged with other comparatively quiescent features of the atmosphere, one underestimates the importance of the small scale features.

Furthermore, when working with a limited data sample, it is important that a diagnostic model be used which maximizes the information which can be extracted from two observational series. As is shown in Appendix V of the original thesis, unbiased polynomial estimates of the temperature and heating provide an unbiased estimate of the generation integral. Thus, with the increased resolution of this model it is possible to investigate the linear contributions of the smaller scale features of the atmosphere in which the spatial variability of the meteorological variables is great.

Because of the limited data sample, daily zonal mean profiles of infrared cooling could not be obtained. Thus, it was necessary to combine the estimates of generation at the transient zonal and eddy scale. Combining the two transient scales of equation (2.14) yields the final diagnostic equation for the infrared component

$$\overline{G} = \{G_{ZS} + G_{ES} + G_T\} \tag{4.15}$$

where the time averaged stationary zonal generation (G_{ZS}) is

$$G_{ZS} = \sum_{s=1}^{7} C_s \overline{\overline{[\bar{\underset{\sim}{A}}]''_s \underset{\sim}{X}_s [\bar{\underset{\sim}{B}}]''_s}} \tag{4.16}$$

The time averaged stationary eddy generation (G_{ES}) is

$$G_{ES} = \sum_{s=1}^{7} C_s \overline{\overline{\underset{\sim}{A}^*_s \underset{\sim}{X}_s \underset{\sim}{B}^*_s}} \tag{4.17}$$

And the time averaged transient generation (G_T) is

$$G_T = \sum_{s=1}^{7} C_s \overline{\overline{(\underset{\sim}{A}')''_s \underset{\sim}{X}_s (\underset{\sim}{B}')''_s}} \tag{4.18}$$

In evaluating the above equations, C_s and the integrated matrix, $\underset{\sim}{X}_s$, are constants for a given layer. The necessary constants to determine C_s and $\underset{\sim}{X}_s$ are presented in Table 3. In these computations the static stability of the US Standard Atmosphere was used. For this reason the upper surface of level four was placed at 234 mb, which is the tropopause of the US Standard Atmosphere.

Since the atmosphere was divided into seven layers, the seven C's and X's of equations (4.16), (4.17), and (4.18) are determined for each level and stored in the computer, thus facilitating the integration.

TABLE 3

CONSTANTS FOR C_s

Layer	ps - ps+1 (mb)	P_{0s} (mb)	$\bar{\bar{T}}_{0s}$ (°K)	$\bar{\bar{\Gamma}}_s$ (°K/km)	C_{1s} (mb)	C_{2s} (mb)
1	1000 - 800	1000	288	6.5	900	100
2	800 - 600	800	275	6.5	700	100
3	600 - 400	600	261	6.5	500	100
4	400 - 234	400	241	6.5	317	83
5	234 - 100	234	218	0	167	67
6	100 - 50	100	218	0	75	25
7	50 - 25	50	218	0	37.5	12.5

$\Gamma_d = 9.8°C/km$; $g = 980\ cm/sec^2$; $R = 2.87 \times 10^6$ ergs/gm-deg

To determine the stationary zonal generation, it was necessary to determine zonal mean profiles of temperature and cooling. This was done by dividing the thirteen stations into three zonal rings surrounding their latitude. This division by ring numbers is presented in Table 1. The stationary zonal component was computed for each ring and the ring averages used to obtain an average zonal generation. The transient and stationary eddy components were computed for each station and the stations averages were used to obtain averages for each zonal ring and also for the entire area. A total generation was obtained from the sum of all three components.

5. Results

Estimates of the transient, stationary eddy and stationary zonal generation of available potential energy obtained by the polynomial integration method are presented in this chapter. As noted before, these estimates are from a limited area and must be regarded as only a linear contribution to the global value of the generation of available potential energy. The estimates, which represent the contribution from a continental region within the westerlies (Zones I and II) and from a maritime area of the subtropics (Zone III), are presented in Tables 4 - 8.

For convenience of discussion, the estimates for the seven layers of integration are combined to form three layers. The first layer extends from the 1000 to the 600 mb surface, thus representing the lower half of the troposphere. The second layer, 600 to 234 mb, represents the upper troposphere, and the third layer, 234 to 25 mb, the stratosphere. Hereafter, the layers will be simply noted as the lower tropospheric, upper tropospheric, and stratospheric layers.

Table 4 gives the estimates of the transient generation. As noted previously, it was necessary to combine the estimates of the transient zonal and transient eddy scales. A comparison of the three layers reveals that the mean transient estimate of Zones I, II, and III, is negative for the lower troposphere (-0.47×10^{-3} watts/m^2-mb), while it is a small positive quantity for the other two layers (+0.14 watts/m^2-mb for the upper troposphere and +0.10 watts/m^2-mb for the stratosphere). The results indicate that during this limited period the phase of the temperature and infrared heating field reversed between the lower troposphere and the upper two layers. This variation of the generation with height will be further discussed after the generation at individual stations is considered.

TABLE 4

TRANSIENT GENERATION

Units: Layers — 10^{-3} watts/m^2 mb
Total — watts/m^2

Zone I

Layer (mb)	Station 405	532	641	645	747	Average
1000-600	-2.67	-1.91	-1.39	1.00	-0.01	-.99
600-234	.84	- .39	-1.29	-0.23	-0.40	-.30
234- 35	.02	- .12	-0.17	0.18	1.13	.21
Total	- .77	- .95	-1.09	0.36	.09	-.47

Zone II

Layer (mb)	Station 202	226	363	Average
1000-600	1.30	- .33	-1.65	-.23
600-234	.36	.45	.93	.58
234- 25	.14	- .21	.64	.19
Total	.70	- .11	-..17	.14

Zone III

Layer (mb)	Station 383	525	866	967	988	Average
1000-600	-0.59	- .14	-1.00	.27	- .05	-.30
600-234	.56	- .72	- .09	- .34	.89	.06
234- 25	.36	-1.66	.52	- .08	.56	-.06
Total	0.04	- .68	- .33	- .03	.41	-.12

Grand Average — Zones I, II, III

Layer (mb)	
1000-600	-.47
600-234	.14
234- 25	.10
Total	-.13

TABLE 5

DAILY CONTRIBUTIONS TO TRANSIENT GENERATION

Station	December									January												
	20	21	22	23	24	25	26	27	28	7	8	9	10	11	12	13	14	15	16	17	18	19	20
										Units: Watts/m^2												
202									-.70	1.17	.32	.71		.56	-1.48	.45	.74		2.02				
226		-.82	-2.88	3.26			1.27		1.33	.05	.79	.20	-4.29	.43	-1.55		.88	3.03	.34	-.60	-1.38	-.05	
405	.02	1.74	.31	-.11	-7.78		-.41	1.66	-.95	-4.45	-3.21	.08	-6.52	1.40	-2.44	-.22	.15	4.87		.19	1.32		
363			-.48		.84	.51	.27			-.24	-.31	-.10	-1.82	-.63			2.43	-.24	-1.17	-.98	-2.03	1.46	
532	-.82		-6.31	-4.45	-1.83	0.81				-4.28	1.16	-.46	.38	1.97	-1.65	-2.66	-.60	2.36		.21	1.60		
641				-1.95					.15			-.34		-.58	-3.06	.72							
645																-.72	1.11	-.91	4.85	.40	.99	-1.36	-.06
747	1.34	-.04	-3.96	.13	.61	-1.08			3.53	-1.53	3.77	-.53	3.92	-.255	-1.43	-2.31	0.11	0.55	.69	3.20	-5.16		
Daily sub-total Zone I and II	.28	.29	-2.66	-2.62	-2.46	.08	.38	1.66	.67	-1.55	.42	-.06	-1.66	.09	-1.93	-.79	.69	1.53	1.29	.39	-.78	-.02	-.06
383	.23	.73	.45	1.66	-1.06	-3.62	3.55	-7.46	1.03	.78	.56	-.88	-.78	-.88	1.19	1.02	.54	.56	1.22	-.34			
525		.55	4.92	-3.21	1.75	-2.30	-2.94	-3.00		.45	-1.99	-.96	-1.16	-.58			-2.24	-1.19	0.98	-1.62	.57	.30	-1.98
866	-.92	.23	-2.27	-1.70	-2.00		-3.58	6.42	-1.15		.34	-3.68	3.27	1.81	.17	1.43	-2.44	-.03	0.52				
967			.76	-1.40	-.26		-3.08	.72	1.65					1.72	.96	.02			-1.27	-.07			
988	-.93	.70	1.68	-.87	-.89	-1.87	-1.60	4.60	.45		.47		-.99	5.75	.55	.75		.20	-.27	.29	-.10		
Daily Sub-total Zone III	-.54	.55	1.95	-1.10	-.49	-2.59	-1.51	.25	.49	.61	-.15	-1.84	.09	1.36	.72	.81	-1.38	-.14	.24	-.49	.24	.30	-1.98

TABLE 6

STATIONARY EDDY GENERATION

Units: Layers — 10^{-3} watts/m^2 mb
Total — watts/m^2

Zone I

Layer(mb)	Station	405	532	641	645	747	Average
	1000-600	-0.39	-0.03	+0.32	-0.62	-1.97	-0.54
	600-234	-0.21	-0.25	-0.02	-0.48	0.00	-0.19
	234- 25	+0.21	0.00	-0.06	-0.68	+0.50	0.00
	Total	-0.19	-0.11	+0.11	-0.58	-0.70	-0.29

Zone II

Layer(mb)	Station	202	226	363	Average
	1000-600	+8.74	-7.79	+2.56	+1.16
	600-234	+0.91	+0.31	-1.46	-0.69
	234- 25	+0.84	-0.58	-0.30	-0.57
	Total	+3.06	-3.21	+0.44	+0.10

Zone III

Layer(mb)	Station	383	525	866	967	988	Average
	1000-600	-0.32	-0.13	+0.06	+0.03	-0.36	-0.14
	600-234	0.00	+0.26	+0.12	+0.21	+0.61	+0.24
	234- 25	-0.55	-0.29	+0.19	-2.21	+0.03	-0.56
	Total	-0.25	-0.02	+0.11	-0.38	+0.09	-0.09

Grand Average

Layer(mb)		
	1000-600	+0.19
	600-234	-0.20
	234- 25	-0.41
	Total	-0.08

TABLE 7

STATIONARY ZONAL GENERATION

Layers (mb)	Zone	I	II	III	Average
	1000-600	-12.47	-2.40	+0.53	-4.13
	600-234	- 0.64	+0.13	-0.74	-0.41
	234- 25	- 0.43	+0.21	-0.80	-0.35
	Total	- 5.44	-0.89	-0.24	-1.93

TABLE 8

TRANSIENT, STATIONARY EDDY, STATIONARY ZONAL, AND AVERAGE INFRARED GENERATION

Layers (mb)	Transient	Stationary Eddy	Transient +Sta. Eddy	Stationary Zonal	Total
1000-600	-0.47	+0.19	-0.28	-4.13	-4.41
600-234	+0.14	-0.20	-0.06	-0.41	-0.47
234- 25	+0.10	-0.41	-0.31	-0.35	-0.66
Total	-0.13	-0.08	-0.21	-1.92	-2.13

Units: layers — 10^{-3} watts/m^2 mb
total — watts/m^2

An examination of the total transient generation in a unit column for each station (Table 4) indicated that contributions are predominantly negative. However, considerable variation in the estimates exists between stations. For example, large positive values are found at Miami (+0.70 watts/m^2) and Curacao (+0.41 watts/m^2), Zone II and III stations, while large negative values are found at Madison (-1.09 watts/m^2) and Peoria (-0.95 watts/m^2), both Zone I stations. The difference between the generation estimates of the higher latitude stations and the low latitude stations is very likely related to the persistence of certain symoptic events during the data period.

Since these data involve time averages, they do not describe time variations of the generation by individual transient disturbances. Thus, one of the perplexing questions which the study cannot entirely resolve is how the generation varies during the life cycle of a transient disturbance. From certain physical arguments based on the distribution of clouds (see Chapter 2), it appears that the contribution is positive during the incipient, developing and mature stage of the disturbance and negative during its dissipating stage. Although exact estimates cannot be made, some information concerning this postulate can be obtained by inspecting the daily contribution of each station to the time averaged transient generation (see Table 5). One notes that there is considerable variation in the daily estimates, which confirms that the time averages estimate of the generation is not the result of the sum of relatively uniform contributions. The best indication that the covariance of temperature and infrared cooling reverses sign is given by the period of 13 January through 17 January. The sums of the estimates for the U. S. stations for each day clearly indicate that during this period the estimates were consistently positive. At this time the eastern continental United States was under the influence of a well developed middle tropospheric trough and two surface lows, one which moved eastward along the U. S. -Canadian border and the other eastward along the Gulf Coast. Evidently, within these traveling disturbances, the cloud distribution and thermal structure were such that the contribution by the eight U. S. stations was predominantly positive. It appears, as suggested in Chapter 2, that the extensive cloudiness in the warm air reduces the cooling by the infrared component while the cooling within the clear cold air is a maximum, thus producing a positive contribution to the generation of available potential energy.

It was noted also in Chapter 2 that above the level of the clouds a negative contribution is likely to occur. An inspection of the daily contribution by each of the seven layers revealed that in many cases the sign of the individual layers reverses one or more times. This result is probably due to the horizontally stratified nature of clouds and water vapor.

In the presence of several layers of clouds, the relative cooling changes sign at the top of each cloud layer. Since within individual airmasses the lapse rate of temperature is nearly constant throughout the troposphere, the relative temperature deviation is constrained to be either a positive or negative quantity while the sign of the heating deviation changes at the top of each cloud layer. Thus, the generation contribution also reverses sign at the top of each cloud layer. For example, at Miami on January 14, 1960, the following generation values were obtained for the seven layers:

Layer (mb)	Transient generation 10^{-3} watts/m^2-mb)
1000-800	0.82
800-600	-0.22
600-400	3.41
400-234	-0.25
234-100	0.17
100- 50	-0.48
50- 25	-1.38

Evidently tops of cloud layers were found at approximately 800 mb, 400 mb and 100 mb. The radiosonde data for that day verifies the existence of moist layers, possibly clouds, at the lower two heights. The humidity observations are missing at the upper level. Large vertical variations of generation such as these indicate that studies using mean values of cooling for atmospheric columns (such as those required when satellite data are employed) may be appreciably constrained. An alternative method which has been presented by Smith (1964) uses satellite data to estimate the cooling within different atmospheric layers. Such a method may be a valuable technique in estimating the infrared generation on a global scale.

There are cloud distributions, however, where the generation will be positive throughout the entire atmospheric column. Consider, for example, a case in which the top of the cirrus shield reaches a height equal to the height of the intersection of the polar and tropical soundings. Although the differential heating field is reversed above this level, the temperature field of horizontal deviations also reverses sign, causing a positive generation throughout the column. Such an example occurred on 23 December, 1960, at Montgomery where all levels were positive except the 100-50 mb level. The total estimate for the column was 3.26 watts/m^2.

Large positive contributions can also be obtained from cloudless regions. These situations occur when there is large infrared cooling from the cold, dry tropospheric air associated with a recent polar outbreak. Under such conditions the generation may be positive throughout the atmospheric column, for the polar stratosphere may be experiencing relative

warming with respect to the colder subtropical stratosphere. The relative warming in the polar stratosphere is produced by direct absorption of the upward radiative flux from the troposphere. At the tropopause the value of the upward radiative flux from the cold clear polar troposphere is significantly greater than the upward radiative flux emitted from regions with high clouds (or moisture layers). Thus, a positive contribution to the generation of eddy available potential energy may again occur throughout the atmospheric column.

An example which illustrates the large generation that can be achieved in fresh polar air and the rapid changes in generation which occur as the air mass is modified are given by the data for International Falls. On 8 January 1961, International Falls experienced a large positive generation (3.92 watts/m^2) while under the influence of an anticyclone associated with a recent outbreak of polar air. On the following three days, the generation became negative (-2.55, -1.43, -2.31 watts/m^2, respectively). An examination of synoptic charts for this period revealed that the cold polar air stagnated over the Eastern United States and warmer more moist air was advected above it. The higher clouds, which resulted, greatly reduced the infrared cooling; and as a consequence, the generation became negative.* Although the mean transient generation for the entire area was -0.13 watts/m^2 the spatial and time variations of the generation noted above indicate that this term may be either a significant source or sink of available potential energy in specific cases. The range of the transient generation estimates in Table 5 is slightly larger than the range of frictional dissipation within the planetary boundary layer for light and moderate winds over the forested region of Northern Wisconsin (W. B. Johnson, 1965). It appears that in an energetically consistent numerical model where frictional dissipation is included, infrared cooling at the scale of the secondary circulation should also be incorporated. Consequently, the time and space variations of the transient generation should be further investigated for individual synoptic events.

The estimates of contributions to the stationary eddy generation are presented in Table 6. The total contribution from the entire area is -0.08 watts/m^2, thus indicating that the stationary eddy component is not a large sink of available potential energy. The mean estimate for the stratospheric layer is considerably more negative than the mean estimate for the tropospheric layers. This indicates that at this scale the stratospheric cooling by infrared radiation is proportional to the stratospheric

*The reader should be reminded that other diabatic effects such as the eddy conduction of sensible heat through the lower boundary are also important in the thermal modification of the air mass.

temperature and is not significantly influenced by factors such as clouds, water vapor and dust. On the other hand, the positive estimate (0.10 watts/m^2-mb) of the transient generation for the stratospheric layer indicates that there are variations in absorbing constituents in the stratosphere associated with transient disturbances.

Further examination of Table 6 reveals that a larger positive generation (1.16 watts/m^2-mb) exists for the lower troposphere of Zone II. This estimate can be misleading because it is in part the result of the difference in the latitude of Miami and the other two stations in the zone. Since computation of the stationary eddy generation involves the product of deviations of the time averaged temperature and cooling profiles from their respective zonal means, the temperature deviation of Miami was unusually large because of the mean north-south temperature gradient. Combined with the large positive deviation was an appreciable relative heating term due to extensive cloudiness in this area. On the other hand, Montgomery had a large negative temperature deviation and a positive heating deviation, thus a large negative estimate. It is interesting to note that although these large temperature deviations are due to the thirteen degree latitudinal extent of the zonal ring, the deviations of the stationary eddy temperature field within a unit zonal ring have the same magnitude as the deviations within Zone II. In view of this fact, it is probable that the range of the contributions (both positive and negative) from different stationary features (continents and oceans) within any unit zonal ring is as great as the difference between Miami and Montgomery. This should be particularly true in the latitudinal belt of 20° to 30° N, where the subtropical highs are most pronounced and in which the temperature field and cloud and water vapor tend to have a systematic distribution.

Although from this study it is not possible to estimate the global averaged stationary generation, the implications of the large positive and negative values for the stationary generation of Zone II are interesting in view of Murakami's (1960) results. Murakami postulates that, if the stationary disturbances transfer available potential energy to the transient disturbances, "the available potential energy of the stationary disturbances should be supplied by the non-adiabatic process of warming of warm air and cooling of cold air." He also notes that the two most probable diabatic components which might generate the available potential energy were infrared heating and sensible heat transfer, since his generation estimate for the latent heat component was an order of magnitude less than the required generation at this scale. The results obtained here tend to indicate that the infrared generation either positive or negative by the stationary disturbance may be important.

In Table 7 the estimate of the stationary zonal generation is -1.92 watts/m^2, a large negative value. Shen's (1963) zonal generation estimate for the infrared component from the use of satellite data was -1.75 watts/m^2 for portions of the period of December, 1959 through February, 1960. Thus the two estimates of zonal generation for the winter hemisphere are nearly equal. One notes that the principal sink of zonal available potential occurs within the lower tropospheric layer, -4.13 watts/m^2-mb. Within the upper tropospheric and stratospheric layers, the negative generation estimate is an order of magnitude less, -0.41 and -0.35 watts/m^2-mb, respectively. This difference between the lower and higher portions of the atmosphere is due to the strong meridional temperature gradient which exists in the lower troposphere during this period. Since during this season the Caribbean tends to be less cloudy than the higher latitudes, the warmer subtropics experienced greater infrared cooling than the polar air over the U.S.

The results of Tables 4-7 are summarized in Table 8. One notes that there is a reversal of sign between the lower tropospheric layer and the two higher layers in both the transient and stationary eddy estimates. However, one cannot necessarily conclude that this is a representative feature of globally averaged generation estimates for these two scales. Within a different time period the results may be quite different for this area, because of different cloud distributions within these two scales.

A subtotal of the transient and stationary eddy contribution is given in the third column. Within the limitations of the study the subtotal is the best approximation to the time averaged infrared eddy generation of equation (2.10). The stationary zonal may be considered as an approximation of the infrared component of equation (2.11). Although the mean generation due to infrared radiation is negative, the large differences between the stationary zonal and transient eddy subtotal stand out, as expected. As noted previously, the small negative values found in the subtotal are the result of the inclusion of a number of significantly positive and negative estimates at these scales.

Another feature presented in the total generation estimate in the fifth column of Table 8 is the pronounced differences in the higher layers. These results indicate that large vertical variations of the infrared generation exist and may be an important feature in different scales of the atmosphere's circulation.

6. Conclusions and suggestions for future research

In this study estimates of the generation of available potential energy have been obtained for a limited area, thus they represent a linear contribution to the average global generation. To obtain these estimates, a diagnostic model with increased resolution and reliability was developed in which the temperature and heating profiles were described by individual approximating polynomials. A technique for integrating the product of the approximating polynomials was devised. As a consequence it was possible to describe the vertical variation of the generation within the scale of the secondary circulation. The method also incorporates a variable vertical static stability factor within individual layers which should be an important consideration in the vertical transfer of moisture and clouds associated with the destabilization of the atmosphere by the infrared component.

The following conclusions may be made concerning the generation of available potential energy:

(1) The total generation during the data period for the limited area was negative.

(2) While the stationary zonal generation was a large negative value, the transient and stationary eddy values were only slightly negative.

(3) An analysis of the daily values indicates that the transient and stationary eddy generations vary considerably from day to day and at times may attain large positive values.

(4) There are pronounced vertical variations in the generation of available potential energy. In general the extreme values, both positive and negative, occur in the lower troposphere. This is undoubtedly the result of varying distributions of cloudiness and water vapor. In individual cases the sign of the generation reverses between different atmospheric layers depending on the distribution of clouds.

(5) Because of the large daily variations as well as vertical variations, it appears that additional intensive studies of the generation for local disturbances should be undertaken. In the life cycle of a disturbance, the infrared generation, both positive and negative, is very likely an important consideration.

(6) The range of the transient generation estimates was slightly larger than the range of frictional dissipation estimates within the planetary boundary layer for light and moderate winds. Consequently, the

satellite estimates of infrared cooling should be considered as necessary information for any future numerical model which includes boundary layer frictional dissipation.

Although the goal of this thesis was a study of the generation of available potential energy and in particular, its vertical variation, a number of serendipitous results were attained. The referenced appendices are available in the original thesis filed with the Memorial Library, University of Wisconsin. They include:

(7) The variance of the downward, upward, and net radiative flux measured by the radiometersonde was firmly established for the first time (Appendix I).

(8) Approximating polynomials were applied to radiometersonde data to obtain continuous cooling profiles which possess a RMS error of only $\pm$0.22°C/day, as opposed to the previous RMS error of $\pm$0.34°C/day for a 100 mb atmospheric layer. The success achieved by approximating polynomials suggests that they may be used to determine vertical derivatives of other meteorological variables, such as wind, temperature, etc.

(9) A technique which permits the integration of two approximating polynomials was developed. It was shown that this method provides unbiased integral estimates when the two approximating polynomials are unbiased and the observational error components are independent (see Appendix V).

BIBLIOGRAPHY

Air Weather Service Technical Report 105-133, 1955: Accuracies of Radiosonde Data, Air Weather Service (MATS), United States Air Force, Washington, D.C.

Box, G.E.P., 1962: Lecture Notes for Mathematical Statistics (237a, 237b), Statistics Dept., University of Wisconsin.

Bushnell, Robert H., 1962: An Investigation of the Problem of the Measurement of Infrared Radiation in the Lower Stratosphere, Ph.D. Thesis, Department of Meteorology, University of Wisconsin.

Clapp, P. F., 1961: Normal Heat Sources and Sinks in the Lower Troposphere in Winter. Monthly Weather Review, Vol. 89, No. 5, pp. 147-162.

Clapp, P. F., and F. J. Winninghoff, 1963: Tropospheric Heat Sources and Sinks at Washington, D. C., Summer 1961, Related to the Physical Features and Energy Budget of the Circulation, Monthly Weather Review, Vol. 91, No. 10, pp. 494-504.

Corcoran, J. L., and L. H. Horn, 1964: The Role of Synoptic Scale Variations of Infrared Radiation in the Generation of Available Potential Energy. University of Wisconsin, Department of Meteorology, Final Report, U. S. Weather Bureau Grant, WBG 10.

Ferrel, W., 1889: A Popular Treatise on the Winds. John Wiley and Sons, New York.

Hadley, G., Concerning the Cause of the General Tradewinds, Phil. Trans. Roy. Soc. London, Vol. 39, No. 58, pp. 1735-36. Reprinted in "The Mechanics of the Earth's Atmosphere. A Collection of Translations by Cleveland Abbe," 3rd collection, Smithsonian Misc. Coll., Vol. 51, No. 4, 1910.

Hildebrand, Francis B., Introduction to Numerical Analysis, New York, McGraw-Hill, 1956. (511p).

Jeffreys, H., 1933: The Function of Cyclones in the General Circulation. Proces-Verbaux del l'Association de Meteorologie, UGG (Lisbon), Part II (Memoires), pp. 219-230.

Johnson, W. B., 1965: Atmospheric Boundary Layer Dynamics Over the Forests of Northeastern Wisconsin, Ph. D. Thesis, Department of Meteorology, University of Wisconsin.

Kendall, Maurice G., and A. Stuart, The Advanced Theory of Statistics, 2 Vols., London, C. Griffin, 1958, Vol. I, Distribution Theory, 1958. Vol. 2, Statistical Inference and Statistical Relationship, 1961.

Korb, G. and F. Möller, 1962: Theoretical Investigations of Energy Gain by Absorption of Solar Radiation in Clouds, Ludwig-Maximilious Universität, Meteorologisches Institut, München, Germany, Contract DA-91-591-EUC-1612.

Kuhn, P. M., 1961: Accuracy of the Airborne Economical Radiometer. Monthly Weather Review, Vol. 89, No. 8, pp. 285-287.

Kuo, H.L., 1957: Energy Releasing Processes and Instability of Thermally Driven Motions in a Rotating Fluid. J. Meteor., Vol. 13, pp. 561-568.

Kuo, H.L., 1957: Further Studies of Thermally Driven Motions in a Rotating Fluid. J. Meteor., Vol. 14, pp. 553-558.

Lorenz, E.N., 1955: Available Potential Energy and the Maintenance of the General Circulation. Tellus, Vol. 7, pp. 157-167.

Margules, M., 1903: Uber die Energie der Sturme. Translated in Smithsonian Miscellaneous Collections, Vol. 51, 1910.

Murakami, T., 1960: On the Maintenance of Kinetic Energy of the Large-Scale Stationary Disturbances in the Atmosphere. Massachusetts Institute of Technology, Department of Meteorology, Scientific Report No. 2, Planetary Circulations Project, Contract No. AF 19(604)-6108.

Palmen, E., 1959: On the Maintenance of Kinetic Energy in the Atmosphere. The Atmosphere and the Sea in Motion. Ed. by B. Bolin, The Rockefeller Institute Press, New York, pp. 212-223.

Plackett, R.L., Principles of Regression Analysis, Oxford, Clarendon Press, 1960. (173 p.)

Rossby, C.G., 1941: "The Scientific Basis of Modern Meteorology," Climate and Man: Yearbook of Agriculture, United States Dept. of Agriculture, Government Printing Office, Washington, p. 599-654.

Rossby, C.G., 1949: On a Mechanism for the Release of Potential Energy in the Atmosphere. Journal of Meteorology, 6, p. 163-180.

Shen, W.C., 1963: The Generation of Available Potential Energy Due to Horizontal Variations in Terrestrial Radiation as Measured by the Satellite Explorer VII. Ph.D. Thesis, University of Wisconsin.

Smith, W.L., 1964: TIROS Radiation Measurements and the Infrared Cooling of the Atmosphere. M.S. Thesis, University of Wisconsin.

Starr, V.P., 1948: An Essay on the General Circulation of the Earth's Atmosphere. Journal of Meteorology, No. 5, pp. 39-43.

Starr, V.P., 1956: Modern Developments in the Study of the General Circulation of the Atmosphere. Journal of Geophysics Research, pp. 61.

Starr, V. P., 1958: What Constitutes Our New Outlook on the General Circulation? Journal of the Meteorological Society of Japan, Series II, Vol. 36, No. 5, pp. 167-173.

Sabatini, R. R., and V. E. Suomi, 1962: On the Possibility of Atmospheric Infrared Cooling Estimates from Satellite Observations. Journal of Atmospheric Sciences, Vol. 19, No. 4, pp. 349-350.

Suomi, V. E., and W. C. Shen, 1963: Horizontal Variations of Infrared Cooling and the Generation of Eddy Available Potential Energy. Journal of Atmospheric Sciences, Vol. 20, No. 1, pp. 62-65.

Wiin-Nielsen, A., and J. A. Brown, Jr., 1962: On Diagnostic Computations of Atmospheric Heat Sources and Sinks and the Generation of Available Potential Energy. Proceedings of the International Symposium on Numerical Weather Prediction, Meteorological Society of Japan, Tokyo, November, pp. 519-613.

Time Structure of Energy Transformations over the Northern Hemisphere

Alfred Carasso
Lyle H. Horn
Donald R. Johnson

Abstract: Variance and Cross-Spectral techniques are applied to time series of the basic energy parameters defined by Lorenz to investigate the nature of energy transformations as a function of time for periods between 50 days and 4 days, in the 850 - 500 mb layer north of latitude 20°N. The results suggest a systematic transformation of available potential energy to kinetic energy at periods less than 10 days but fail to reveal any preferred periodicities for longer periods, possibly because of a transfer of energy from outside the region.

1. Introduction

By averaging the generation and conversion terms that enter into the atmospheric energy equations over a period of several months, Lorenz (1955) arrived at the following picture of the average tropospheric energy cycle:

> Basic radiation processes create zonal available potential energy which is converted into eddy available potential energy by the action of the large scale eddies in the general circulation. Eddy available potential energy is the source of atmospheric kinetic energy, at least in the troposphere. It is first converted into eddy kinetic energy by overturnings in east-west planes, at the scale of the cyclones and anticyclones, and the

kinetic energy associated with these eddies feeds the zonal flow against the dissipative effects of the smaller scale turbulent eddies. Although most of the zonal kinetic energy is dissipated by friction, a small portion is reconverted into zonal available potential energy by a net indirect meridional circulation.

Several features of this cycle have been substantiated by empirical and theoretical evaluations. (See White and Saltzman 1956, N. A. Phillips 1956, Kuo 1956, Wiin-Nielsen 1959, Wiin-Nielsen and Brown 1960, Wiin-Nielsen, Brown and Drake 1963, Saltzman and Fleisher 1960, 1961, Jensen, 1961, Winston and Krueger, 1961). Such energy calculations have also been extended to the stratosphere, notably by White and Nolan (1960), Reed, Wolfe and Nishimoto (1963), R. E. Newell (1964), and A. H. Oort (1964). However, the question as to what cycle, if any, prevails over periods of less than a month has not yet been resolved. In this study a contribution to this problem is made by examining the way in which atmospheric kinetic energy responds to changes in available potential energy when such changes take place over periods of between 50 days and 4 days.

In studying atmospheric energy transformations, two approaches are possible, a direct and an indirect. The direct approach consists of calculating the conversion and generation terms over a given time period and averaging the values to yield the average energy flow over that period. The empirical studies enumerated above fall into this category. Since the conversion of available potential energy into kinetic energy involves the vertical wind speed ω, such calculations may not be realistic if the vertical velocity computations are not realistic. In most cases the vertical speed was obtained either from the adiabatic method or as a by-product of a numerical prediction model where the adiabatic assumption is implicit. The use of such data has been criticized recently by Holopainen (1963), Wiin-Nielsen, Brown and Drake (1963) and Wiin-Nielsen (1964). Pending the advent of more realistic vertical velocity data, an indirect approach to the study of energy transformations may be desirable. It is the object of this paper to make a preliminary investigation of the feasibility of such a procedure.

2. The Approach Used in this Study: Time Series Analysis

The method used here consists of studying time series of daily values of some of the energy parameters introduced by Lorenz (1955) and relating them by the methods of cross-spectra analysis. A cross-spectra analysis yields two components, each a function of frequency, called the coherence and phase angle (Panofsky and Brier, 1958). The

coherence measures the degree of correlation between the corresponding harmonics of each series, while the phase angle describes the phase difference between the harmonics. Suppose that a time series of daily values of the total available potential energy and a similar series of the total kinetic energy are correlated. If the coherence is high at a certain period, say 10 days, it is very likely that changes in kinetic energy over such a period are related to changes in available potential energy at the same period. If the phase angle is small, this means that there is a tendency for increases in kinetic energy to occur with increases in available potential energy. If, on the other hand, the phase difference is 180°, then increases in kinetic energy occur with decreasing available potential energy. This is the situation that would occur in the case of an adiabatic frictionless atmosphere, where kinetic energy increases solely at the expense of the available potential energy. There may be practically no correlation between harmonics of a certain period which would be the case if, for example, changes in kinetic energy are derived mainly from a transfer of mechanical energy from without the region being considered rather than from a conversion of the available potential energy in the region. A lack of correlation could also occur if the generation of available potential energy very nearly balanced the conversion into kinetic energy. Thus a judicious examination of the characteristics of the cross spectra between any two energy parameters may reveal certain features of the energy transformations. This is the essence of the indirect approach employed in this study.

Through a program of daily computations initiated at the Meteorological Satellite Laboratory of the U. S. Weather Bureau, time series of the daily values of the following energy parameters were made available to the authors: A_e, A_z, K_e, K_z, C_a, and for comparison purposes, C_e and C_z estimated by numerical computation of ω values. These data cover the period October 1958 - June 1963 and refer to that portion of the atmosphere lying between 20°N and the pole and between 850 and 500 mb. The necessary computations are discussed in detail by Winston and Krueger (1961).

3. The Kinetic Energy Equation for the Region Considered

In general, the symbols and definitions used here are the same as used by Lorenz (1955).

Φ : geopotential
Θ : potential temperature
P : pressure
T : temperature

$\underline{v}$: horizontal wind velocity
V : magnitude of horizontal velocity
v : meridional component of horizontal velocity
g : acceleration of gravity
R : gas constant for air
Γ : lapse rate
Γ_d : dry adiabatic lapse rate
ω : individual pressure change or vertical speed
$\bar{P}_0$: average surface pressure
$\underline{F}$: frictional force per unit mass
$\underline{\quad}$: areal average over the whole area of the earth
$\underline{\underline{\quad}}$: areal average over the area of the earth lying north of 20°N
$[\ ]$: zonal average
$*$: deviation from zonal average
$'$: deviation from areal average
A_z : zonal available potential energy
A_e : eddy available potential energy
K_e : eddy kinetic energy
K_z : zonal kinetic energy
C_a : conversion of A_z into A_e
C_e : conversion of A_e to K_e
C_K : conversion of K_e into K_z
C_z : conversion of A_z into K_z
D_z : dissipation of zonal kinetic energy
D_e : dissipation of eddy kinetic energy
G_e : generation of eddy available potential energy
G_z : generation of zonal available potential energy

Upon consideration of the whole atmosphere, Lorenz (1955) has obtained the following energy equations:

$$\left.\begin{aligned} \frac{\partial \bar{A}_z}{\partial t} &= -\bar{C}_z - \bar{C}_a + \bar{G}_z \\ \frac{\partial \bar{A}_e}{\partial t} &= -\bar{C}_e + \bar{C}_a + \bar{G}_e \end{aligned}\right\} \qquad (1)$$

$$\left.\begin{aligned} \frac{\partial \bar{K}_z}{\partial t} &= \bar{C}_z - \bar{C}_K - \bar{D}_z \\ \frac{\partial \bar{K}_e}{\partial t} &= \bar{C}_e + \bar{C}_K - \bar{D}_e \end{aligned}\right\}$$

We wish to derive an analogue of this system when the region considered is not the whole atmosphere, but the polar cap region lying north of 20°N, between 850 and 500 mb.

With the aid of the hydrostatic equation, the kinetic energy equation at a point takes the form:

$$\frac{\partial k}{\partial t} + \nabla_p \cdot (k + \frac{\Phi}{g})\underline{V}_p + \frac{1}{8}\frac{\partial}{\partial p}(\omega \Phi) + \frac{\omega \alpha}{g} + \frac{\partial}{\partial p}(\omega k) + d = 0 \qquad (2)$$

where $k = \frac{V_p^2}{2g}$ and $d = \frac{\underline{V}_p \cdot \underline{F}}{g}$. Integrating over the polar cap region gives:

$$\frac{\partial \bar{\bar{K}}}{\partial t} + \int_{500}^{850} \overline{\overline{\{\nabla_p \cdot (k + \Phi/g)\}}}\, dp + \int_{500}^{850} \frac{\partial}{\partial p}\overline{\overline{(\omega k)}}\, dp + \frac{1}{g}\int_{500}^{850} \frac{\partial}{\partial p}\overline{\overline{(\omega \Phi)}}\, dp$$

$$+ \frac{1}{g}\int_{500}^{850} \overline{\overline{(\omega \alpha)}}\, dp + \int_{500}^{850} \bar{\bar{d}}\, dp = 0 \qquad (3)$$

where $\bar{\bar{K}} = \int_{500}^{850} \frac{V_p^2}{2g}\, dp$ is the average kinetic energy inside the polar cap, per unit area.

We note that equation (3) does not explicitly contain any conversion terms (i.e., terms which clearly express the physical mechanism by which energy transformations take place). For example $\int \overline{\overline{(\omega \alpha)}}\, dp$ occurs instead of $\int \overline{\overline{(\omega' \alpha')}}\, dp$ which is the transformation of available potential into kinetic energy by the sinking of colder air masses and the rising of warmer air masses. To eliminate the mean motion terms in (3), aiming at an equation containing only eddy correlations between various pairs of quantities, we use the following expansion:

$$\frac{1}{g}\int_{500}^{850} \frac{\partial}{\partial p}\overline{\overline{(\omega \Phi)}}\, dp = -\frac{1}{g}\int_{500}^{850} \bar{\bar{\Phi}}\, \overline{\overline{(\nabla_p \cdot \underline{V}_p)}}\, dp - \frac{1}{g}\int_{500}^{850} \bar{\bar{\omega}}\, \bar{\bar{\alpha}}\, dp + \frac{1}{g}\int_{500}^{850} \frac{\partial}{\partial p}\overline{\overline{(\omega' \Phi')}}\, dp \qquad (4)$$

together with the identity

$$\int_{500}^{850} \overline{\overline{\nabla_p \cdot (h\underline{V}_p)}}\,dp = \frac{-2\pi a \cos 20°}{\text{Area of earth north of } 20°N} \int_{500}^{850} [hv]_{20°N}\,dp \qquad (5)$$

which holds by virtue of Gauss's theorem for any differentiable function h (x, y, p, t). Here "a" is the radius of the earth. With these substitutions the kinetic energy equation for the polar cap takes the form:

$$\frac{\partial \bar{\bar{K}}}{\partial t} = \frac{1.41}{a} \int_{500}^{850} [kv]_{20°N}\,dp + \left\{ \overline{\overline{(\omega k)}}_{500} - \overline{\overline{(\omega k)}}_{850} \right\} + \frac{1.41}{ag} \int_{500}^{850} [\Phi' v]_{20°N}$$

$$- \frac{1}{g} \int_{500}^{850} \overline{\overline{(\omega' \alpha')}}\,dp + \frac{1}{g} \left\{ \overline{\overline{(\omega' \Phi')}}_{500} - \overline{\overline{(\omega' \Phi')}}_{850} \right\} - \frac{1}{g} \int_{500}^{850} \overline{\overline{(\underline{V}_p \cdot \underline{F})}}\,dp \qquad (6)$$

If the wind at 20°N can be assumed to be geostrophic, at least above the surface layer as the findings of Jordan (1953, 1956) indicate, the third term on the right of (6) vanishes. The physical interpretation of the remaining terms in (6) is as follows:

The first term is the advection of kinetic energy at the southern boundary. Its value can be estimated, using data published by Saltzman, Gottuso and Fleisher (1961) for the geostrophic wind at 500 mb. These data show that the winter average value is about 35 ergs $cm^{-2}sec^{-1}$ compared to some 6 ergs $cm^{-2}sec^{-1}$ during the summer.

The second term on the right of (6) represents the net vertical flux of kinetic energy into the region. Jensen (1961) gives a value of about 260 ergs cm^{-2} sec^{-1} for this term, averaged over the month of January 1958, and computed from adiabatic vertical velocities. An average value of about 1490 ergs $cm^{-2}sec^{-1}$ is also given by Jensen for the conversion term, the fourth term on the right of (6). This value agrees with those obtained by other authors. (See Introduction.)

The interpretation of the fifth term is more difficult. A similar term was encountered by Jensen (1961) and by Reed, Wolfe and Nishimoto (1963). In fact, this term is identical to Jensen's "potential energy flux" term, if we assume the wind to be geostrophic at 20°N. Jensen obtained a value of about -3870 ergs $cm^{-2}sec^{-1}$ for the 850 - 500 mb layer. A large negative value was also found by Reed, Wolfe and Nishimoto (1963)

during the second phase of the stratospheric warming of early 1957; it accounted for the large decrease in the zonal kinetic energy of the stratospheric layer they were studying, despite the indications that both zonal available potential and eddy kinetic energy were being converted into zonal kinetic energy.

In both of these studies adiabatic vertical velocities were used; but if such data preserve at least the relative order of magnitude of the different terms in (6) which involve ω, the conversion and geopotential flux terms must be the two most important ones in influencing the kinetic energy of the polar cap region considered in this study.

The available potential energy in the layer is also subject to the effect of flux processes, which may increase or decrease the available energy. All of these considerations must be borne in mind in interpreting the results of the spectral analysis.

4. Computation of the Spectra

In this section the particular methods employed in carrying out the spectral computations are discussed. The reader is referred to Panofsky and Brier (1958), Blackman and Tukey (1958), and Holloway (1958) for a more detailed treatment of time series techniques. Before attempting any spectral computations it is important to know the time structure of the data, i.e. which frequencies are the most important in accounting for the overall variation in the data. Such knowledge determines the methods that need be employed in obtaining meaningful estimates. Figure 1 which presents the variation of monthly mean values of the energy parameters was kindly made available to the authors by Messrs. J. S. Winston, A. F. Krueger and D. A. Haines of the Meteorological Satellite Laboratory.* It indicates that, with the exception of C_Z, all parameters have a well-defined and in most cases marked seasonal variation. Apart from this large annual variation there may be other important periodicities whose effect is perhaps too small to be detected by taking monthly averages, as was done in the case of Figure 1. To find these periodicities a variance spectrum can be computed for each parameter. A variance spectrum is, basically, equivalent to a graph of the square of the amplitude versus frequency after each series has been resolved into its Fourier components. Unfortunately,

*The data pertaining to this figure have now been published in somewhat revised form. See Krueger, Winston and Haines (1965).

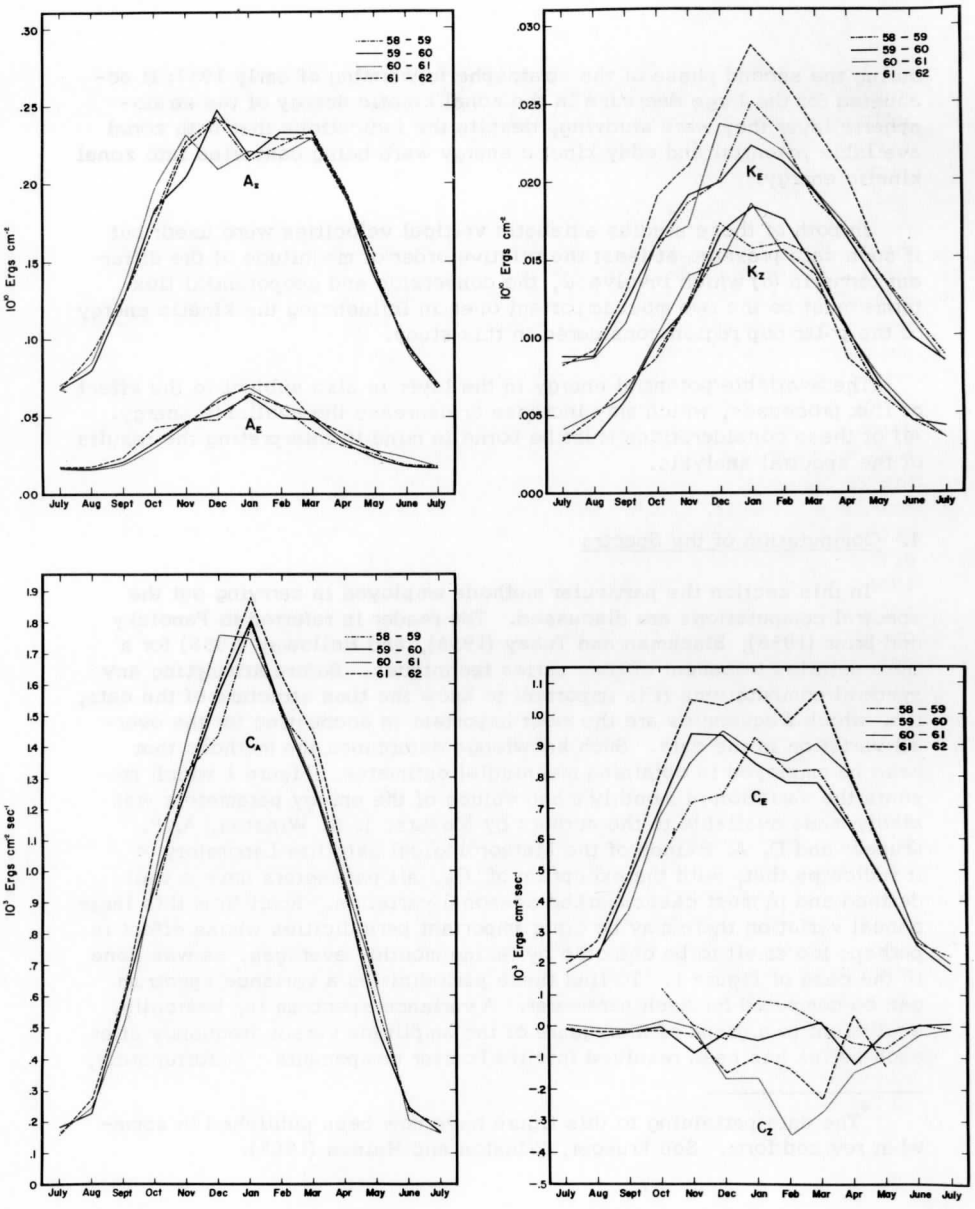

FIGURE 1. Annual Variations of Various Energy Parameters (after Winston, Krueger and Haines).

due to the presence of noise in all measurements the method of squaring Fourier coefficients yields unreliable estimates. Consequently, the method outlined by Tukey (Blackman and Tukey, 1958) was adopted here. This method yields variance estimates by calculating the Fourier transform of the autocorrelation function.

In applying the method to five years of data it is permissible to sample the record at fifty lags without losing statistical significance, giving variance estimates at periods of 100 days and less. In the case of data with a large annual variation a technique equivalent to prewhitening (i.e., a type of filtering that reduces the annual variation) is necessary prior to computing by Tukey's method. If the large annual variation is not attenuated prior to computing, there results "a diffusion of spectral energy toward lower spectral levels" (Munk, Snodgrass and Tucker, 1959) so that the estimates at the shorter periods appear larger than they really are. Here, both the very low frequencies, associated with the seasonal variation, and the very high ones, due to noise, were attenuated by passing the data through a suitably designed band pass filter. Once the approximate shape of the true spectrum is known, such a filter can be constructed with the aid of two exponential smoothing functions of the form $e^{-t^2/2\sigma^2}$ (Holloway, 1958). The frequency response of the filter is selected by choosing the parameter σ in each function in such a way that the intermediate frequencies are emphasized so that the filtered data now displays the characteristics of "white noise." The variance spectrum can then be estimated from the filtered data and later corrected for the effect of smoothing by dividing each estimate by the square of the frequency response of the filter at the frequency of the estimate (Holloway, 1958).

By and large, the same precautions are necessary in computing cross-spectra to assure stability. Once the cross-spectra are estimated from the filtered series, it is not necessary to correct for the effect of smoothing because in our case the smoothing operator is an even function (Munk, Snodgrass and Tucker, 1959). In this manner power and cross-spectral estimates were obtained at periods of 100 days, 50 days, 33.3 days, 25 days ... and 2 days. Each period listed here is that corresponding to a central frequency. Thus, a period of 50 days corresponds to the central frequency, 4/200, of a frequency band which extends from 3/200 to 5/200 or from periods of 66.7 days to 40 days. The estimate at 50 days is a measure of the average spectral density in that frequency band, but with much greater weight given to the central frequency. The same holds true in the case of the coherence and phase angle.

The definition of coherence used here is that given by Goodman (1957). Under the hypothesis that the process generating the time functions is Gaussian, Panofsky and Brier (1958) have calculated the probability that the coherence will have a value greater than or equal to a certain limit β, when it is really zero. This is expressed by

$$\beta = \sqrt{1 - (p)^{1/f-1}}$$

which says that if the number of degrees of freedom is f, the probability is p, that a coherence greater than or equal to β will be found by accident. This expression is used to establish the statistical significance of the coherences obtained in this study.

5. Discussion of Results: The Variance Spectra

The normalized variance spectra for periods less than or equal to 33 days are exhibited in Figures 2, 3, 4, and 5. The curves appearing on each diagram are the result of joining the point estimates by means of straight lines. Because of relatively large intervals between periods greater than 33 days (for example, the interval from 33 to 50 and from 50 to 100 days) the results at these longer periods (50 and 100 days) are not included. It is not possible to make convincing statements concerning the behaviour of the spectra within these large time intervals, and to obtain estimates at intermediate periods would require the computation of a larger number of lags than that used in this preliminary study. Toward the very short periods the spectrum has been truncated either because the estimates became erratic due to the presence of noise or because the variance reached a value less than 10^{-10}.

a) available potential energy: Although the spectra for both zonal and eddy available potential energy possess the same quasi-monotonic decrease in variance with decreasing period, there is more concentration of variance at longer periods in the case of A_z. At periods shorter than 25 days the normalized variance in A_e is always larger than that in A_z, so that as a function of time A_e tends to fluctuate relatively more rapidly than A_z. This difference may be a reflection of the different physical mechanisms that can cause changes in each of these parameters. Changes in A_z are mainly due to changes in the north-south temperature gradient and the latter is a very persistent feature of the atmosphere. By contrast, A_e is subject to more irregular effects such as varying amounts of conversion of A_z to A_e and of direct generation or destruction by non-adiabatic effects. The latter include differential heating due to radiation,

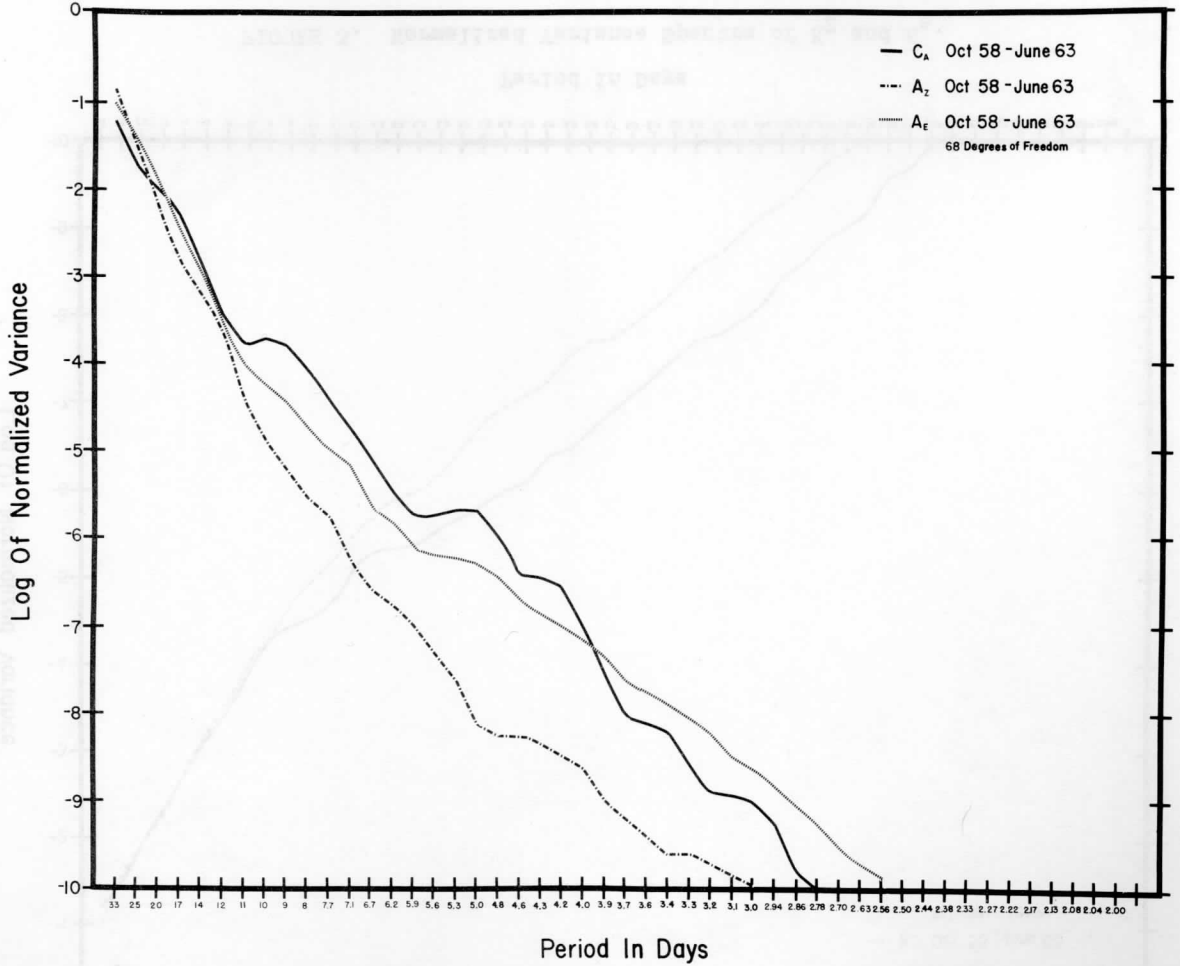

FIGURE 2. Normalized Variance Spectra of A_Z, A_e, and C_A.

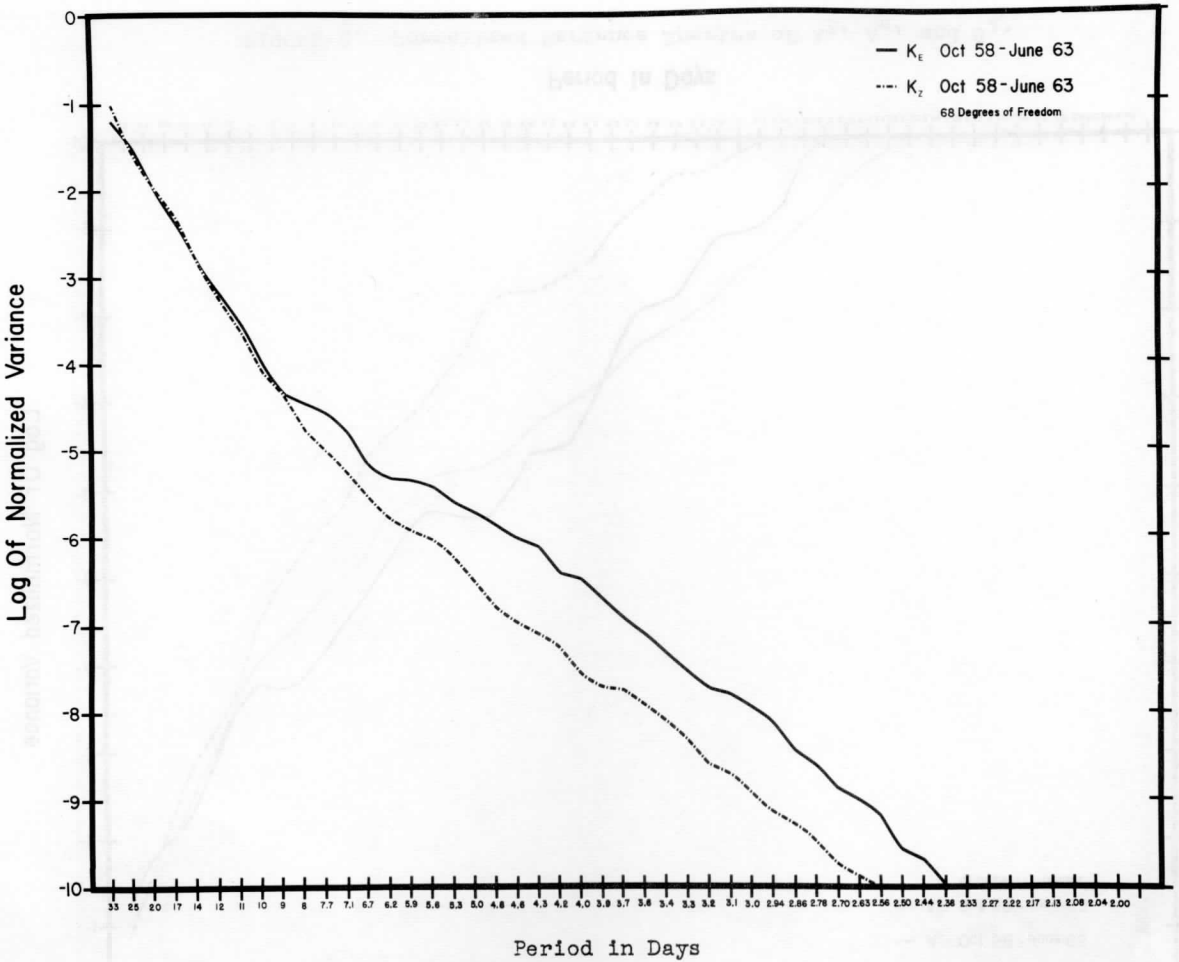

FIGURE 3. Normalized Variance Spectra of K_Z and K_e.

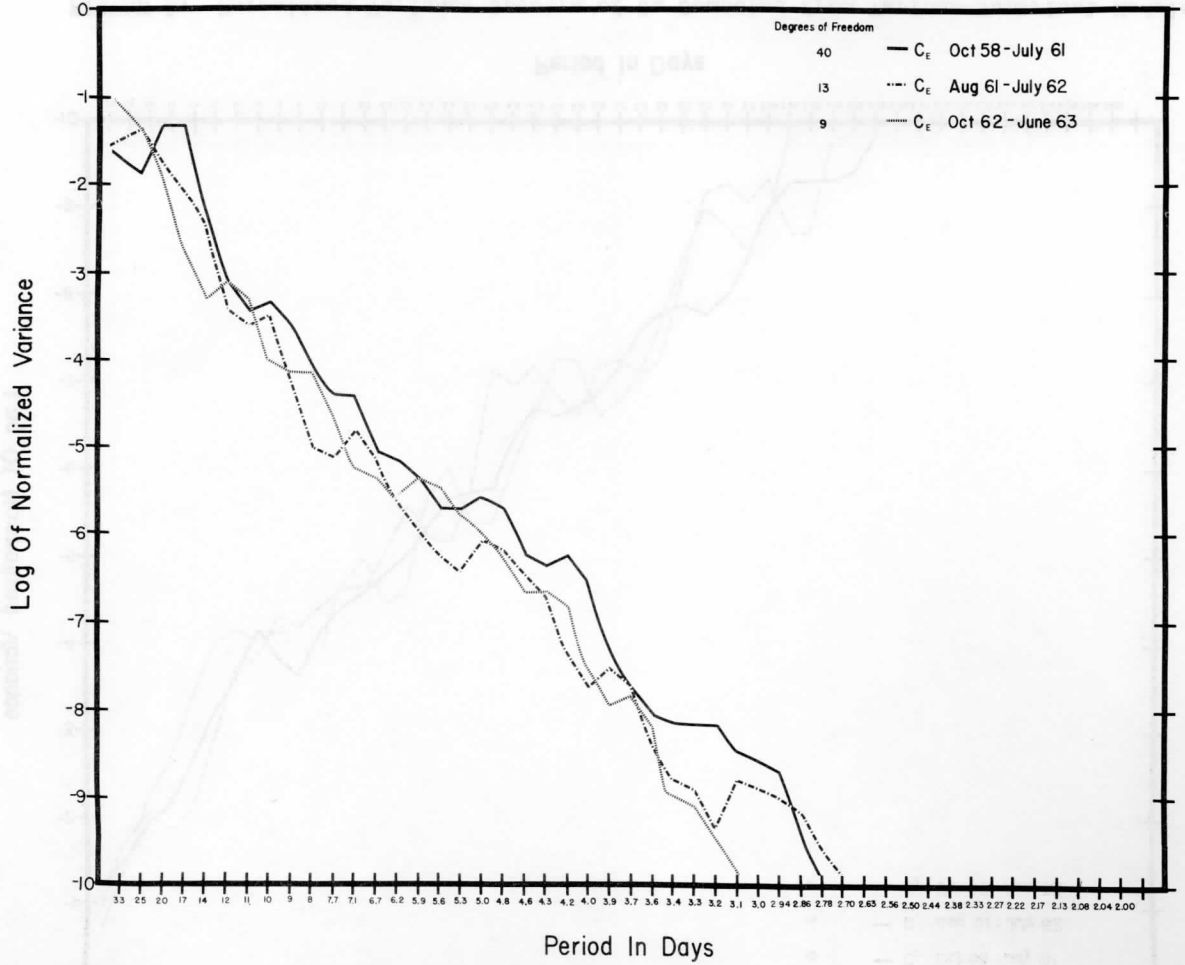

FIGURE 4. Normalized Variance Spectra of C_E Computed from Various Numerical Models

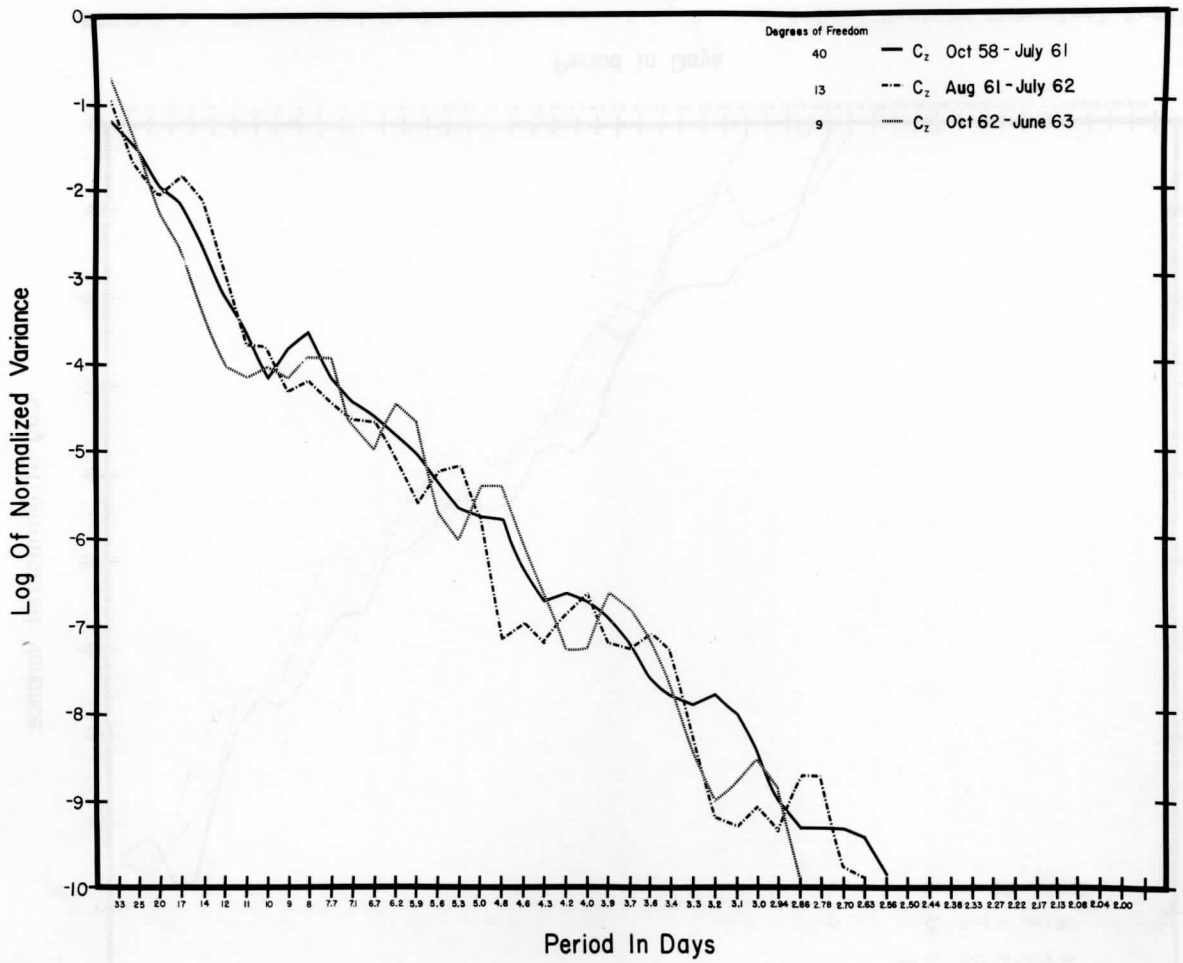

FIGURE 5. Normalized Variance Spectra of C_Z Computed from Various Numerical Models

latent heat release and eddy conduction. Such effects could serve to introduce substantially higher frequency oscillations in A_e, resulting in the relatively greater variance at shorter periods. It is perhaps this difference in character of the two time series that accounts for the low coherence at all periods between these two parameters as will be shown later. Another feature of these spectra is the absence of holes or peaks. Every discrete frequency contributes some variance to the spectrum and there are no indications of preferred periodicities in either parameter.

b) kinetic energy: As in case (a) the normalized spectra of eddy and zonal kinetic energy have similar appearances but the variance is more equitably shared in the case of the eddy kinetic energy. In fact the spectra for K_e and K_z practically coincide until a period of 10 days is reached after which K_z begins to decrease faster with increasing frequency. Thus, periodicities of less than 10 days contribute more variance in K_e than in K_z, indicating perhaps the influence of forming and dissipating storm systems. There are again no indications of preferred modes of oscillations in either parameter. It is quite possible that such modes may prevail in the atmosphere but not in the data analyzed in this study, since the daily statistic used here represents a quantity integrated over such a large portion of the atmosphere that these modes may have been obscurred in the averaging process.

c) the conversion terms: The spectrum for C_a (Figure 2) has the same characteristics as those already discussed. In the case of C_e and C_z (Figures 4 and 5) where the data record was divided into three parts owing to inhomogeneity,* the spectra vary depending on the method used in obtaining the vertical speed ω. Thus for the period October 1958 — July 1961 (two level model) C_e and C_z have relatively smooth spectra with only occasional small peaks. For the period October 1962 — June 1963 (three-level model) more fluctuations appear probably because with its greater vertical resolution, the three-level model is more capable of detecting higher frequency oscillations in $\overline{\omega'\alpha'}$ than is the two-level model. Whether or not such oscillations are significant is considered

*From October 1958 through July 1961 vertical velocities were obtained as a by-product of the two-level model. The vertical velocity data from August 1961 to July 1962 are not consistent. During that period tests were being conducted at the National Meteorological Center using various multi-level models prior to adopting the three-level model. The latter was put into operation in October 1962. Thus it was necessary to divide the data record for C_e and C_z into three parts: October 1958 - July 1961, August 1961 - July 1962, October 1962 - June 1963.

later when the cross-spectra of C_e vs K_e are discussed. For the period August 1961 - July 1962 the spectra also fluctuate, but little meaning can be attached to the individual peaks owing to the inconsistency in the data. In fact, it will be shown later that this portion of the data is poorly correlated with K_e and K_z in comparison to the portions already discussed.

6. Discussion of Results: The Cross-Spectra

The coherence estimates obtained for time series of various energy parameters are presented in Table 1 where the distribution of coherence estimates with respect to the 1, 5, 10, 20, 30, and 50 percent probability levels is displayed. This table is divided into three groups of periods. In the first group, the estimates for periods ranging between 100 days and 10 days are shown. The spectral analysis yields 10 estimates in that range; i.e., at about 100, 50, 33, 25, 20, 17, 14, 12, 11, and 10 days. This group will be referred to as "long periods." The second group consists of 23 estimates between 9 days and 3 days and will be denoted "intermediate periods." The last group, which will be called "the short periods," contains 17 estimates at periods between 2 days and 3 days. Because of the presence of noise at these high frequencies, not a great deal of significance can be attached to these short periods. The number of estimates which exceed or equal the probability levels listed at the top of each column is given for each group. For example, in the case of K_e vs K_z there are no estimates better than or equal to the 50 percent limit at long periods. At intermediate periods all 23 estimates are better than the 50 percent limit, 19 being greater than the 1 percent limit.

We shall consider coherence values greater than the 5 percent limit as indicative of a direct or indirect physical mechanism linking the two parameters. This is most likely to be the case when large coherence values occur consecutively within a certain group of periods. In the following the discussion of the cross-spectra will be organized about the general circulation theory outlined in the introduction as well as its modification for the region considered in this study.

Let us begin with a consideration of the parameters involved in the transformation of zonal available to eddy available potential energy: A_z, A_e, C_a. The zonal and eddy generations of available potential energy also enter here but were not available for analysis. Significant correlations are found for A_z versus C_a and A_e versus C_a but the coherences in the A_e versus A_z spectra are generally low. In the case of A_z versus C_a, 10 out of 10 estimates at long periods are better than of equal to the 5 percent limit. At intermediate periods there is a group of 12 consecutive estimates better than the 10 percent limit extending

TABLE 1

DISTRIBUTION OF COHERENCES FOR VARIOUS PAIRS OF ENERGY PARAMETERS

Period Range (in days)	A_e vs A_z (percent)						A_z vs C_a (percent)					
	1	5	10	20	30	50	1	5	10	20	30	50
10 - 100 (10 estimates)	2	2	4	6	9	10	9	10	10	10	10	10
3.03 - 9.09 (23 estimates)	0	0	0	1	3	3	8	10	12	14	15	16
2.0 - 2.94 (17 estimates)	6	6	6	6	6	7	7	7	7	7	8	8
	K_e vs K_z (percent)						A_z vs K_z (percent)					
10 - 100 (10 estimates)	0	0	0	0	0	0	0	0	0	0	0	1
3.02 - 9.09 (23 estimates)	19	20	20	21	22	23	0	0	0	0	0	0
2.0 - 2.94 (17 estimates)	17	17	17	17	17	17	6	6	6	6	6	6

TABLE 1 (continued)

Period Range (in days)	A_e vs C_a (percent) 1	5	10	20	30	50	A_e vs K_e (percent) 1	5	10	20	30	50
10 - 100 (10 estimates)	7	9	9	10	10	10	10	10	10	10	10	10
3.03 - 9.09 (23 estimates)	2	3	3	4	4	4	23	23	23	23	23	23
2.0 - 2.94 (17 estimates)	6	6	6	6	6	6	17	17	17	17	17	17
	K_z vs C_z (1) (percent)						K_z vs C_z (2) (percent)					
10 - 100 (10 estimates)	0	0	0	0	0	1	0	0	0	1	1	1
3.03 - 9.09 (23 estimates)	0	0	2	3	4	6	0	0	0	0	1	1
2.0 - 2.94 (17 estimates)	12	14	15	15	15	16	3	3	3	4	4	5

(1) indicates data from October 1, 1958, through July 31, 1961, when vertical velocities were obtained from two level model.

(2) indicates data from August 1, 1961, through July 31, 1962, when vertical velocities were obtained from a variety of models

TABLE 1 (continued)

Period Range (in days)	K_e vs C_e (percent) [1]						K_e vs C_e (percent) [2]					
	1	5	10	20	30	50	1	5	10	20	30	50
10 - 100 (10 estimates)	5	6	8	8	9	9	0	0	1	2	2	5
3.03 - 9.09 (23 estimates)	0	6	8	9	9	11	0	0	0	0	0	0
2.0 - 2.94 (17 estimates)	11	11	11	11	11	11	0	0	0	0	2	4
	K_z vs C_z (percent) [3]						A_e vs K_z (percent)					
10 - 100 (10 estimates)	2	3	3	5	6	6	0	0	0	0	2	3
3.03 - 9.09 (23 estimates)	4	5	6	7	8	10	20	20	21	21	21	23
2.0 - 2.94 (17 estimates)	3	4	4	4	4	4	17	17	17	17	17	17
	K_e vs C_e (percent) [3]						A_z vs K_e (percent)					
10 - 100 (10 estimates)	4	4	5	8	8	8	2	3	3	3	5	9
3.03 - 9.09 (23 estimates)	0	1	1	1	4	10	0	0	0	0	0	0
2.0 - 2.94 (17 estimates)	12	12	12	13	14	14	3	3	3	3	3	3

[1] indicates data from October 1, 1958, through July 31, 1961, when vertical velocities were obtained from two level model.

[2] indicates data from August 1, 1961, through July 31, 1962, when vertical velocities were obtained from a variety of models.

[3] indicates data from October 1, 1962, through June 30, 1963, when vertical velocities were obtained from three level model.

from periods of nine to four days. Thus there is evidence for a systematic relationship between A_z and C_a from periods of 100 days down to about four days. In the case of A_e versus C_a we find significant correlations at long periods where 9 out of 10 estimates exceed the 5 percent limit. At intermediate periods only 3 out of 23 estimates are better than the 10 percent limit and at short periods there are no significant estimates other than those expected from noise. Thus, here the relationship is not maintained at intermediate periods as was the case above, probably because the generation or destruction of A_e and its conversion to K_e became involved at intermediate periods. Such a conclusion is consistent with the results of the variance spectra analysis where it was inferred that A_e as a function of time fluctuates more than A_z. A tendency for A_e to behave more irregularly than A_z was also found by Horn (1961), but for a much smaller data sample. It is probably this difference in character of the two parameters that accounts for the low coherence at most periods in the A_e-A_z spectra.

In the second stage of the cycle the parameters involved are A_e, K_e and C_e. Data for C_e (and also C_z) are labeled (1), (2) and (3) in the coherence table corresponding to the numerical weather model or models that were used in obtaining the vertical speed ω. This is indicated in the table. Excellent results are obtained in the case of A_e versus K_e, all estimates being greater than the 1 percent limit. Consideration of the variance spectra of these two parameters indicates the probable existence of noise at very short periods so that the estimates at these periods are unreliable. Nevertheless it seems fairly certain that a close relationship exists between K_e and A_e from periods of about 100 days down to about 2.5 days. Such a relationship may appear to merely verify the fact that geostrophic balance and the thermal wind relationship are good approximations in the atmosphere. If this were the case one would expect nearly simultaneous correlations, (i.e., a phase lag of nearly zero at most periods). However, at the longer periods, the magnitude of the phase difference between corresponding harmonics is near 25°, the magnitude generally decreasing with decreasing period. The sign of the angle appears doubtful at most periods in this cross-spectrum as well as in the other cross-spectra. What is really needed to resolve this uncertainty is a means of estimating the probable error in the phase angle.

In the case of K_e versus C_e there is no indication of any relationship with the data for period (2) during which values were obtained from a variety of models. This lack of coherence is not surprising. On the other hand, K_e versus C_e for period (1), (two-level model), produced 8 out of 10 estimates which exceeded the 10 percent limit at long periods. For period (3), (three-level model), only five out of ten estimates are

significant at the 10 percent level at long periods. At periods shorter than ten days, the two-level model consistently seems to portray the eddy conversion better than the three-level model (19 versus 13 estimates above the 10 percent level).

The coherence between K_e and K_z has values below the 50 percent limit at long periods, but the relationship improves markedly at intermediate and short periods where the majority of estimates are better than the 1 percent limit. This is also the case for A_e versus K_z, although here the relationship must be of an indirect nature since there is no mechanism that can convert eddy available potential energy directly into zonal kinetic energy (Lorenz, 1955).

By way of summary, the following pairs are very well related at periods shorter than 10 days: $A_e - K_e$, $A_e - K_z$, $K_e - K_z$. This tends to support a systematic relationship between the three energy parameters A_e, K_e, K_z, although it is not possible to say in which direction the energy flow takes place at any one group of periods. By contrast, K_z is poorly correlated at periods greater than 10 days to every other energy parameter. This is the situation which would prevail if K_z were not appreciably influenced, at longer periods, by the energy processes inside the polar cap, but rather that changes in K_z were brought about by large transfers of energy from outside the polar cap region (for example, the transfer expressed by the fifth term of equation 6). In this connection it is interesting to note that in the stratospheric studies of Reed, Wolfe and Nishimoto (1963) a similar situation was encountered; during the second phase of the warming, changes in K_z were due mainly to an abnormally high value of the zonal component of the geopotential flux term.

In the last stage of the energy cycle, zonal kinetic energy is dissipated by friction with a small residual being reconverted into zonal available potential energy. The mechanism that can affect such a conversion is a net indirect meridional circulation. Empirical studies (Starr, 1953) have revealed that such a circulation is very weak. The low coherences between A_z and K_z at all periods would tend to support these findings.

7. Conclusion

In the preceding, a method was presented for studying certain aspects of energy transformations which avoids the difficulties involved in a direct study of the conversion terms. The variance and cross-spectra analyses of time series of the basic energy parameters for the 850 - 500 mb polar cap north of 20° N, may be interpreted as supporting an energy cycle at periods between 3 days and 10 days. It appears that at longer periods any

preferred periodicity of the energy cycle within the polar cap is destroyed due to the transfers of energy from outside the region as well as the effects of heat sources and sinks within the region.

The indirect approach used here is limited by the fact that the interpretation of the spectra is not unequivocal in view of the several factors acting simultaneously on any one parameter. Furthermore, the details of the processes are obscured because of averaging over such an extensive area. With data from additional levels it should become possible to study more limited areas such as a specific latitude belt. The partitioning of the data according to wave number before undertaking time series analyses may yield insight into the significance of scale size in energy transformations.

8. References

Blackman, R. B., and J. W. Tukey, 1958: The measurement of power spectra from the point of view of communications engineering. Bell System Tech. J., 37, pp. 185-282 and 485-569.

Goodman, N. R., 1957: On the joint estimation of spectra, cospectrum, and quadrature spectrum of a two dimensional stationary Gaussian process. Scientific Paper No. 10, Engineering Statistics Lab., New York University.

Holopainen, E. O., 1963: On the dissipation of kinetic energy in the atmosphere. Tellus 15, 1, pp. 26-32.

Holloway, J. L., 1958: Smoothing and filtering of time series and space fields. Advances in Geophysics, Vol. 4, Academic Press, New York, pp. 351-389.

Horn, L. H., 1961: A statistical investigation of the relationship between the potential energy and the kinetic energy of the atmosphere. Ph. D. thesis, Department of Meteorology, University of Wisconsin, Madison, Wisconsin.

Jensen, C. E., 1961: Energy transformations and vertical flux processes over the northern hemisphere. J. Geophys. Res. 66, 4, pp. 1145-1156.

Jordan, C. L., 1953: A comparison between observed and geostrophic winds in low latitudes. Quart. J. R. Meteor. Soc., 153-156.

Jordan, C.L., 1956: An experiment in low latitude numerical prediction with the barotropic model. J. Meteorology, 13, pp. 223-235.

Krueger, A.F., Winston, J.S., and D. A. Haines, 1965: Computations of atmospheric energy transformations for the northern hemisphere for a recent five year period. Monthly Weather Review, 93, 4, pp. 227-238.

Kuo, H.L., 1956: Energy releasing processes and stability of thermally driven motion in a rotating fluid. J. Meteorology, 13, pp. 82-101.

Lettau, H.H., 1954: Notes on the transformation of energy to and from eddying motion. J. Meteorology, 11, pp. 196-201.

Lorenz, E.N., 1955: Available potential energy and the maintenance of the general circulation. Tellus 7, 2, pp. 157-167.

Munk, W.H., F. E. Snodgrass, and M. J. Tucker, 1959: Spectra of low frequency ocean waves. Bulletin of the Scripps Institution of Oceanography, 7, 4, pp. 283-312.

Newell, R. E., 1964: Stratospheric energetics and mass transport. Pure and Applied Geophys., 58, pp.

Oort, A.H., 1964: On the energetics of the mean and eddy circulations in the lower stratosphere. Tellus, 16, pp. 309-327.

Panofsky, H.A. and G. Brier, 1958: Some applications of statistics to Meteorology. Pennsylvania State University, University Park, pp. 113 and 155-158.

Pfeffer, R.L., 1957: On the physical significance of energy transformation functions. Final Report 1957, Contract No. AF 19(604)-1000, Studies of the Atmospheric General Circulation II, Mass. Inst. Tech., pp. 42-45.

Phillips, N.A., 1956: The general circulation of the atmosphere: A numerical experiment. Quart. J. R. Meteor. Soc., 82, pp. 123-164.

Reed, R.J., J. L. Wolfe, and H. Nishimoto, 1963: A spectral analysis of the energetics of the stratospheric sudden warming of early 1957. J. Atmospheric Sciences, 20, 4, pp. 256-275.

Saltzman, R. and A. Fleisher, 1960: The modes of release of available potential energy. J. Geophys. Res., 65, 4, pp. 1215-1222.

Saltzman, B. and A. Fleisher, 1961: Further statistics on the modes of release of available potential energy. J. Geophys Res., 66, 7, pp. 2271-2273.

Saltzman, B., R. M. Gottuso and A. Fleisher, 1961: The meridional eddy transport of kinetic energy at 500 mbs. Tellus 13, 2, pp.

Starr, V. P., 1953: Note concerning the nature of the large scale eddies in the atmosphere. Tellus, 5, pp. 494-498.

White, R. M., and B. Saltzman, 1956: On conversions between potential and kinetic energy in the atmosphere. Tellus, 8, pp. 357-363.

White, R. M. and G. F. Nolan, 1960: A preliminary study of the potential to kinetic energy conversion process in the stratosphere. Tellus, 12, pp. 145-148.

Wiin-Nielsen, A. and J. A. Brown, Jr., 1960: On the distribution of heat sources and sinks in the lower troposphere and the corresponding generation of available potential energy. Proceedings of the International Symposium on Numerical Weather Prediction, Tokyo, 1960.

Wiin-Nielsen, A., J. A. Brown, and M. Drake, 1963: On atmospheric energy conversions between the zonal flow and the eddies. Tellus, 15, pp. 261-279.

Wiin-Nielsen, A. 1964: On energy conversion calculations, Monthly Weather Review, 92, pp. 161-167.

Winston, J. S. and A. F. Krueger, 1961: Some aspects of a cycle of available potential energy. Monthly Weather Review, 89, 9, pp. 307-318.

The Role of Latent and Sensible Heat for the Development of a High Pressure System over the Subtropical Andes, in the Summer

Gabriel Jules Gutman and Werner Schwerdtfeger

Department of Meteorology
University of Wisconsin

Abstract: The circulation over the Altiplano of Bolivia gives evidence of a high reaching anticyclone during the summer months, whereas in winter there is a straight West-East flow, at least in the layers between 500 and 100 mb.

The wind and thermal wind over Antofagasta (West Coast of South America, at the Tropic of Capricorn) indicate that there must be a heat source to the East of the station, that is over the interior of the continent in the warm season, November through March. From an analysis of these winds and surface reports for the month of January, the vertical structure of the atmosphere over the Altiplano is derived, for conditions with and without thunderstorms. On this basis, the limits for the magnitude of the high pressure system can be established.

TIROS II radiation data (8-12 microns) are used to illustrate the change of the cloud pattern over the area during the course of the day. A tentative heat budget of the region is calculated, leading to the conclusion that the high pressure system is maintained by the latent heat released in the violent thunderstorms which characterize the weather conditions of the Altiplano in summer, and to a lesser degree by the sensible heating of the atmosphere over the plateau.

1. Introduction

It is a characteristic of the general circulation of the Earth's atmosphere that there are some persistent deviations from the ideal, average planetary pattern of zonal winds. Thus, an anticyclonic

deformation of the streamfield is commonly found over middle-latitude mountain chains where these present a major obstacle to the main flow. The position of subsequent, quasi-stationary troughs appears to be related to the orographic features of our planet (Namias and Clapp, 1951).

The question then arises whether these phenomena are to be interpreted as the consequence of "thermal" or of "dynamic" processes. More adequately, however, one may ask over which part of the Earth and in which season one or the other of these two processes must be considered the dominating one.

For the Andes of South America, for instance, Bolin (1950) has stated (and this notion has been carried over into various textbooks) that the apparent deviation from the ideal planetary pattern is dynamically produced. He accounted for a ridge over this mountainous terrain, applying the theorem of conservation of potential vorticity. This consideration may be appropriate when one refers to the middle latitude part of the Andes, south of the latitudes of the subtropical high pressure belt at sea level where pressure and temperature in the lower troposphere decrease polewards and thus the wind field in the lower layers west of the Andes shows a component from the West (that is, against the mountains) and where the assumption of adiabatic motions is to a certain degree justified. However, the conditions in the region of the subtropical Andes, between 30 and 15°S, are different. Nevertheless, in this subtropical region there is, in the summer, and only in summer, a pronounced anticyclonic ridge at least in the upper half of the troposphere and lower stratosphere.

Various studies of the atmospheric circulation pattern over mountainous terrain with extended elevated plateaus, such as in Tibet and Bolivia, have led to conflicting opinion. In several papers, since 1950, Flohn (1950, 1953, 1959, 1960) described the high reaching summer anticyclone over the central Asian highlands and related this phenomenon mainly to the pronounced sensible heating of the air over the Tibetan plateau. Rangarajan (1963), however, claims that the sensible heat transfer in the lowest layers, surface to about 500 mb, could not explain the anticyclonic pattern deduced from his analysis of 500 mb heights; he attributes this feature to the heating of the Asian continent as a whole.[1] In this context, it is of interest that Rangarajan quotes Guibaut (1948) as saying ". . and the best season for travelling in Tibet

---

1. Flohn's comments on this contention will also appear in the Australian Meteorological Magazine, 1965. (personal communication).

is autumn. In high summer, the rainfalls are so frequent that they hinder the caravans. The soil of the upper valleys,drenched with water which the ice has settled on it, is dotted with swamps and pools.... The Himalayas cannot stop the progress of the clouds which the monsoon carries along with it." This is meant to illustrate the point that there is too much cloudiness for the plateau to be a source of great sensible heat but no mention is made of the pronounced diurnal variation of cloudiness, which must be an important characteristic.

For the Altiplano of the subtropical Andes, the main subject of the present study, Schwerdtfeger (1961) stated that the summer anticyclone must be thermally produced and maintained, by the intense sensible heating of the plateau and by the latent heat released in thunderstorms. For this region, there exists much evidence of severe thunderstorm activity during the summer months, the most impressive reports provided not by the synoptic observations nowadays made at relatively protected places, but by explorers of the past century who travelled through the almost unihabited mountains, and by old pilots who have flown in Bolivia in the early years of commercial aviation. The description given by Reck (1865) is probably the best illustration of this. He states, "Almost always, the rainshowers are accompanied by violent thunderstorms, hail, and snow. The thunderstorms seldom appear before noon, and much more frequently in the afternoon, evening, and night; their intensity surpasses all imagination of anybody who has experienced thunderstorms in the old continent, even in its highest inhabited regions. The ground is trembling, massive stone buildings shaking, windows and doors rattling and chattering as if there were an earthquake. During my journeys at the High Plateau proper, I have observed the thunderstorms between 2 and 5 P.M."

This study is an attempt to demonstrate that the summer high formed over the subtropical Andes is thermally produced by a combination of sensible heating and the release of latent heat, the latter process being the more important one. Similar considerations may apply to the Tibetan Highland.

2. Description of Wind Field

On the basis of mean monthly wind data over Antofagasta (23°25'S, 70°28'W, 137 m, on the west coast of the continent) for 1957-1963 (United States Weather Bureau, 1957-1963), one can readily see the march of the resultant winds with seasons at 200 mb (fig. 1). The annual variation is similar, but not as striking at 300 mb. In the summer season, the resultant wind (parallel to the mean contour lines of the constant

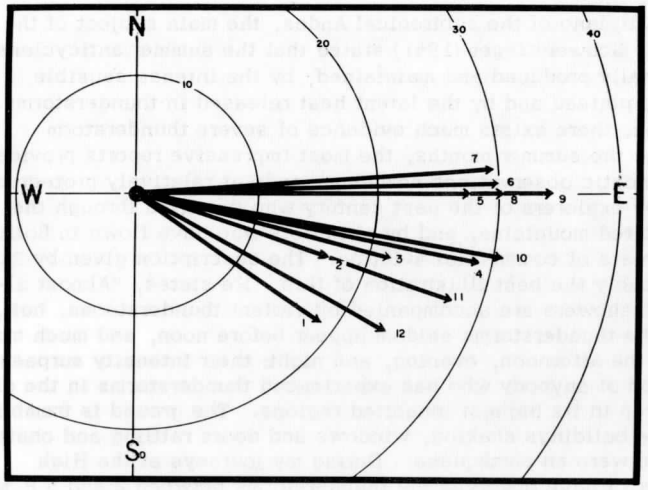

FIGURE 1. Mean monthly resultant winds at 200 mb, in m/sec, Antofagasta, 1958-63.

pressure surfaces) indicates greater height values at the 200 mb level toward east, that means over the Altiplano. In the winter, the resultant winds shift to a slightly south of west direction and the feature of the relatively high pressure over the Andes is thus absent.

Correspondingly, the thermal winds, computed between 300 and 200 mb using the same data as previously, indicate a pattern that changes with season. The isobaric temperature gradient, which is perpendicular and proportional to the thermal wind, has been plotted (fig. 2); it will be taken, in future discussion, as the vector pointing towards higher temperature. It is in the direction of the High Plateau in the summer months; in the winter months, it is directed towards the tropical Pacific Ocean.

Using the daily wind observations as given on form WBAN 33 of the National Weather Records Center, U.S. Weather Bureau, one can test whether this change is likely to be a chance effect. This has been done for the 200/300 mb thermal wind vectors of January and July. It is found that their difference is significant, i.e., it differs from zero for both the x (W-E) and y (S-N) component at the 99.9% probability level. More generally, fig. 2 also suggests that the isobaric temperature gradient in the upper troposphere over Antofagasta for the 4 months period, June through September, differs remarkably from that for the 5 warm months period, November through March. No further significance test was considered necessary.

The following analysis will now be based mainly on the data for the month of January as a typical summer month over the Altiplano. The isobaric temperature gradients in various layers between 500 and 150 mb were plotted for both times of day, i.e., 0000 and 1200 GCT,[2] (fig. 3). It is obvious that the differences between 8 A.M. and 8 P.M. l.t. are not significant. However, an interesting result does come to light from this illustration. From 500 mb to 200 mb there is a strong onshore directed temperature gradient; 200-175 mb is characterized by a weak and indistinct temperature gradient, while above 175 mb the gradient is strong and approximately opposite in direction.

---

2. GCT is defined as Greenwich Civil Time. Local time will be denoted by l.t.; 1200 l.t. is 1200 local time. Local time is approximately 4 1/2 hours earlier than Greenwich Civil Time (1200 GCT = 0730 l.t.; 0000 GCT = 1930 l.t.)

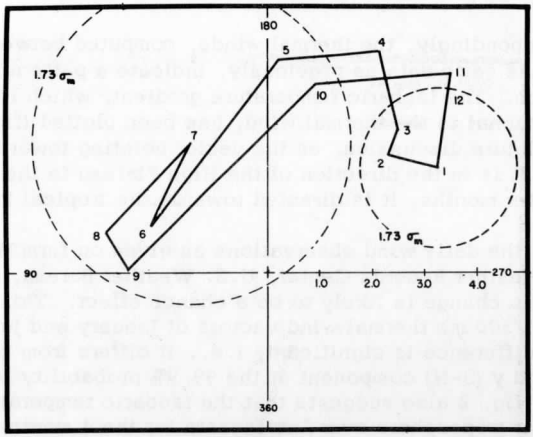

FIGURE 2. Mean monthly isobaric temperature gradient of the 200/300 mb layer, Antofagasta, 1958-63; units: °C/100 km. The values are plotted in hodograph form, with the number of the month at the end point of each vector.

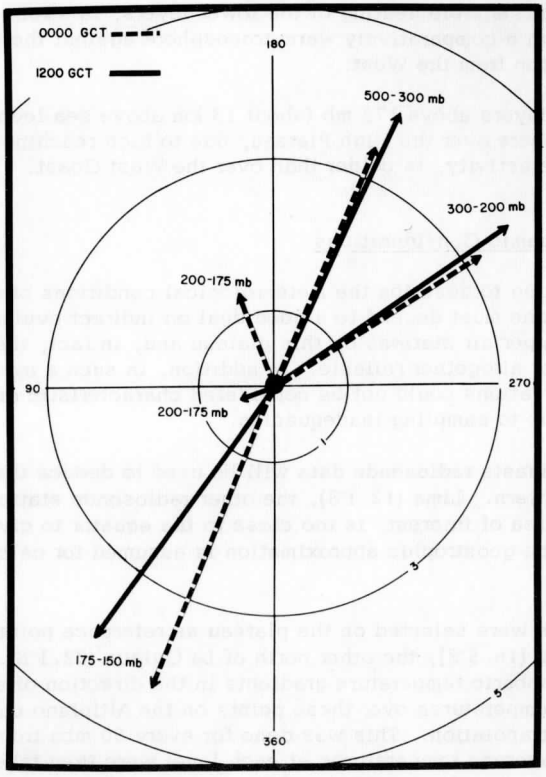

FIGURE 3. Mean January isobaric temperature gradients for various layers, Antofagasta, 1958-63; units: °C/1000 km. The arrows point in the direction of increasing temperature.

It will be shown that these features are in agreement with the following concepts:

a. latent heat is released in the thunderstorms over the Altiplano from the cloud base to about 200 mb. This heat source, together with sensible heating of the lower layers, is strong enough to maintain a comparatively warm troposphere against the cold air advection from the West.

b. in the layers above 175 mb (about 13 km above sea level) the atmosphere over the High Plateau, due to high reaching convective activity, is colder than over the West Coast.

3. Thermodynamic Considerations

In attempting to describe the meteorological conditions of the Altiplano region, one must depend to a good deal on indirect evidence. There are no upper air stations on this plateau and, in fact, the surface stations are not altogether reliable. In addition, in such a mountainous area any observations could not be considered characteristic of the region as a whole, due to sampling inadequacies.

The Antofagasta radiosonde data will be used to deduce the upper air temperature pattern. Lima (12.1°S), the other radiosonde station at the border of the area of interest, is too close to the equator to give reliable results when the geostrophic approximation is assumed for calculating thermal winds.

Two points were selected on the plateau as reference points, one south of La Paz (16.5°S), the other north of La Quiaca (22.1°S). By applying the isobaric temperature gradients in the direction of each point, the upper air temperatures over these points on the Altiplano can be constructed by extrapolation. This was done for every 50 mbs from 500 to 100 mb. The average temperatures at each level were then taken to be the mean of both soundings. This gave a sounding which one could assume approaches that actually over the plateau from 500 mb upward. Values of temperature and humidity for the lower levels, i.e., from surface to 500 mb, can be approximated by taking these parameters for various stations which are at different elevations (U.S. Weather Bureau, 1957-1963, Table 1) in order to obtain the temperatures and dew points in the lowest layers. The hypothetical sounding can be completed (fig. 4) if one takes the conditions at La Quiaca as characteristic for the diurnal variation of temperature; hourly temperatures are available from

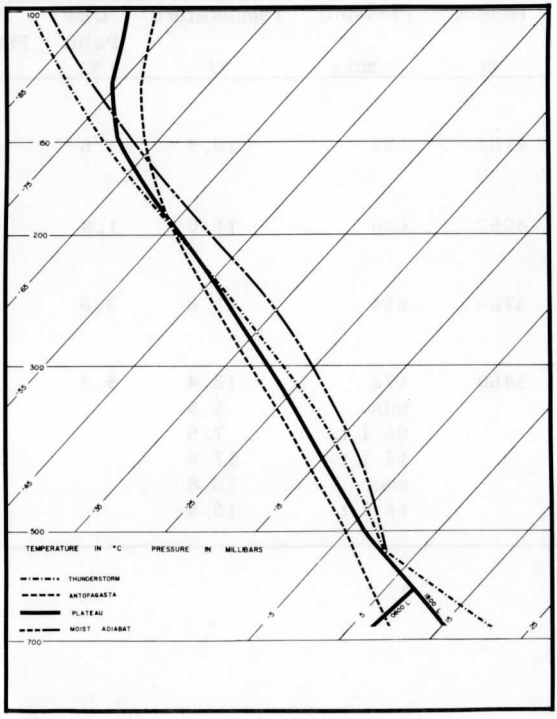

FIGURE 4. Average vertical structure of the atmosphere over Antofagasta and the Altiplano, in January.

TABLE 1.

Mean January Surface Station Data

Station	Height	Pressure	Temperature	Dew Point	Vapor Pressure
	m	mb	°C	°C	mb
LA PAZ					
16.5°S; 68.1°W	4103	622	10.3	3.6	8.0
CHARANA					
17.6°S; 69.5°W	4059	626	11.0	1.8	7.0
ORURO					
18.0°S; 67.1°W	3706	654	13.6	3.6	7.4
LA QUIACA					
22.1°S; 65.6°W	3460	672	12.4	5.3	9.1
" "		min	5.5		
" "		06 l.t.	7.5		
" "		12 l.t.	17.0		
" "		max	20.8		
" "		18.l.t.	15.6		

this station at an elevation of 3460 m (app. 672 mb), representative for the lower parts of the High Plateau.

A skew-T, log P diagram (fig. 4) has been applied to determine the heating during the day and the subsequent convection, using the daily mean maximum temperature for January at La Quiaca (Servicio Meteorologico Nacional, Republica Argentina, 1957) and the average mixing ratio in the lowest 50 mb to obtain the convective condensation level. By following the moist adiabat from this point, and assuming an entrainment rate of 100% per 300 mb as suggested by Saucier (1955), we find that an average thunderstorm over the Altiplano will rise to approximately the 125 mb level (13.5 km above sea level). Thus, we now can compare the observed vertical temperature distribution over Antofagasta (I) with two computed sets of data:

(II) Altiplano without thunderstorms, as given near the surface by observed temperatures in the Altiplano region, and at each level of the free atmosphere (above 500 mb) by "temperature gradient in the direction toward the center of the Altiplano times distance", and

(III) Altiplano with thunderstorms.

These data are listed in Table 2. Consequently, the corresponding height differences can be determined through the thickness equation, Table 3. Here, the values belonging to III - I must be considered maximum values obtained if the whole area were thunderstorm covered, and the II - I values can be accepted as lower limits, because there are some thunderstorms over the Altiplano practically every summer day.

The cumulative thickness differences ALTIPLANO minus ANTOFAGASTA clearly show the deformation of the thickness fields over the Altiplano in summer, in comparison to the general West-East course of the thickness isolines which must be assumed over the Pacific Ocean. Since the absolute height-differences between ANTOFAGASTA and the Altiplano for the lowest levels, surface to 600 mb, are very small and practically insignificant (as indicated by the weak resultant winds over ANTOFAGASTA and their little constancy), it follows that the cumulative differences given in the last two columns of Table 3 also describe the deformation of the contour fields of the upper constant pressure surfaces.

---

3. Unpublished data of the Servicio Meteorologico Nacional, Buenos Aires, for La Quiaca: 1911-1940.

TABLE 2.

Upper Air Temperatures, January Averages

Pressure mb	I Antofagasta	II Temperature (°C) Plateau without thunderstorms 0600 l.t.	1800 l.t.	III Plateau with thunderstorms
672	9.6	7.5	15.7	20.4
650	7.8	7.8	13.8	17.5
600	4.0	8.5	8.5	11.0
550	- 0.3	3.0		3.9
533	- 2.0	1.0		1.3
500	- 5.0	- 3.0		- 1.5
450	-10.6	- 8.6		- 6.5
400	-16.8	-14.8		-12.3
350	-23.7	-21.7		-19.5
300	-32.0	-30.2		-28.3
250	-41.9	-40.2		-39.4
200	-53.4	-52.4		-53.0
175	-59.8	-60.8		-61.4
150	-66.1	-69.0		-70.6
125	-72.4	-75.9		-80.6
100	-78.0	-81.0		-91.7

TABLE 3.

Thickness values (in gpm) for layers of the atmosphere over Antofagasta and the Altiplano and cumulative differences

Layer (mb)	I Antofagasta	II Altiplano 06 a. m.	III Altiplano (Thunderstorms)	Layer (mb)	II-I	III-I
672-650	285	283	295	672-650	- 2	10
650-600	658	680	698	672-600	20	50
600-550	696	714	718	672-550	38	72
550-500	790	799	799	672-500	47	81
500-450	823	829	834	672-450	53	92
450-400	893	899	907	672-400	59	106
400-350	991	997	1,006	672-350	65	121
350-300	1,108	1,117	1,126	672-300	74	144
300-250	1,272	1,284	1,290	672-250	86	162
250-200	1,473	1,484	1,484	672-200	97	171
200-175	847	847	844	672-175	97	168
175-150	949	941	936	672-150	89	155
150-125	1,085	1,069	1,052	672-125	73	122
125-100	1,294	1,274	1,223	672-100	53	51

4. Radiation Evidence

Other than brief descriptions in numerous travelogs (Tschudi, 1846; Reck, 1865; Bowman, 1916), there is little, if any, detailed observational evidence of the cloud type and amounts and their characteristic diurnal vairation over the whole of the Altiplano at any one time. For this reason, it is difficult to state how widespread the thunderstorm activity over the area is. With the advent of the TIROS satellites, large portions of the area can now be "seen" as never before feasible. By use of the radiation data from TIROS II in the window region (8-12 microns), one can obtain an idea of the development of cloud patterns with time of day. Figure 5 illustrates this rather well, and Bowman's description (1916) of a small portion of this area can be compared with the evidence gathered from radiation data. He states: "Light, highlying cirrus clouds are most characteristic of early morning hours. They produce some very striking sky effects just before sunrise as they catch the sun's rays aloft. An hour or two after sunrise, they disappear and small cumulus clouds begin to form. These grow rapidly as the winds begin, and by afternoon become bulky and numerous. In the wet season, they grow into nimbus and stratus types that precede a sudden downpour of water or a furious hailstorm." In other portions of his book, Bowman makes note of unusual weather phenomena, among them the violent "tempests" during the day and the absence of many starry nights during the wet (thunderstorm) season.

All available descriptions of the weather over the Altiplano indicate that the development of the sky conditions in the great majority of all summer days follows the above pattern, and it thus seems reasonable to look for the corresponding evidence of such a development in the satellite radiation data obtained at different local times, in order to see how the change of effective black body temperatures during the day indicates the presence of certain cloud patterns. Of course, this must be understood as only an illustration, not as a proof, because not more than a few orbits of TIROS II with a record of long-wave radiation data over the Altiplano are available for the summer of 1960-1961, and the evaluation of such data in fig. 5, therefore, necessarily refers to different days.

In the exposures of fig. 5a,about 30 minutes after sunrise, through c, 0907 l.t., early morning conditions are shown. Later in the morning, (5d; 1127 l.t.) the cumulus clouds seem to build up and through the afternoon (5e, f; 1410 l.t., 1732 l.t.) the areas with the taller cumulonimbus are characterized by the lowest temperatures. The cloud tops can penetrate into the layers above about 100 mb where winds from the East can carry cirriform clouds westward. Cirrus and decaying cumulonimbus may

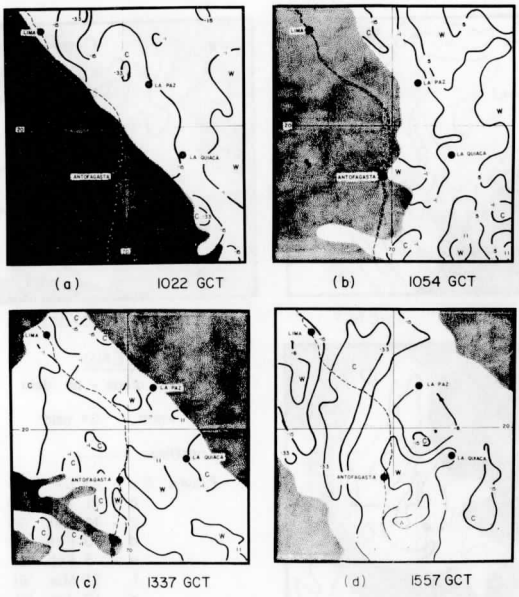

FIGURE 5. TIROS II radiation data converted to effective black body temperatures, °C, stippled areas = no data; W = warm; C = cold; ------ = coastline.

a) 23 Dec. 1960,
b) 21 Dec. 1960,
c) 14 Dec. 1960,
d) 10 Feb. 1961,
e) 3 Feb. 1961,
f) 29 Mar. 1961,
g) 17 Jan. 1961

next page

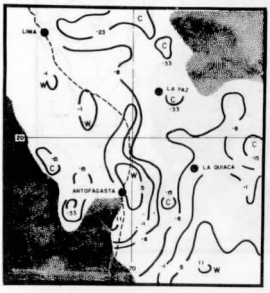

(e) 1840 GCT

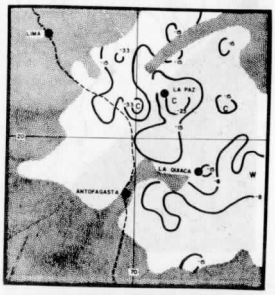

(f) 2202 GCT

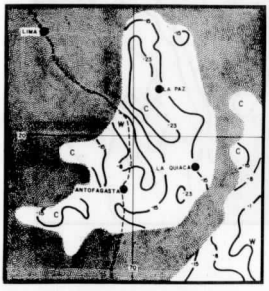

(g) 0110 GCT

LEGEND

Stippled areas - no data

W = warm C = cold

Coastline ---------

Figure 5 a - 23 Dec. '60
b - 21 Dec. '60
c - 14 Dec. '60
d - 10 Feb. '61
e - 3 Feb. '61
f - 29 Mar. '61
g - 17 Jan. '61

FIGURE 5 - CONTINUED

FIGURE 5 (continued) (See page 109)

thus continue through a good part of the night (5g; 2040 l. t.) until the cycle starts once again the following day.

The authors are aware of the work of Wark et. al. (1962) and Kern (1963) who showed that the absolute temperature values obtained through the "window" radiation data of the satellites cannot be considered accurate. This difficulty, however, is not important as long as the data are used for purposes of comparison, as in this part of the study. Actual cloud observations from surface at the approximate times of the radiation maps are available for Oruro, Cochabamba, and La Paz, and are presented in Table 4. These compare favorably with the interpretation of the radiation data.

TABLE 4.

Cloud Types and Amount Over Three Stations on the Altiplano*

Station	23 Dec. 1022 GCT	21 Dec. 1054 GCT	14 Dec. 1337 GCT	10 Feb. 1557 GCT	3 Feb. 1840 GCT	20 Mar. 2202 GCT
Oruro	2/8 Ci	4/8 Ci	1/8 Cu	2/8 Cu 600 m	4/8 Sc	1/8 Cb
67 07'W	4/8 Cs		5/8 Ci	3/8 Cu 900 m	2/8 Cu	2/8 Cu
17 58'S				3/8 Cs	2/8 As	1/8 Ci
Cochabamba	2/8 Ci	Trace Ci	3/8 Cu, Sc	Trace Sc, Cu	5/8 Cu, Cb	2/8 Sc, Cu
66 10'W			2/8 Ac	7/8 Ci, Cs	3/8 As	Trace Ac
17 24'S			2/8 Cs			1/8 Cs
La Paz	no report	no report	6/8 Cb, Sc, Ci	6/8 Cb, Sc	8/8 Fc, Cu, As, Cs	8/8 Cu, Ci
68 08'W						
16 30'S						

*Data obtained by courtesy of the SERVICIO METEOROLOGICO DE BOLIVIA, LA PAZ

TIROS photographs have only recently become available for the Altiplano region during the southern hemisphere summer, and the authors have examined several series of TIROS V pictures for January and February 1963. A comparison of pictures taken at different times of the day confirm the strong development of heavy convective cloudiness over the Altiplano from the late morning hours and through the afternoon. No reproduction of such photographs is here intended, as more detailed and sharper NIMBUS pictures can soon be expected.

5. A Tentative Heat Budget

As the wind observations of ANTOFAGASTA indicate, there is, during the summer months in the layers between 500 and 200 mb, an almost continuous cold air advection towards the Altiplano, and much less advection of the opposite sign in the lower and higher layers. Nevertheless, the troposphere over the Altiplano remains considerably warmer than over the coastal regions. This situation calls for a discussion of the various terms of the heat budget of the atmosphere over the region in question, and in particular of the role of the available latent heat.

To do so, an approach has been carried through to which H. H. Lettau (1956, and unpublished course notes) called the attention to the authors. It is based on the fact that the heat budget terms as incoming, absorbed, and out-going radiation, gains and losses of sensible and latent heat and the respective storage terms must all be interrelated to fulfill the following conditions: the total energy budget at the lower boundary of an air column over the Antiplano (summer) and likewise the sensible heat budget of such an air column must both become zero; the net import of energy across the boundaries of the column has to correspond to the energy storage within; and the water budget must be kept in agreement with the observed data and with a reasonable appreciation of the regional circulation.

This approach is schematically represented in fig. 6, the meaning of the letters being given in Table 5 together with a logical, and likely, combination of the observed, computed and estimated terms. These values refer to the Southern part of the Altiplano, for which La Quiaca (22 06'S; 65 36'W; 3460 m) is a representative station, with more and better surface observations than there are available for the Northern part. Of course, the arrangement of Table 5 is not the only possible one, and the reasoning why this combination was chosen will be given in the following discussion of the more important, and more uncertain, terms of the budget.

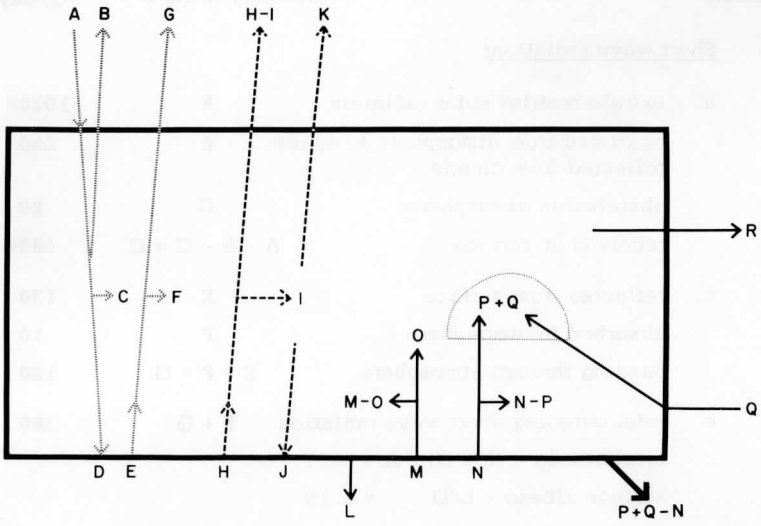

FIGURE 6. Scheme of the heat budget used and explained in Table 5.

TABLE 5.

A tentative heat budget for the Altiplano. Units: ly/day.
Asterisk: Values based on measurements or computations.

Terms		Symbols in fig.6	ly/day
1.	Short wave radiation:		
a.	extraterrestrial solar radiation	A	1020*
	scattered from atmosphere to space reflected from clouds	B	260
	absorbed in atmosphere	C	80
	received at surface	A - B - C = D	680*
b.	reflected from surface	E	130
	absorbed in atmosphere	F	10
	passing through atmosphere	E - F = G	120
c.	total outgoing short wave radiation	B + G	380
	total albedo = (B + G) / A = 0.37		
	surface albedo = E/D = 0.19		
2.	Long wave radiation:		
	emitted from surface	H	770*
	absorbed in atmosphere	I	660
	passing through	H - I	110
	back radiation	J	600
	effective radiation from surface	H - J	170*
	to space from atmosphere	K	440
	total outgoing to space	H - I + K	550*
	heat loss from atm. (corresponding to a l.w.rad. cooling rate of about 2.5 C/day	I- J - K	380

3. Total energy budget at lower boundary:

a.	radiation:	short wave incoming	D	680*
		short wave outgoing	E	130
		effective long wave out	H - J	170*
		net radiation	D - E - (H - J)	380
b.	heat transports:	storage into ground	L	20
		sensible heat up	M	120
		latent heat up	N	240
		total transports	L + M + N	380
		Bowen ratio = M/N = 0.5		

Balance: D - E - (H - J) = L + M + N

4. Heat budget, interior of column:

a.	gains:	absorbed short wave radiation (not stored)	C + F	90
		absorbed long wave radiation (not stored)	I	660
		conducted into air from below (not stored)	O	110
		latent heat effectively released (not stored)	P + Q	*
		from evaporation at surface (not stored)	P	230
		from lateral advection (not stored)	Q	40
	total gain:	C + F + I + O + P + Q		1130
b.	losses:	back radiation	J	600
		long wave to space	K	440
		by advection (laterally, out)	R	90*
		total loss:	J + K + R	1130
c.	storage:	sensible heat	M - O	10
		latent heat	N - P	10
		sum of storage terms:	M - O + N - P	20

Balance: losses equal gains

5. Net import of total energy:

across	upper boundary	A - B - G - (H - I) - K	90
	lower boundary	L	20
	lateral boundaries	R - Q	50

5. Net import of total energy (cont'd)

net amount: A - B - G - (H - I) - K - L - (R - Q) 20
Balance: sum of storage terms (4 c) equals net amount (5).

6. Water budget:

precipitation	P + Q	270*
evaporation	N	240
water storage at and in ground + run off:	P + Q - N	30

D: The global radiation has been measured at La Quiaca with a ROBITZSCH-actinograph, for several years. The January mean for the uninterrupted series 1943-56 (Angstrom - scale) is 759 ly/day, (unpublished data, courtesy of F. Prohaska). As the ROBITZSCH-pyranograph was never designed to be an instrument which gives exact absolute measurements, it appeared necessary to compare this value of 750 ly/day with the results of computations on the basis of various formulas known in the literature (Albrecht 1955, Budyko 1956, Hinzpeter 1958, List 1958) and with unpublished data determined by H. and K. Lettau. For the station CALAMA (22 28'S, 68 56'W, 2250 m, at the westslope of the Andes) Linke (1942) gives for the month of January a turbidity factor T of 2.4. With the assumption of T = 2.0 for the atmosphere over the Altiplano, the direct solar radiation (cloudless sky) for a surface pressure of 600 mb, at January 21, becomes 840 ly/day and the global radiation (D_o) to 910 ly/day. For a relative duration of sunshine of .65 (Campbell-Stokes records, La Quiaca, January average) and with the relation for D/D_o as given by Fritz (see List, 1958, Table 151), one obtains for D, as an estimate of the global radiation received at the surface of the Altiplano in January, 680 ly/day. This value will be used for tentative heat budget.

H and H - J: The long wave radiation emitted from surface, H in the notation of Table 5, corresponds to an average (black body) surface temperature of 11°C. The effective long wave radiation from the surface has been computed using nine different formulas (see Budyko 1956, Lönnqvist 1950 and 1953, Penman 1956) on the basis of surface observations, i.e., the January means of temperature, vapor pressure, cloudiness, and relative duration of sunshine of La Quiaca. The values thus obtained lie between 103 and 173 ly/day, the highest values resulting from the formulas of Lönnqvist and Penman. In Lönnqvist's, the ratio between the liquid equivalent (precipitable water) and the vapor pressure at surface can be varied. It is thus possible to allow for realistically low values of this

ratio, and the relatively high amount of 170 ly/day appears to be the best estimate.

H - I + K: The total long wave radiation outgoing to space has been evaluated (by G. Gutman) from TIROS II radiation data on the basis of the records of seven orbits of various summer days when the satellite was passing over the Altiplano at different local times, in intervals of approximately 3 hours. The result is a value of about 550 ly/day, but it remains an open question whether this is really representative of average January conditions. No better estimate, however, was available because no aerological soundings have been made on the Altiplano and, therefore, a computation with one of the various radiation-diagrams could not be regarded as any improvement. On the basis of this value of 550 ly/day together with the estimates for the long wave radiation emitted from the surface (H) and the effective radiation from surface (H - J), the long wave radiation outgoing from the atmosphere (K) was determined to be about 440 ly/day.

L, M - O, N - P: These are the storage terms which can be assumed to be rather small in the month under consideration. In view of the inexactness of the estimates of the much larger terms of the tentative heat budget, no effort was made to determine these rather insignificant terms more precisely. They are included in Table 5 mainly in order to maintain a logical build-up of the total budget.

M + N: The sum of these two terms is, in the first place, a consequence of the balance requirement for the total energy budget at the earth-atmosphere interface. The value for N also depends upon the estimate of the average monthly sum of precipitation over the Altiplano. Finally, the ratio of M/N, the regional Bowen ratio, must reasonably correspond to the surface properties and rainfall characteristics of the Altiplano. These three conditions are important; they severely restrict the limits within which various other terms of the budget have to be found.

O, P: These terms follow from the conclusions regarding M and N and the assumptions made for the storage terms.

P + Q: The value accepted as the sum of these two terms represents the equivalent of our estimate of the average regional January precipitation falling on the Altiplano. The value chosen, 270 ly/day, corresponds to a rainfall of 135 mm per 30 days. This assumption needs some lengthier comments: generally, the observed rainfall amounts appear to be the best basis of estimating the latent heat released and becoming available, even if in a terrain as the Altiplano, with thunderstorm activity producing most of the precipitation, the sampling network is inadequate. However,

a comparison of the remarks on the enormous intensity of the daily thunderstorms given by various authors who have travelled through the subtropical Andes and the Altiplano in summer (Tschudi 1846, Reck 1865, Bowman 1916) with the precipitation records of Bolivia and the extreme Northwest of Argentina clearly suggest that the most violent storms are to be found over the uninhabited mountains. Furthermore, conventional rain gauges cannot give representative results when the precipitation falls with strong and gusty winds.

In Bolivian and Argentine climatological records (Escobar Vallejo 1948, Servicio Meteorologico Nacional 1943, 1957, 1958), there are in the region of the Altiplano 50 stations with an elevation of more than 3000 m above sea level, with precipitation series of 5 or more years. The overall January mean of these 50 stations amounts to 108 mm, the yearly variation is represented in fig. 7. This average sum for January must be considered an underestimate, first because of the above mentioned reasons, and second because with such a small amount of monthly precipitation, the total energy budget at the lower boundary (Table 5, part 3) could be brought into balance only with an unrealistic high value of the Bowen ratio, M/N, and/or some improbable assumptions regarding the radiation terms.

Q: A positive import of H_2O by lateral advection into the region of the Altiplano is a logical necessity, because there must be some storage of water (falling mainly during the summer months) in the ground (and lakes) and some surface—and subsurface run off. As the air masses of the upper half of the troposphere over the subtropical Pacific Ocean and the coastal region which are advected toward the Altiplano area are drier than the air masses over the Altiplano itself where the daily summer thunderstorms develop, there must be a considerable moisture advection in the lowest layers. This notion is supported by local weather observations and by the predominance, only in summer, of surface winds from the Northeast quadrant, together with comparatively high vapor pressure values at the surface. These characteristics of the summer climate of the Altiplano are discussed in a more detailed form by Prohaska (1964). Table 7 summarizes his data of the relative frequency of the direction of surface winds. The winter values have been added in order to prove that the predominance of the NE-winds in the summer is not due to local terrain features.

R: The advective sensible heat loss follows as a balance requirement in the sensible heat budget for the interior of an air column, as mentioned in the discussion of the total amount of long wave radiation outgoing to space. On the other hand, R can be computed from the wind analysis for Antofagasta, the key aerological station used in the first part of this

study. The computed value is about 80 ly/day (see Table 6), obtained under the reasonable assumption that the small contribution of the layers below 500 mb and above 100 mb can be disregarded. In the tentative heat budget, Table 5, a slightly higher value of 90 ly/day has been used. It is admitted, of course, that valid arguments can be brought forward as well against our estimate of the outgoing radiation as against the assumption that the wind and thermal wind evaluation for Antofagasta gives a quantitatively correct value of the temperature advection towards the Altiplano.

P + Q - N: The sum of water storage and run off results as the difference between the precipitation reaching the ground and the evaporation at its surface. It must be understood that the term "run off" refers to the amount of water definitively lost from the Altiplano, not to the run off within the mountain-encircled High Plateau itself. The rate of 30 ly/day corresponds to 0.5 mm of rain per day, equivalent to about 600 m^3 of water per second per an area of 10^5 km^2, which should be in the right order of magnitude.

TABLE 6.

Temperature advection at ANTOFAGASTA, expressed in ly/day, determined from the daily wind observations and average values of the thickness of the standard layers for the month of January of the 5 years, 1959-63.

Layer	Advection
500-400 mb	- 8
400-300 "	-15
300-200 "	-70
200-150 "	+ 6
150-100 "	+ 4
Sum	-83

In conclusion, it appears that this heat budget gives an adequate description of the mechanism by which the warm, stationary summer-anticyclone in the region of the Altiplano, with intense thunderstorm activity in its center, is kept alive. It is only presented in order to show that an estimate of the magnitude and the interaction of the physical processes involved leads to a consistent, meteorologically probable picture. It is not pretended to be a "proof".

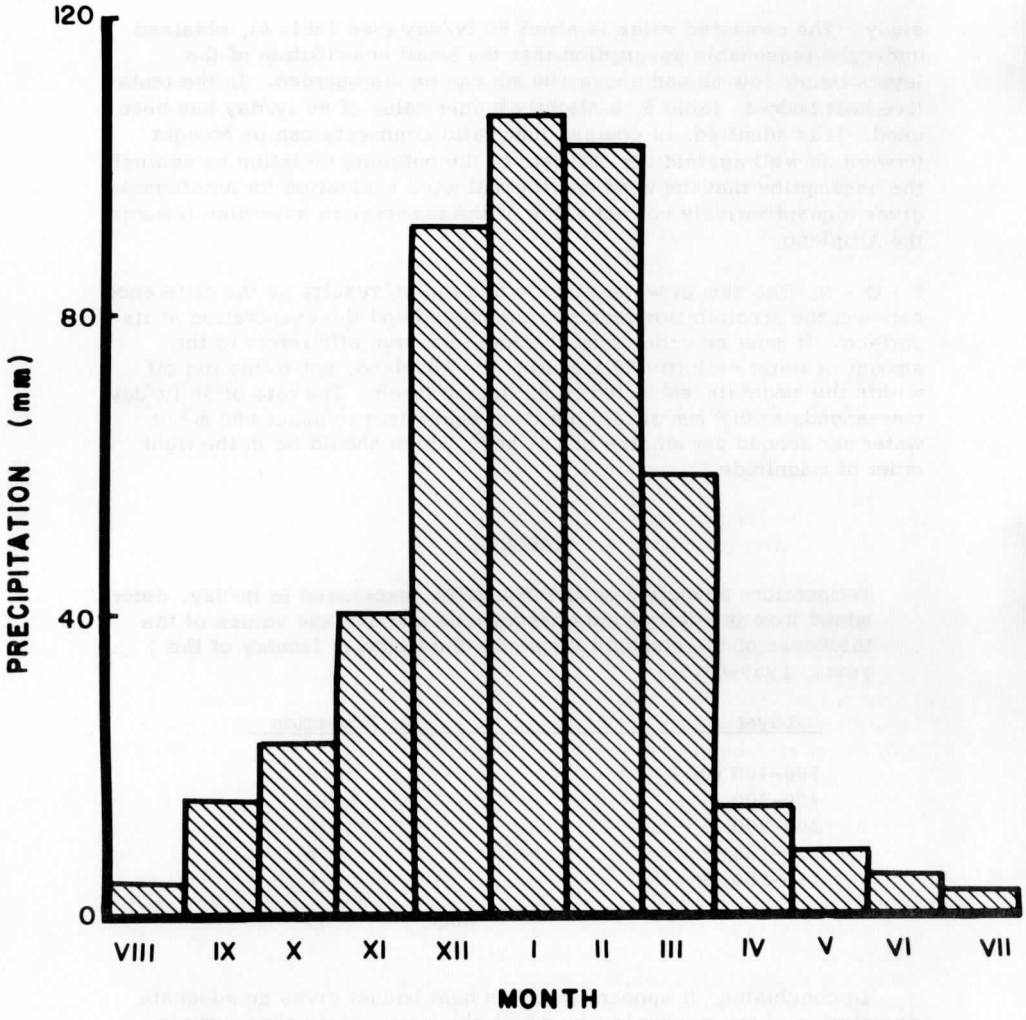

FIGURE 7. Average monthly sum of precipitation (reduced to months of equal length) of fifty stations in the region of the Altiplano, all of them located at elevations between 3000 and 4600 m above sea level.

In this context, it is interesting to note that the wind pattern in the surface layer and its change from summer to winter (Table 7) can be understood as a large scale, seasonal valley—and mountain-wind system (Prohaska 1964). One thus may say that the intensified sensible heating of the Altiplano in spring brings about the moisture-supplying "valley" winds, that the latent heat of this moisture plays the dominating role for the maintenance of the anticyclone in summer, and that the phenomena disappear when the heating of the High Plateau and its slopes decreases.

TABLE 7.

Relative frequency of the direction of surface winds LA QUIACA, hourly observations 1935-43, (Prohaska 1964).

Season	N	NE	E	SE	S	SW	W	NW	Calm
Summer (XII-II)	18	35	8	7	11	6	5	8	2%
Winter (VI-VIII)	8	8	6	12	24	10	15	12	5%

This concept can now be employed to interpret the seasonal change of the upper wind pattern as shown in fig. 1, and the characteristics of the thickness field, figs. 2 and 3. The remarkable deformation of the upper tropospheric streamfield only in the warmer season should be due to a thermal effect, the comparatively high temperatures of the upper half of the troposphere in the anticyclonic ridge over the subtropical Andes being maintained through the latent heat released in thunderstorms.

As far as the comparatively larger area of the Highlands of Tibet is concerned, recent studies of Flohn (1965) strongly suggest that similar conditions indeed exist. In both cases, the upper troposphere anticyclone is a quasi-stationary system, persisting through the warm season. For a much shorter time interval, an analogous phenomenon in the region of the Gulf of Mexico was analyzed by Riehl (1959). He writes: ". . . . a situation is presented where a warm high was of thermal origin, produced and maintained by release of latent heat of condensation. The interior of the high was filled with cloud and rain; maximum precipitable water content of the air was found in the central parts of the high. . . . It is now known that this type of circulation occurs fairly frequently in subtropical and tropical latitudes."

It thus appears that anticyclogenesis and the persistence of an upper high pressure system is <u>not</u> "invariably accompanied by subsiding motion",

as it is generally said in meteorological textbooks (e.g., Petterssen, 1956), but rather that condensation heating can produce the same effect.

6. References

Albrecht, F.H.W., 1955: Methods of computing global radiation. Geofisica Pura e Applicata, Vol. 32, 131-138.

Bolin, B., 1950: On the influence of the earth's orography on the general character of the westerlies. Tellus, 2, 184-195.

Bowman, I., 1916: The Andes of Southern Peru, New York, Henry Holt and Company, 336 pp.

Budyko, M.L., 1956: The heat balance of the earth's surface. U.S. Weather Bureau Translation, 1958.

Escobar Vallejo, I., 1948: Régimen Pluviométrico de Bolivia, La Paz, Dirección General de Meteorología, 57 pp.

Flohn, H., 1950: Tropische und aussertropische Monsunzirkulation. Berichte des Dt. Wetterdienstes U.S. Zone, No. 18, p. 34-50.

Flohn, H., 1953: Hochgebirge und die allgemeine Zirkulation. II. Die Gebirge als Wärmequellen. Archiv für Meteorologie, Geophysik und Bioklimatologie, Serie A, Vol. 5, p. 265-279.

Flohn, H., 1959: Bemerkungen zur Klimatologie von Hochasien. Abhandl. Math. Naturwiss. Kl. Akademie der Wiss. und Lit. Mainz, Vol. 14, p. 309-331.

Flohn, H., 1960: Recent investigations on the mechanism of the "Summer Monsoon" of southern and eastern Asia. Symposium on Monsoons of the World, New Delhi, Hind Union Press, pp. 75-88.

Flohn, H., 1965: Remarks on the thermal effects of the Tibetan Plateau during summer. Australian Meteorological Magazine, in press.

Guibaut, A., 1948: Tibetan Venture. London, John Murray Ltd., 206 pp.

Hinzpeter, H., 1958: Vergleichende Prüfung von Formeln zur Berechnung von Globalstrahlungssummen. ARCHIV für MET., GEOPHYS. und BIOKLIM., Serie B, vol. 9, pp. 60-72.

Kern, C.D., 1963: Desert soil temperatures and infrared radiation received by TIROS III. Journal of Atmospheric Sciences, 20, pp. 175-176.

Lettau, H.H., 1956: A study of the mass, momentum and energy budget of the atmosphere. ARCHIV für MET., GEOPHYS. und BIOKLIM., Serie A, Vol. 7, pp. 133-157.

Linke, F., 1924: Ergebnisse von Messungen der Sonnenstrahlung und Lufttrübung über dem Atlantischen Ozean und in Argentinien. Meteorologische Zeitschrift, Vol. 59, p. 42-46.

List, R.J., 1958: Smithsonian Meteorological Tables, sixth revised edition, Smithsonian Miscellaneous Collections, Vol. 114, Table 151.

Lönnqvist, O., 1950: A general method and a simplified formula for calculating effective radiation. ARKIV für GEOFYSIK, Vol. I. pp. 79-115.

Lönnqvist, O., 1953: Calculating effective radiation with due regard to its diffuse nature. ARKIV für GEOFYSIK, Vol. I, pp. 441-451.

Namias, J. and P.F. Clapp, 1951: Observational studies of general circulation patterns. Compendium of Meteorology, Waverly Press, Inc., pp. 551-567.

Penman, H.L., 1956: Evaporation; An Introductory Survey. Netherlands Journal of Agricultural Science, Vol. 4, No. 1, pp. 9-29.

Petterssen, S., 1956: Weather Analysis and Forecasting, Second edition, Vol. I. McGraw-Hill Book Company, New York.

Prohaska, F.J., 1964: Factores advectivos en el clima de la Puna Argentina, Boletín de Estudios Geográficos, Universidad Nacional de Cuyo, Vol. IX, in press.

Rangarajan, S., 1963: Thermal effects of the Tibetan Plateau during the Asian monsoon season. Australian Meteorological Magazine, 42, pp. 24-34.

Reck, H., 1865: Geographie und Statistik der Republik Bolivia, Petermann's Geogr. Mitteilungen, pp. 281-295.

Riehl, H., 1959: On production of kinetic energy from condensation heating. In The Rossby Memorial Volume, The Rockefeller Institute Press and Oxford University Press, New York, pp. 381-399.

Saucier, W.J., 1955: Principles of Meteorological Analysis, Chicago, The University of Chicago Press, 438 pp.

Schwerdtfeger, W., 1961: Strömungs und Temperaturfeld der freien Atmosphäre über den Anden. Meteor Rundschau, 14. Jahrgang, 1. Heft, 1-6.

Servicio Meteorológico Nacional, 1943: El Régimen Pluviométrico de la República Argentina, Normales de Lluvia de 25 Años. Publ. Serie F, No. 2, Buenos Aires.

Servicio Meteorológico Nacional, 1957: Estadísticas Climatológicas 1901-1950. Publ. Serie B, No. 1, Buenos Aires.

Servicio Meteorológico Nacional, 1958: Estadísticas Climatológicas 1941-1950. Publ. Serie B, No. 3, Buenos Aires.

Tschudi, J.J.V., 1846: Peru. Reiseskizzen 1838-1842. 2, 71 St. Gallen.

U.S. Weather Bureau, 1957-1963: Monthly Climatic Data for the World, 10-16, Asheville.

Wark, D.Q., G. Yamamoto and J.H. Lienesch, 1962: Methods of estimating infrared flux and surface temperatures from meteorological satellites. Journal of Atmospheric Sciences, 19, pp. 369-384.